Adapting to the Future Storm and Ice Regime in the Great Lakes

Stream 1 Report

May 1, 2019

Prepared by:

Contact the Author:
Peter J. Zuzek
905-719-8980
pzuzek@zuzekinc.com

Zuzek inc.
ONE WORLD

Supported by Natural Resources Canada's Climate Change Adaptation Program

Natural Resources Canada | Ressources naturelles Canada

Canada

Great Lakes Ice Cover March 25, 2019 from the MODIS Satellite

Disclaimer:

Zuzek Inc. assumes no responsibility for the use of this report by a third party. Furthermore, if used by a third party, they agree that the information is subject to change without notice and Zuzek Inc. assumes no responsibility for the consequences of such use or changes in the information. Under no circumstances will Zuzek Inc. be liable for direct, indirect, special, or incidental damages resulting from, arising out of, or in connection with the use of the information in this report by a third party.

EXECUTIVE SUMMARY

Zuzek Inc. was the lead Consultant for the study "Adapting to the Future Storm and Ice Regime in the Great Lakes". Other members of the Consulting Team include Linda Mortsch from the University of Waterloo, RWDI, and Baird. Funding and in-kind support were provided by the Municipality of Chatham-Kent, the Lower Thames Valley Conservation Authority, the Credit Valley Conservation Authority, the Region of Halton, the 20 members of the Conservation Authorities Coastal Working Group, and the Ontario Centre for Climate Impacts and Adaptation Resources. The study also received significant financial support from Natural Resources Canada's Climate Change Adaptation Program.

There were two primary objectives of the study. First, in Stream 1 the potential influence of climate change on coastal storms on the Great Lakes was investigated to project possible future impacts on wave heights and storm surges. In Stream 2 case studies were used to co-develop knowledge and expertise on how to integrate this new information for coastal management and develop adaptation alternatives to increase the resilience of coastal communities and ecosystems.

The Stream 1 investigation was completed at the end of March 2019. The detailed findings are summarized in two technical reports, attached to this Executive Summary. The first authored by RWDI Inc. was entitled "Adapting to the Future Storm and Ice Regime in the Great Lakes; Future Storm Frequencies" and is included in Appendix A. It included the following analysis: 1) synoptic weather typing for the severe storm events association with large waves and storm surges, 2) analysis of sea-level pressure gradients across the Great Lakes region for historical and projected future conditions, and 3) changes between historical and future ice cover for the RCP8.5 late-century emission scenario. These studies did not identify any statistically significant change in future storm intensity compared to historical conditions. In short, the storm surge magnitude and wave height associated with severe storm events in the future is expected to be consistent with historical conditions.

The second component of Stream 1 was focused on numerical modeling of waves and storm surges by Baird and based on the climate inputs from the RWDI analysis. The work by Baird is summarized in a technical report entitled "Adapting to the Future Storm and Ice Regime in the Great Lakes; Lake Erie and Ontario Nearshore Wave and Surge Modelling". The full report is provided in Appendix B. In the first half of the analysis, detailed wave and hydrodynamic models were set up and calibrated for Lake Ontario and Lake Erie. Then, 15 of the largest storm events between 2000 and 2013 (baseline period) were simulated to generate shallow water wave heights for the case studies and spatially varying storm surges. The storms were then re-run using the ERA-Interim reanalysis for the RCP8.5 emission scenario to generate future conditions from the 15 storms. For some events, peak wave heights were higher for the baseline period, for others the wave heights were higher for the future conditions. This trend is consistent with the RWDI (2019) finding that no statistical change in storm intensity is expected in the future due to Climate Change.

The second aspect of the Baird (2019) analysis was an hourly wave hindcast for Lake Ontario and Lake Erie using the WAVAD second generation spectral wave model. The model uses a coarse grid of 2,200 m to cover the lakes and simulated hourly wave conditions (height, period,

and direction) from 2000 to 2013. For the historical hindcast, the model incorporated the NOAA GLERL ice charts to represent the actual ice cover conditions. For the future scenario, the hourly wind data from the ERA-Interim RCP8.5 emission scenario reanalysis was used to drive the wave hindcasting model. Given the amount of atmospheric and lake warming in this future late-century scenario, both lakes were assumed to be ice-free in the future simulation. On Lake Erie, the winter wave energy is predicted to more than double in Western Basin. See the plot below. Across the remainder of the north shore, the increase ranges from 60% to 80%.

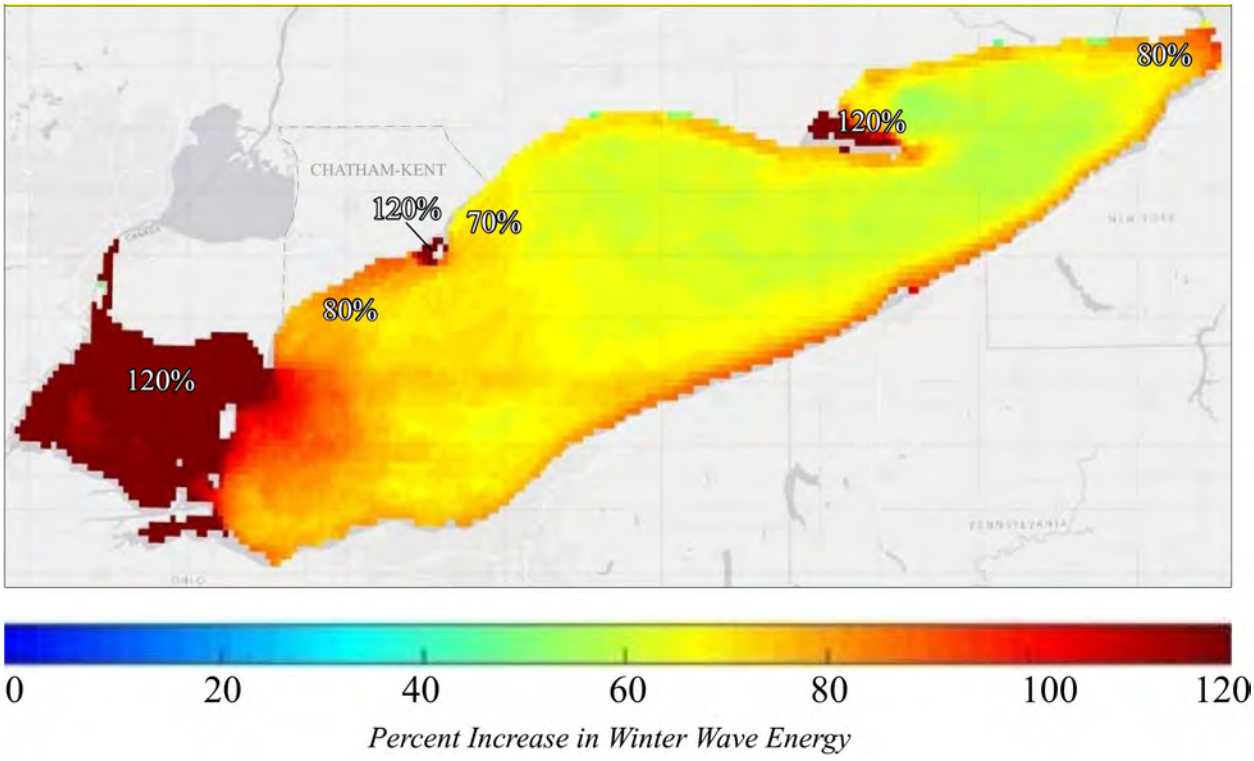

Percent Increase in Lake Erie Wave Energy, December to March, for the Late-Century Projection Compared to the Baseline Period (2000 to 2013)

For Lake Ontario, the Kingston Basin will see the greatest change in energy, with roughly a doubling in the winter (map on next page). Historically, this basin was ice covered every winter, so an ice-free future will dramatically increase the wave energy regime (by ~100%).

Across the north shore of Lake Ontario, the projected increase in wave energy will be 20% to 60%, with higher increases in sheltered embayments. Along the western shore of Lake Ontario, ice cover is often limited to shore-fast ice, as seen in the February 2019 photograph from Burlington Beach on the next page. While narrow, this ice still protects the shoreline and infrastructure from direct wave attack during storms. Since these narrow bands of ice are not captured in the NOAA satellite-derived ice-cover database, their influence on our wave energy analysis is not captured at this time. However, the loss of this shore-fast ice in the winter due to rising air and water temperatures across the western basin of Lake Ontario will result in significant increases in wave energy exposure.

The Stream 2 case studies are all underway and working to integrate this new information on the projected impacts of Climate Change on Great Lakes storms. A report summarizing these findings will be prepared in March 2020. The time series wave data for the historical and future period can be downloaded from the following website: http://www.zuzekinc.ca/waves/.

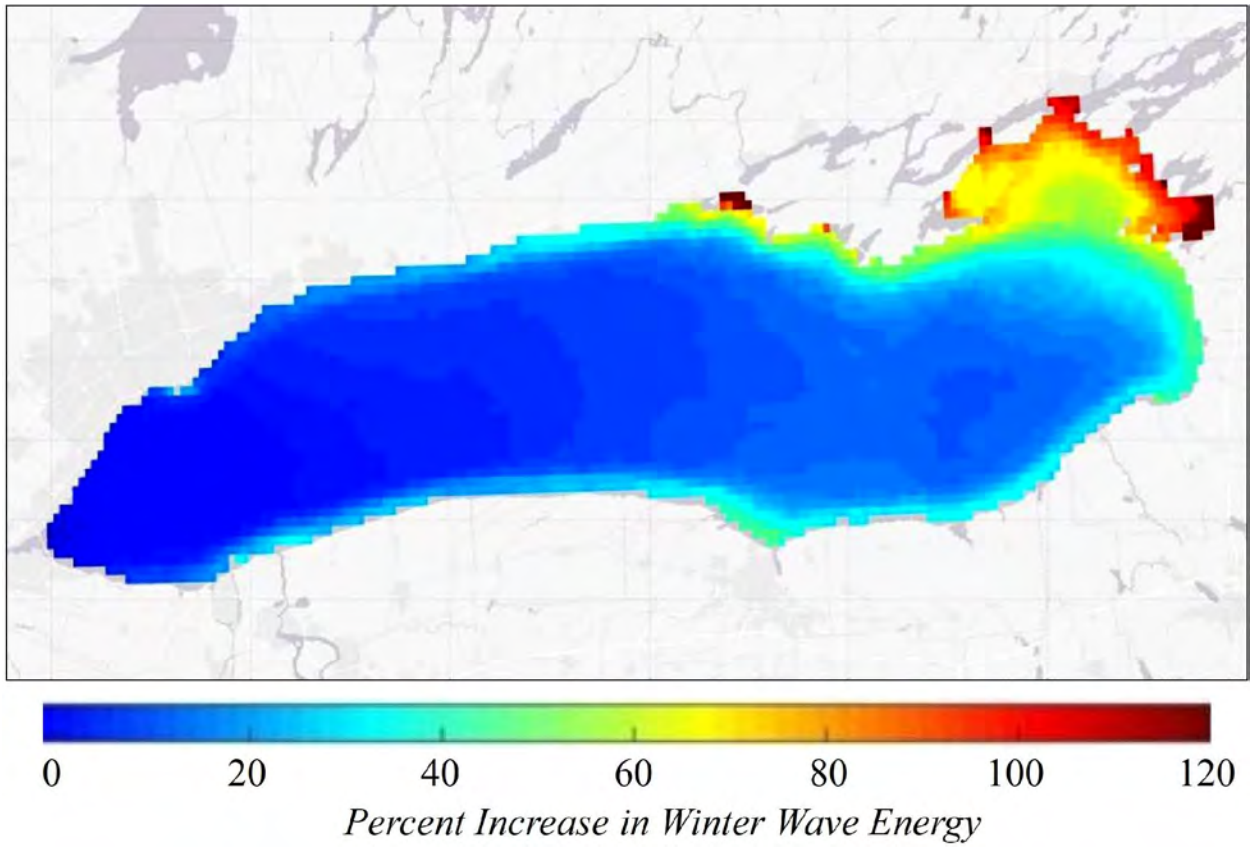

Percent Increase in Lake Ontario Wave Energy, December to March, for the Late-Century Projection Compared to the Baseline Period (2000 to 2013)

Example of a Narrow Band of Shore Fast Ice at Burlington Beach, February 28, 2019

APPENDIX A

Future Storm Frequencies

REPORT

ADAPTING TO THE FUTURE STORM AND ICE REGIME IN THE GREAT LAKES: FUTURE STORM FREQUENCIES

RWDI #1801772
June 1, 2020

SUBMITTED TO
Peter Zuzek
Zuzek Inc.
125 Wimberly Ave
Waterdown, Ontario
L8B 0S2

SUBMITTED BY
Ron Chapman
Project Manager
ron.chapman@rwdi.com

Christian Reuten, Ph.D., ACM
Technical Directory / Associate
Christian.reuten@rwdi.com

Jeff Lundgren
Technical Directory / Principal
Jeff.lundgren@rwdi.com

RWDI
600 Southgate Drive,
Guelph, Canada, N1G 4P6
T: 519.823.1311
F: 519.823.1316

TABLE OF CONTENTS

LIST OF TABLES

LIST OF FIGURES

APPENDICES

VERSION HISTORY

Index	Date	Pages	Author
1	March 29, 2019	All	Ron Chapman, Jeff Lundgren, Christian Reuten
2	April 11, 2019	All	Ron Chapman, Jeff Lundgren, Christian Reuten
3	April 06, 2020	All	Christian Reuten, Jeff Lungren, Ron Chapman
4	May 29, 2020	All	Christian Reuten, Jeff Lungren, Ron Chapman

1 EXECUTIVE SUMMARY

This report summarizes RWDI's contribution to a multi-team climate study that analyzed future storms and their impact on shore flooding and erosion in the Great Lakes. Changes in synoptic weather patterns, sea-level pressure (SLP) differences, and ice cover were considered to assess future changes in the frequency of storm events over Lake Erie and Lake Ontario.

Using wave heights from the USACE WIS hindcast stations closest to the site and storm surge data from the closest water level gauge, historical storms were chosen from each lake and analyzed and characterized by synoptic weather types. Output from five global climate models (GCMs) that were part of the Coupled Model Intercomparison Project Phase 5 CMIP5 project for high emission Representative Concentration Pathway (RCP8.5) for the 2071-2100 period were analyzed to determine whether the identified storm types would change in frequency due to climate change. Future changes in synoptic weather patterns were estimated to decrease storm frequencies by 2% of over both lakes with uncertainties of 2-3%.

Sea-level pressure differences are a driving force for storms. Future changes in SLP differences over both lakes were estimated to decrease the frequency of storms by 8% over Lake Erie and 5% over Lake Ontario with uncertainties of 6% and 12% respectively. With the high uncertainty, the future changes are indeterminant.

Finally, ice cover can completely suppress large wave height events even in the presence of strong storm conditions. A preliminary analysis for this study suggested the possibility of complete absence of ice cover by the end of the century under RCP8.5 and increases of storm frequencies of 25% for Lake Erie and 13% for Lake Ontario during the winter storm season which typically runs October through April. The uncertainty of these estimates could not be determined in the preliminary analysis.

The overall balance between changes in synoptic weather patterns, SLP differences, and ice cover is estimated to be an increase of 15% for Lake Erie (standard deviation 6% plus additional uncertainties from changes in ice cover) and 6% for Lake Ontario (standard deviation 12% plus additional uncertainties from changes in ice cover). Hence, ice cover arises as the most critical determinant of future storm frequencies over both lakes. It is highly recommended to perform a thorough analysis for future ice cover and the effect that ice cover has had historically to improve these critically important estimates and to assess their uncertainties.

In addition to the analysis of storm frequencies, high resolution simulations of the historical and future climate of North America were used to provide gridded wind and pressure fields to drive storm surge and wave simulations over Lakes Erie and Ontario. The historical simulation was driven using the ERA-Interim reanalysis for a 13-year period from October 1, 2000 through September 30, 2013. The future simulation used a pseudo global warming approach, in which the same reanalysis-derived boundary conditions used to drive the historic period are perturbed by an amount equal to the increment predicted by a large ensemble of CMIP5 global climate models. These outputs were used in the Baird (2019) storm surge and wave modeling.

Understanding the mechanism driving storm events over the Great Lakes, how these storms will change in intensity and frequency in the future, along with the reduction in lake ice during these same storms in the future will lead to better understanding of shore erosion and flooding hazards, which in turn informs land use planning in/around the Great Lakes and the development of climate change adaptation alternatives.

2 GLOSSARY

Acronym	Description
CFSR	Coastal Forecast System Reanalysis
CMIP5	Coupled Model Intercomparison Project (CMIP) Phase 5
ECMWF	European Centre for Medium-range Weather Forecasts
EOF	Empirical Orthogonal Function
GCM	Global Climate Model (in the scientific literature, sometimes used for 'General Circulation Model', a more specific type of global climate model)
GPH	Geopotential Height (here used in short to refer specifically to 500-hPa GPH)
GLERL	Great Lakes Environmental Research Laboratory
IPCC	Intergovernmental Panel on Climate Change
LLNL	Lawrence Livermore National Laboratory
NCAR	National Center for Atmospheric Research
NOAA	National Oceanic and Atmospheric Administration
PCA	Principal Component Analysis
PGW	Pseudo Global Warming
RCP	Representative Concentration Pathway
SLP	Sea-Level Pressure
Storm	Or 'storm event': A day when the modelled peak wave height was within a chosen percentile of all wave heights, e.g. the top 100 wave heights from 1979 to 2013.
SSTSK	Sea Surface Skin Temperature
T2	Dry Bulb Air Temperature at 2 meters height above ground
U10	West-East Grid Relative Wind Speed
V10	South-North Grid Relative Wind Speed
WAM	Spectral Wave Model
WIS	Wave Information Studies
WRF Model	Weather Research and Forecasting Model

3 PROJECT OBJECTIVES AND DESCRIPTION

RWDI partnered with Zuzek Incorporated (Zuzek), W.F. Baird & Associates Coastal Engineers Ltd (Baird), and Linda Mortsch from the University of Waterloo to advance the knowledge base and enhance the adaptive capacity of practitioners managing the coastal zone in the Great Lakes Basin by developing climate change information on crucial but under-investigated drivers of coastal processes such as ice cover and large storm events to address key physical knowledge gaps that determine the magnitude of coastal hazards and appropriate adaption responses.

The project was divided into two streams, the first was to simulate future climate change hazards based on historical extreme wind, wave and storm-surge climatologies. The second stream used the results from Stream 1 to complete detailed climate adaptation case studies with conservation authorities, municipalities and stakeholders.

This report summarizes RWDI's contribution to Stream 1, specifically an analysis of future changes in storm frequencies over Lake Erie and Lake Ontario and the collection and preparation of historical and future meteorological input data for wave and surge modelling by Baird. Separate reports will be provided by Baird on their modelling efforts and by Zuzek/Mortsch on the use of the modelling results to inform stakeholders.

4 BACKGROUND AND APPROACH

The part of the project that was performed by RWDI comprised of a frequency analysis and preparatory work for Baird's wave and storm surge modelling. The frequency analysis followed a similar approach as presented in Reuten et al. (2011). The frequency of large wave height events can be affected by changes in synoptic weather patterns or in environmental parameters that affect wave height, even when synoptic weather patterns do not change. For example, future temperatures might be higher under the same synoptic pattern and cause ice-free conditions that permit large wave height events to reach the shoreline when historically, the lake surface was covered with ice.

Several data sets were needed to perform the analyses in this report. Characteristics, sources, and pre-processing of the data are explained in section 4.1.

Figure 1 outlines the approach used to address whether the frequency of storms will change due to climate change impacting know weather patterns. Historical storm data was used to generate a list of the top 100 storms on Lake Erie and Lake Ontario. Historical weather data sets were then used to identify weather patterns for each storm, then synoptic weather typing was performed using k-means clustering and used to characterize large wave height events. Changes in the frequencies of the synoptic weather types for historical and future GCM output provided insights into the changes of large wave height events (section 4.2).

The effect of changes in other environmental parameters on the frequency of large wave height events is covered in section 4.3. Specifically, changes in sea-level pressure (SLP) gradients (Figure 2) and ice cover (Figure 3) across the buoy locations on Lake Erie and Lake Ontario were investigated

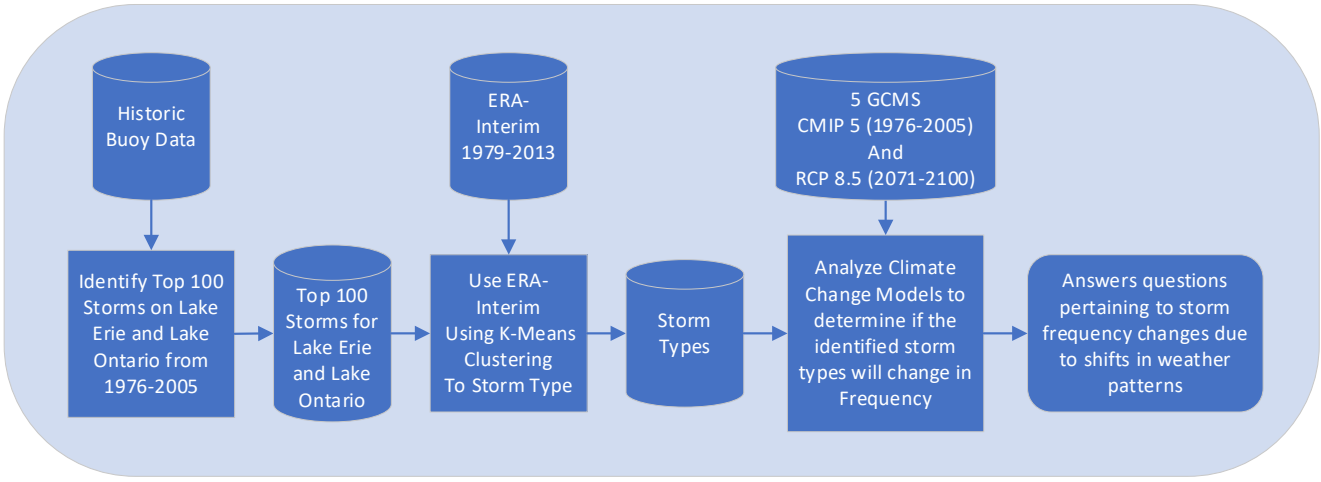

Figure 1: Steps performed to investigate whether shifts in weather patterns impact the frequency of future storm events

Section 4.4 describes the approach taken to prepare input and other relevant information for the wave and storm surge modelling performed by Baird (Figure 4). The objective of the latter work is to estimate how wave heights and storm surge magnitude during large storm events might change in the future.

Finally, section 6 concludes with a summary of caveats and assumptions associated with the approach.

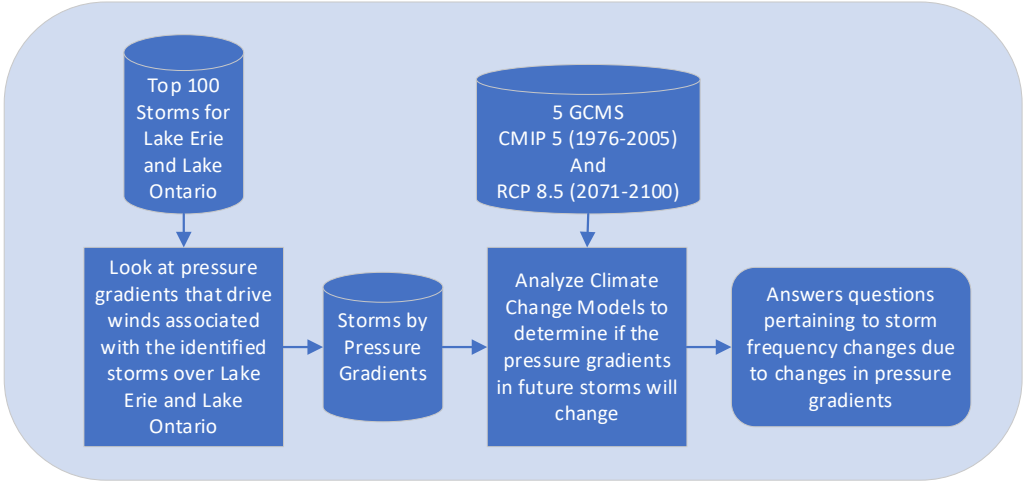

Figure 2: Steps performed to investigate whether pressure gradient changes impact the frequency of future storm events

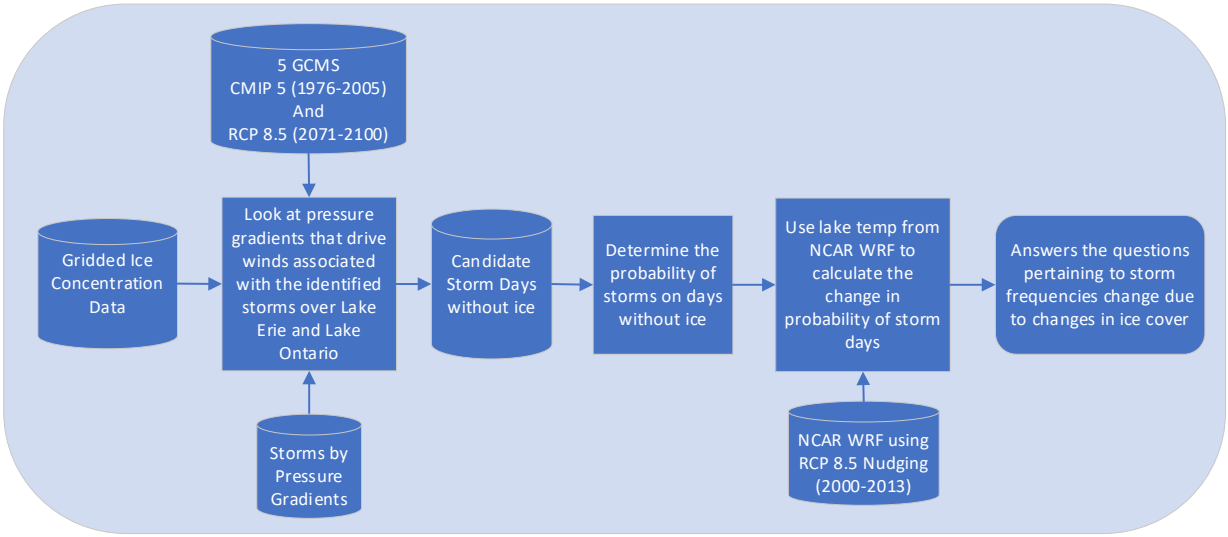

Figure 3: Steps performed to investigate whether ice cover changes impact the frequency of future storm events

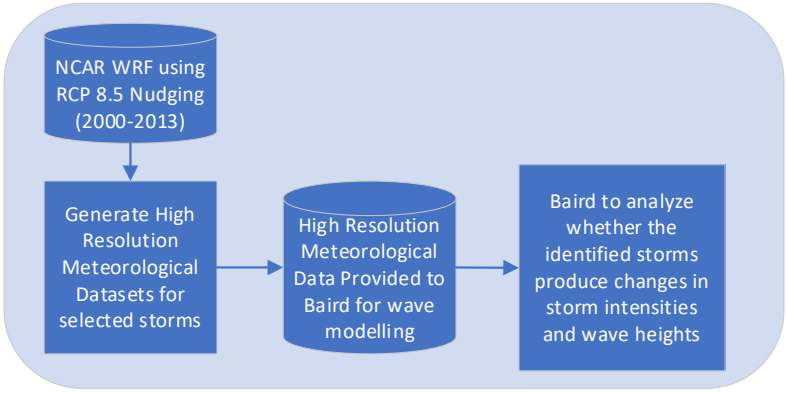

Figure 4: Steps performed to generate high resolution weather data for wave modelling

4.1 Data Used

The analyses performed by RWDI required several data sets. The following subsections explain the characteristics of the data sets, where and how the data were accessed, and the pre-processing steps that were necessary to prepare the data for further analyses.

The frequency analysis required long daily time series (on the order of decades) with a spatial resolution sufficient to resolve synoptic weather fields of sea-level pressure and geopotential height (on the order of hundreds of kilometres). The output from GCMs meets these requirements (section 4.1.1). Ground truthing of GCM output over the historical period was performed against ERA-Interim reanalysis output (4.1.2).

By comparison, the input to Baird's wave modelling required meteorological information for short periods (on the order of days) at higher temporal resolution (on the order of hours) and spatial resolution (on the order of kilometres) since it was event-driven. The National Center for Atmospheric Research (NCAR) Weather Research and Forecasting (WRF) downscaled historical and future 'pseudo global warming' model output was utilized for that purpose (4.1.3).

Wave-height data were required over a sufficiently long historical period of several decades at a temporal resolution on the order of hours and sufficient spatial accuracy on the order of kilometers to meet the requirements of both frequency and strength analyses (4.1.4). Finally, information on ice cover was utilized in the frequency analysis and used to inform the strength analysis (4.1.5).

4.1.1 Global Climate Model Output

Key to the synoptic weather typing approach was to quantify the change in the frequency of synoptic weather types using GCM output for the historical period from 1976 to 2005 to the future period from 2071 to 2100. Within the scope of the study, only one RCP could be considered. The highest RCP considered in the IPCC's Fifth Assessment Report (IPCC, 2013), RCP8.5, was selected to be consistent with the NCAR climate simulations covered in section 4.1.3. Details on the RCPs are available in section 12.3 of IPCC (2013).

At the time when the research reported in Reuten et al. (2011) was performed, the use of only one GCM was a major limitation caused by limited access to GCM output. For this study, more than one GCM was used in order to have a measure of uncertainty associated with changes in the frequency of weather types. All GCM output for this study was part of the Coupled Model Intercomparison Project Phase 5 (CMIP5) and was accessible from the Lawrence Livermore National Laboratory (LLNL) at the web address: https://esgf-node.llnl.gov/search/esgf-llnl/.

Since LLNL is hosting millions of data files, a systematic tree-like search is necessary to narrow down the available data. Repeated searches were necessary until a final set of GCMs was found that met all the requirements. Matching pairs of historical 1976-2005 and future 2071-2100 RCP8.5 GCM output were needed. As a major constraint, 500-hPa geopotential height (GPH), which was used for the weather typing described in section 4.2, is only available on daily time scales. Many search criteria failed to deliver the correct data sets, because naming conventions were not strictly enforced on many search terms. The final search options in the check boxes in the left column of the LLNL website were as follows. For "historical" and the future ("rcp85") period:

1. Project: "CMIP5"
2. Experiment: "historical" for the 1976-2005 period and "rcp85" for the future 2071-2100 period
3. Time frequency: "day"
4. Variable: "zg"

The variable "zg" is GPH. Data sets containing GPH also contain the other variable of interest, SLP, which is denoted as "psl" in the data sets. The search results comprise more than 50 data sets. Many of these are duplicates, repetitions of simulations with somewhat different characteristics, or simulations that are not part of a

matching historical-future pair of data sets. Among the remaining GCM pairs, we were specifically looking for models with the following characteristics:

- Used by NCAR for deriving climate perturbations for the pseudo global warming simulations with WRF
- Highest spatial resolution for the atmospheric component (where different resolutions were available)
- Well-established model that has participated in more than one IPCC cycle
- Sea-ice component

Among the remaining choices, we sought a broad range of modelling centres and host countries. The final set of GCMs, for which daily SLP and GPH were downloaded for the historical 1976-2005 and future 2071-2100 RCP8.5 simulations, is presented in Table 1. All GCMs included a sea-ice component.

Table 1: GCM output used for this study.

Model Name	Modelling Centre	Grid Resolution (Lat x Lon, degrees)
CanESM2	Canadian Centre for Climate Modelling and Analysis	2.79 x 2.81
CMCC-CM	Centro Euro-Mediterraneo per I Cambiamenti Climatici, Italy	0.75 x 0.75
GFDL-CM3	Geophysical Fluid Dynamics Laboratory, USA	2.0 x 2.5
HadGEM-CC	Met Office Hadley Centre, UK	1.2 x 1.875
MRI-CGCM3	Meteorological Research Institute, Japan	1.12 x 1.12

4.1.2 ERA-Interim Reanalysis

ERA-Interim is a global reanalysis from the European Center for Medium Range Weather Forecasts (ECMWF). Reanalysis is effectively forecasted weather for a past period based on historical input, also called 'hindcast'. ERA-Interim provides three-dimensional reanalysis meteorological fields every 6 hours at 0.75°x0.75° resolution for the period from 1979 to 2013.

Sea-level pressure and 500-hPa geopotential height (matching the variables derived from GCM as described above) for the full 1979-2013 were downloaded from the ECMWF data portal at (https://apps.ecmwf.int/datasets/data/interim-full-daily/levtype=sfc/. ERA-Interim is freely available for commercial use for registered ECMWF users.

4.1.3 NCAR High Resolution Climate Simulations

To provide estimates of both the historical and future climate of the Great Lakes, publicly available data derived from high resolution climate simulations over North America conducted by the National Center for Atmospheric Research (NCAR) were used (Liu et al., 2017). The simulations cover most of North America, including all the continental United States and large portions of Canada and Mexico at 4 km spatial resolution. The extents of the NCAR WRF modelling domain are shown in Figure 5.

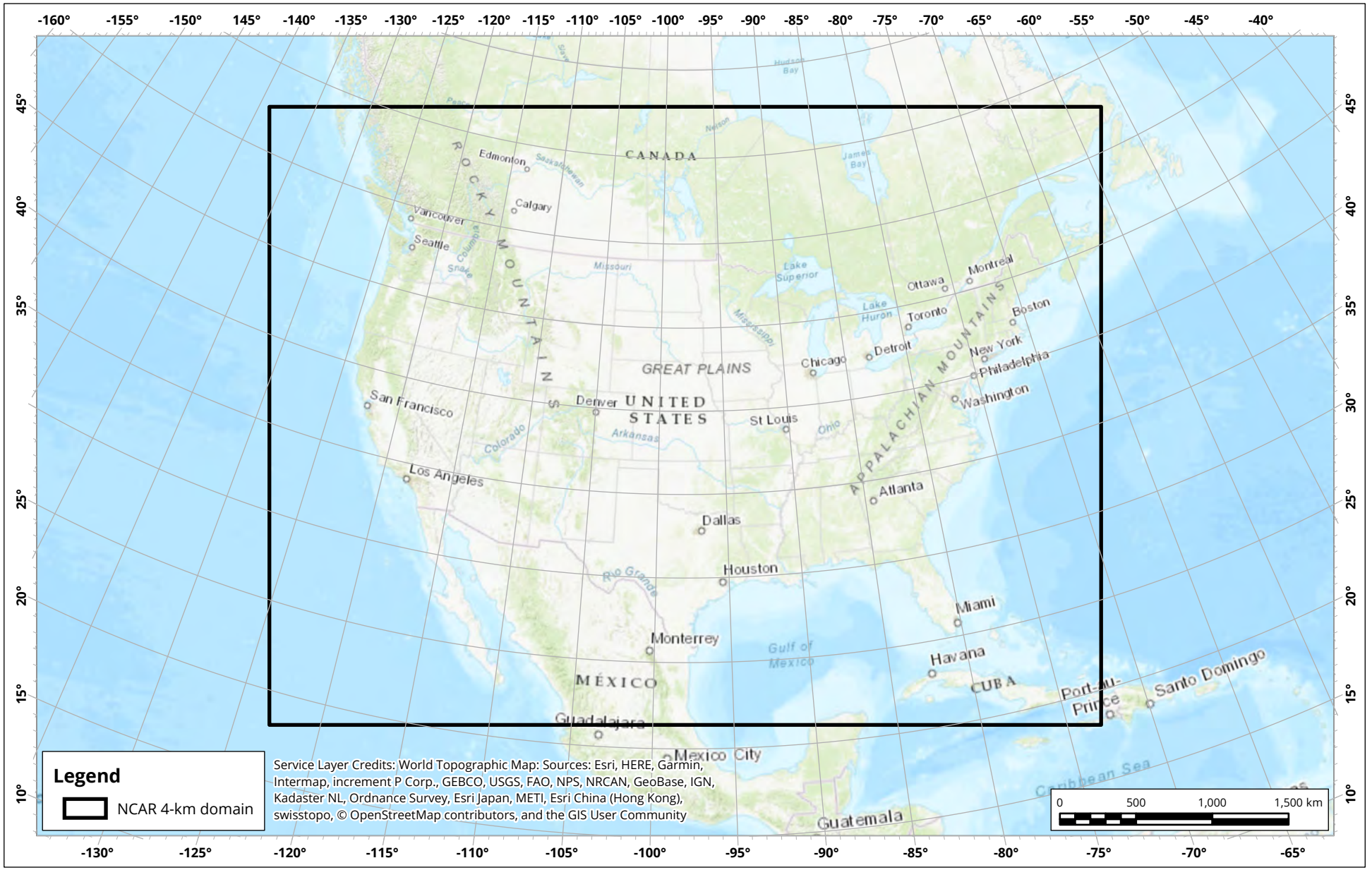

Domain extents of the NCAR 4-km high resolution WRF-based North American climate simulations

True North

Drawn by: DJH | Figure: 5

Approx. Scale: 1:35,000,000

Date Revised: Apr 10, 2019

Map Projection: Canada Lambert Conformal Conic 1

NRCAN Great Lakes Future Wave Climate - Canada

Project #: 1801772

Map Document: F:\2018\1801772 - RJC - NRCAN Great Lakes Future Wave Climate\4. Analysis\99 GIS\1801772_NRCan_Great_Lakes.aprx

The NCAR simulations were applied over a 13-year period from October 1, 2000 to September 30, 2013. These dates include 13 contiguous winter periods. The 13-year period was repeated twice: once for a historical base period and once for a future climate realization.

The boundary conditions for the historical period were derived using the ERA-Interim reanalysis fields described in the previous section.

The future case uses a 'pseudo global warming' (PGW) approach in which the historical period is repeated but with the boundary conditions perturbed by an amount equivalent to the predicted climate change increment. This is an alternative approach to using a future climate GCM simulation to directly provide boundary conditions to a limited area prognostic model as is typically done in a regional climate modelling (RCM) approach. The NCAR WRF essentially is similar to the implementation of an RCM, but in this case the boundary conditions are supplied by a climate-change-perturbed historical reanalysis rather than by a GCM directly.

The advantage of the approach is that the ERA-Interim output is available at higher spatial and temporal resolution than are typically available from GCM outputs. This allows the limited area model regional climate model to be run at a much higher resolution than when GCM output is used directly. In the case of the NCAR simulation, the 4-km resolution allows, for example, for convective processes to be explicitly resolved rather than parametrized as is necessary in GCM simulations and in more coarse resolution RCM applications. The 4-km resolution also allows for better resolution of land-water interfaces and resulting mesoscale thermally and orographically forced flows that may be of importance over the Great Lakes.

The perturbations of the ERA-Interim for the PGW scenario were based on the ensemble average of the RCP8.5 for the CMIP5 experiment for the 2071-2100 period. Thus, the NCAR PGW scenario is approximately equivalent to the climate change increment from the historical 2000-2013 reference period to the end-of-century RCP8.5.

Details of the modeling methodology including model physics options and inputs are provided in Liu .et .al (2017). Of interest to the current study is the revised treatment of inland water bodies in the NCAR WRF simulations. By default, the in-land water temperature in WRF is calculated from an interpolation of the nearest sea surface temperature. In the referenced paper, the authors note that this procedure has been found in other studies to generate water surface temperatures that are too warm in cold seasons in some instances, with Great Salt Lake cited as one notable example. To improve lake surface temperature predictions, Liu et al (2017) developed an alternative algorithm which calculates time-varying lake water temperatures from the diurnal average of surface skin-temperatures of surrounding land surfaces. Thus, as the land surface in the Great Lakes region within the model simulation heat up or cools down, so will the simulated lake surfaces. This process will more accurately approximately the real-world drivers and resulting lake temperature than would assuming the nearest sea-surface temperature as is the default approach.

It should also be noted that authors claim that the revised lake surface algorithm should *reduce* a prior warm bias for lake surface in similar WRF simulations. In other words, the predicted lake surface temperature in the NCAR PGW scenario are *lower* than they would have been using the default WRF model configuration the modelling. This fact should be recalled when considering lake surface temperatures later in this report.

The data were downloaded under free public license from the NCAR Research Data Archive (https://rda.ucar.edu/datasets/ds612.0/). Details of the methodology and results are provided in Rasmussen and Liu (2017).

4.1.4 Wave Heights

The Wave Information Studies (WIS) is a U.S. Army Corps effort to provide high-quality continuous coastal wave hindcast model estimates for at least 20 to 30 years. The current dataset runs from 1979 to 2014 (http://wis.usace.army.mil/hindcasts.html). Hindcast datasets generated on the Great Lakes provide wave information for locations every few kilometres along the shoreline at a water depth of approximately 10 to 20 metres. For Lake Ontario and Lake Erie, the WIS hindcast was developed using the spectral wave model (WAM) and Coastal Forecast System Reanalysis (CFSR) wind fields developed by NCAR. Lake bathymetry was discretized on a spherical 0.02-degree resolution grid, and the model included mean daily ice concentration maps derived from Assel's atlas (https://www.glerl.noaa.gov/data/ice/atlas/). Wave data were extracted at one location near the case study sites on each lake (refer to Figure 6 in section 4.2.1) and used to develop the storm listings for this study.

4.1.5 Ice Cover

Ice coverage on the Great Lakes during the winter months can reduce or entirely suppress wave formation. It is therefore, a key environmental parameter beyond driving parameters such as wind speed and considered in the frequency analysis of large wave height events in section 4.3.

Gridded ice concentration data were obtained through NOAA's Great Lakes Environmental Research Laboratory (https://www.glerl.noaa.gov/data/ice/#historical). An example of an ice chart and a table with additional details, developed by the U.S. National Ice Center and the Canadian Ice Service, are shown in Baird's report. Data were available from 1973 to 2018 and typically had a daily timestep during periods with ice.

4.2 Weather Typing for Lake Ontario and Lake Erie

Climate change may affect the frequency of large wave height events through a shift in the frequency of synoptic weather patterns, because large wave height events are more likely to occur under some weather patterns than others, for instance when large pressure gradients across the water cause strong winds. The steps involved in characterizing changes in the frequency of large wave height events are described in the following subsections.

Section 4.2.1 provides an overview of the physical parameters, the domain size and resolution, and the period and temporal resolution used to characterize synoptic weather patterns.

In a preliminary step in section 4.2.2, the high dimensionality of the synoptic weather fields is reduced through principal component analysis (PCA). Section 4.2.3 describes how k-means clustering was used to assign weather

types to the lower-dimensional representation of the synoptic weather fields. The number of weather types is chosen to optimize the separation between types with low and high probability of large wave height events (4.2.4). Weather typing was first performed on reanalysis output, which represent true historical weather with high fidelity. It was then repeated for GCM output for the same historical period. Section 4.2.5 describes how reanalysis and GCM output were linked before the weather typing was repeated for future GCM output (4.2.5).

4.2.1 Characterization of Synoptic Weather Patterns

In this study, RWDI characterized synoptic weather patterns by spatial fields of SLP and GPH as has been done previously in Reuten et al. (2011) and references therein, such as McKendry (1994). Every daily spatial field was assigned to one of a set of representative weather types following the approach described in the following sections. RWDI tested the weather typing on three different domains as further described in the 'Results and Discussion' section. The final domain size is shown in Figure 6 (from N36° to N51° and W65° to W100°).

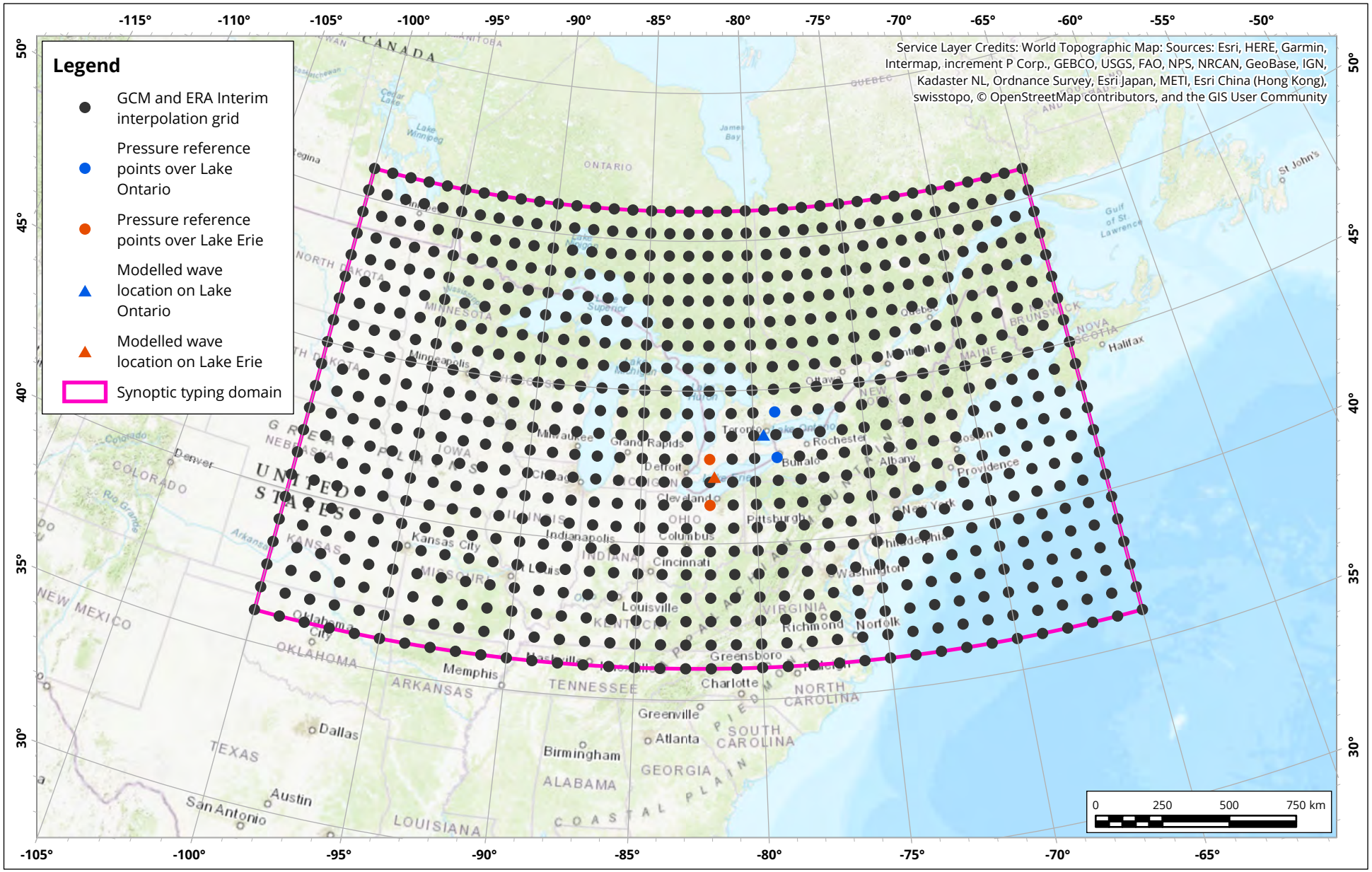

Domain and grid points for synoptic weather typing

True North

Drawn by: DJH | Figure: 6

Approx. Scale: 1:20,000,000

Date Revised: Apr 9, 2019

Map Projection: Canada Lambert Conformal Conic

NRCAN Great Lakes Future Wave Climate - Canada

Project #: 1801772

Map Document: C:\Users\djh\OneDrive - ROWAN WILLIAMS DAVIES & IRWIN INC-\GIS Temp\1801772\1801772_NRCan_Great_Lakes.aprx

Figure 6 also shows the surface location of the 756 grid points to which SLP and GPH were interpolated bi-linearly using the linint2_Wrap function in the NCAR Command Language (NCL) (https://www.ncl.ucar.edu/Document/Functions/Contributed/linint2_Wrap.shtml). The grid points are spaced 0.75° in north-south direction and 1° in east-west direction. That ensures roughly square grids while minimizing information loss in the 0.75° x 0.75° for ERA-Interim. The information loss would mostly affect spatial SLP details caused by complex terrain such as in the lee of the Rockies, which was of little concern. However, near Lake Erie and Lake Ontario, the depth of low-pressure systems would be reduced. GCM output ranged from 1.12° to 2.81° (Table 1), so this fine grid avoids information loss for the highest-resolution GCM.

4.2.2 Principal Component Analysis

The combined spatial field of SLP and GPH has 2 x 756 = 1512 parameters, which are strongly correlated in space. PCA substantially reduced the dimensionality. Every daily synoptic weather pattern was then expressed as a linear combination of eight empirical orthogonal functions (EOFs). An intuitive mathematical analogue is the approximation of points in a two-dimensional plane that lie roughly on a straight line through the origin. Each point requires two coordinates to describe its exact position in the plane. However, every point could be approximated by its distance from the origin. Much of the variability across all the points in the plane would, therefore, be 'explained' by only one coordinate. For example, across all daily ERA-Interim weather patterns during the storm seasons from 1979 to 2013, the selected 8 EOFs explained 94% of the variance.

4.2.3 K-Means Clustering of Historical Weather Patterns

After the dimensionality of the weather patterns was reduced, k-means clustering was carried out in the EOF space. 'Centroids' were determined via least-squares, i.e. as the points in the EOF space that had the lowest sum of the squared distances of all the (dimensionally reduced) synoptic weather patterns from these centroids. Using the same analogy as above, one could determine for example two points on the straight line using least-squares, which in turn are approximations of the points in the plane. This approach is particularly useful when the points tend to cluster within two regions along the straight line.

4.2.4 Isolating Large Wave Height Events

Almost all historical large wave height events between 1979 and 2013 occurred during the 'storm season' from October 2 to April 15. Limiting k-means clustering to the storm season reduced the noise caused by weather patterns that are primarily associated with non-storm conditions over the non-storm season.

The clustering was first performed on ERA-Interim synoptic weather patterns during the storm seasons from 1979 to 2013. For each centroid, the frequency of large wave height events was determined from all synoptic patterns

associated with the centroid. The number of centroids was adjusted to find a good isolation of weather patterns associated with large wave height events from those that had a low frequency of storms.

4.2.5 Future Changes in Large Wave Height Events

The k-mean clustering was repeated for ERA-Interim fields over the period of overlap, 1979-2005, between ERA-Interim (1979-2013) and the historical GCM simulations (1976-2005) to ensure that the slightly shortened period did not alter the results.

Historical GCM simulations do not reproduce actual daily weather patterns but only the statistical occurrence over sufficiently long periods. Therefore, a statistical link had to be established between large wave height events and GCM weather patterns. An independent k-means clustering was performed for all five historical GCM simulations to evaluate if the GCMs produced similar centroids.

In the next step, GCM weather patterns were mapped to the ERA-Interim centroids. Some ERA-Interim centroids were associated with high frequencies of large wave height events, and a future shift in the occurrence of these centroids would be an indication of a shift in the frequency of large wave height events in the future. Therefore, it was important to verify that the GCM simulations reproduced similar centroid frequencies as ERA-Interim.

Finally, those GCMs that showed good agreement with the frequency of centroid occurrences were used to perform k-means clustering on the RCP8.5 2076-2100 GCM output. The change in the frequency of clustering centroids together with the frequency of large wave height events for each centroid provided estimates of changes in future large wave height events as a result of changes in the frequency of weather patterns.

4.3 Changes in Other Environmental Parameters

Reuten et al. (2011) did not find that climate change will cause “significant” changes in the frequency of ozone exceedances in the Lower Fraser Valley due to changes in the frequency of synoptic weather types. The use of only one GCM was a major limitation of the work in Reuten et al. (2011) compared to this study. However, the shift in the frequency of weather types was such that the overall frequency of ozone exceedances showed only a change of a few percent which was deemed insignificant compared to the expected differences across different GCMs. In this study, a better quantification of uncertainty was possible due to the use of several GCMs.

Reuten et al. (2011) amended their analysis by noticing that temperature (and of less relevance, precipitation) could change in the future without the frequency of weather types changing. They concluded that higher temperatures under the same weather types (and assuming the same emissions characteristics) would lead to a substantial increase in exceedances of ambient ozone standards.

A similar extension of the analysis in this study is necessary with respect to two environmental parameters that could change without, or in addition to, changes in weather types: SLP gradients over Lake Erie and Lake Ontario (which cause winds) and ice cover (affected by temperature).

4.3.1 Changes in Sea-Level Pressure Gradients

As a measure of SLP gradients specifically over the two reference points in Figure 6 in section 4.2.1 (the wave locations selected from the U.S. Army Corps WIS modelling), RWDI explored different SLP differences between grid cells near the reference points, including the sign of the SLP differences which determines the wind direction. The two grid cells that were selected over Lake Erie and Lake Ontario are also shown in Figure 6. Large SLP differences between those two grid cell centres over both lakes, independent of their sign and therefore the subsequent wind direction, were shown to be strong predictors of storm events.

Given the differences between ERA-Interim reanalysis and GCMs, in particular a coarser spatial resolution of GCMs, the distribution of SLP differences over the common period from 1979 to 2005 was different between ERA-Interim and the GCMs. Bias correction to SLP differences from GCM output to ERA-Interim were determined following the same approach as in Reuten et al. (2011): Daily SLP differences over the common period were sorted and assigned to bins with equal number of entries, for example the 20 highest SLP differences were assigned to the first bin, the next 20 SLP differences to the second bin, etc. This was done for SLP from the GCM output and the ERA-Interim. The boundaries of the bins for the GCM were then matched with the corresponding boundaries of the ERA-Interim bins. This was repeated for a range of entries per bin to determine how robust the approach is and how much uncertainty is associated with the choice of bin sizes and the bias correction.

Some minor reductions were made to the total number of days entering the binning: The length of a calendar year differs between GCMs, e.g. by neglecting leap years or assuming that every month has 30 days. To ensure that ERA-Interim and all GCMs have the same number of days in the data set and that the total number of days is a multiple of the selected number of entries in each bin, an appropriate number of days with the lowest SLP differences was removed from each data set before the binning was performed.

Once the bias correction was applied, the frequency of storms was equal between corresponding bins for GCMs and ERA-Interim. SLP differences from the future RCP8.5 2071-2100 GCM output were then assigned to the same bin boundaries. Finally, for each bin, changes in the frequency of occurrence of SLP differences were combined with the frequency of storms and tallied up over all bins to determine changes in the overall frequency of storm events.

4.3.2 Changes in Ice Cover

In the historical storm record since 1979, it is apparent that both the number of storms and the number of ice-free winter days has increased. This triggered an investigation if ice cover on Lake Erie or Lake Ontario near the reference points during days with high SLP differences were reducing or entirely suppressing the formation of large waves.

A thorough quantification of lake-ice amount and spatial distribution on the two lakes relative to the reference locations was beyond the scope of this study. Ice cover is sensitive to temperatures integrated over several days and wind speed and direction. However, some threshold behaviours and statistical relationships could be

established and quantified between historical ice cover and associated temperatures that suppressed storms on days with large SLP differences and ice-free days that did not experience storms despite large SLP differences. Projecting the relationship between temperature and ice cover into the future with the GCMs provided statistical changes in the probability of storms at the end of the century under the RCP8.5.

4.4 High-Resolution Input to Wave Modelling

4.4.1 Extract Past and Future Inputs Fields for Wind and Wave Model

To drive storm surge and wave modelling conducted by Baird, 2-dimensional fields of grid relative wind speeds (i.e. U and V wind components) and surface pressure are required. To reduce file size and more easily facilitate data transfer and limit input data required for storm surge and wave analysis, separate subdomains over each of Lake Erie and Lake Ontario were extracted.

The subdomains of the NCAR outputs used for modelling over Lake Erie and Lake Ontario are shown in Figure 7 and Figure 8, respectively.

In addition, to examine potential effects of air-water temperature differences, near surface air temperature and water temperature were extracted as well. The air temperature at 2 meters above ground was used as the near surface air temperature and the sea surface skin temperature was extracted as a proxy for water temperature. Both fields were extracted from the NCAR outputs for the historical and PGW cases over the Erie and Ontario domains in NetCDF format. The resulting data files were transferred to Baird for use in the storm surge and wave modelling.

The dimensions of the Lake Erie subdomain are 111 grid cells (444 km) west-east and 81 grid cells (324 km) or south-north. The Lake Ontario subdomain is 91 grid cells (364 km) west-east and 71 grid cells (284 km) south-north.

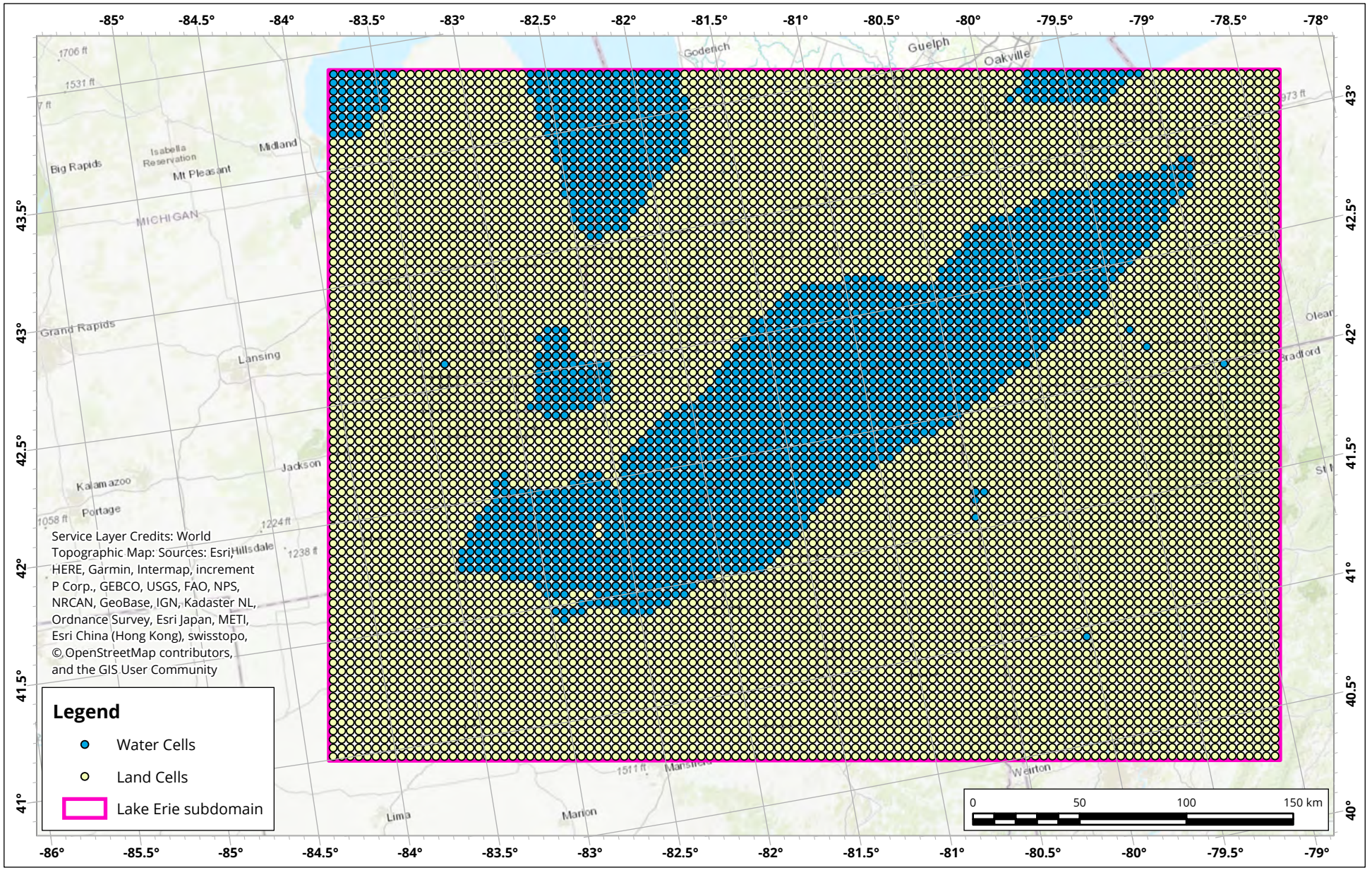

Subdomain of the NCAR WRF extracted for wind and wave modelling of Lake Erie

Map Projection: Canada Lambert Conformal Conic 1

NRCAN Great Lakes Future Wave Climate - Canada

True North

Project #: 1801772

Drawn by: DJH	Figure: 7
Approx. Scale:	1:2,500,000
Date Revised:	Apr 9, 2019

Map Document: C:\Users\djh\OneDrive - ROWAN WILLIAMS DAVIES & IRWIN INC-\GIS Temp\1801772\1801772_NRCan_Great_Lakes.aprx

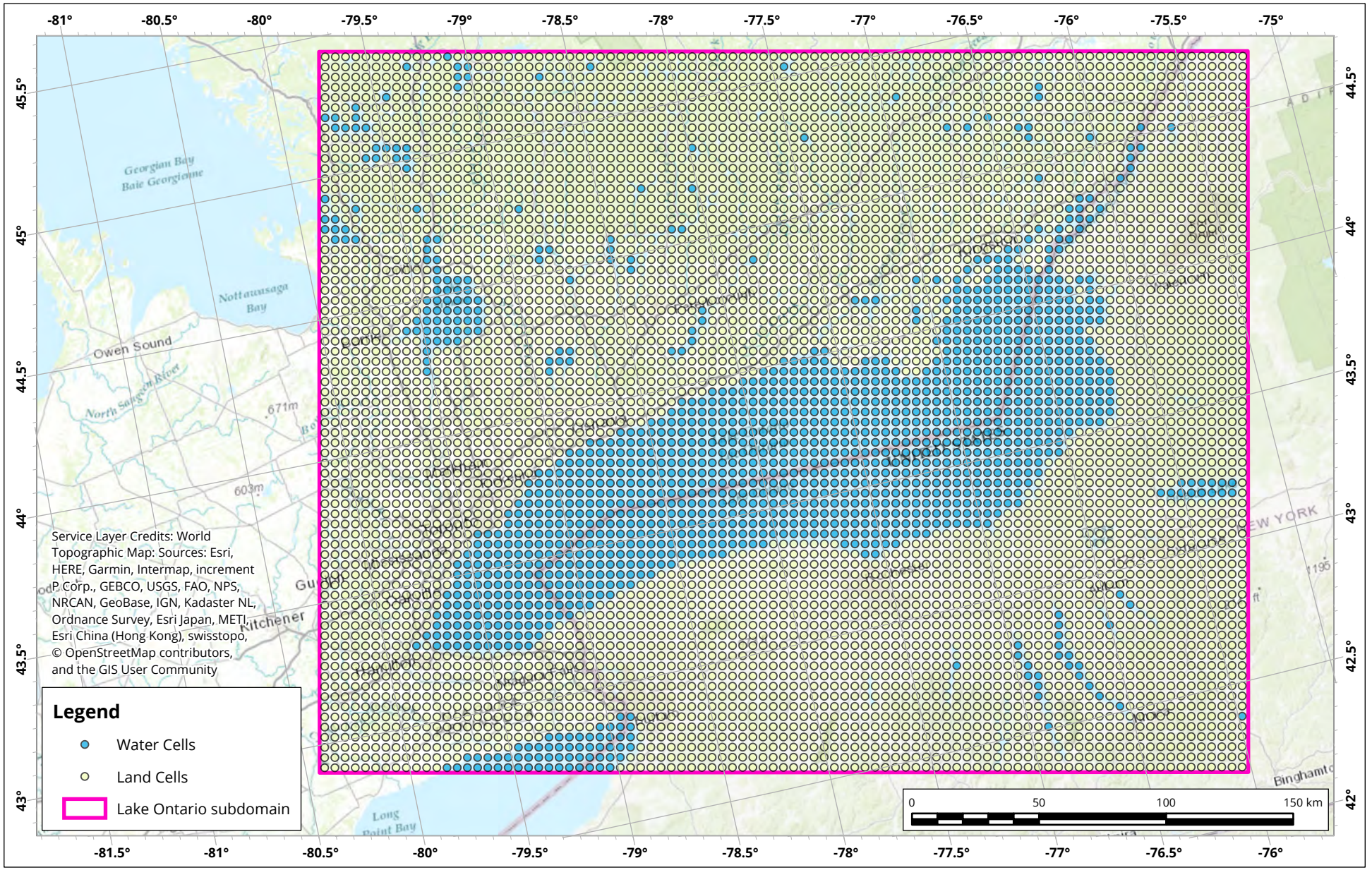

Subdomain of the NCAR WRF extracted for wind and wave modelling of Lake Ontario

Map Projection: Canada Lambert Conformal Conic 1

NRCAN Great Lakes Future Wave Climate - Canada

True North

Project #: 1801772

Drawn by: DJH	Figure: 8
Approx. Scale:	1:2,100,000
Date Revised:	Apr 9, 2019

Map Document: C:\Users\djh\OneDrive - ROWAN WILLIAMS DAVIES & IRWIN INC-\GIS Temp\1801772\1801772_NRCan_Great_Lakes.aprx

4.4.2 Storm Occurrence in Past and Future Simulations

The NCAR WRF simulations are being used to estimate how the strength or intensity of specific storms will change under the impact of future climate change. For this to be tenable, the same set of storms that have been identified in the historical record must also be present in the PGW NCAR WRF simulations.

However, given the PGW method, in which only the model boundary is perturbed and the model interior is allowed to develop restricted only by the model physics, it is possible that the PGW perturbation could result in a climate realization with differing synoptic patterns than the historical case. Therefore, it was critical to the storm analysis to confirm that synoptic patterns are similar in the historic and future case and that each storm that did occur in the historical record has a corresponding perturbed analogue in the PGW case.

To ensure the synoptic patterns in the historic and PGW cases are similar, the surface pressure in the extraction subdomain was spatially averaged over each hour of the 13-year period producing an hourly time series of domain-wide average surface pressure that will be indicator of synoptic systems passing over the region. Plots of the time series for the historic and future cases were then overlaid to examine in the synoptic patterns in the two cases are consistent.

Figure 9 show time series plots of the domain wide surface pressure for the historic and PGW simulations for the 2012-2013 winter period. In the plot the major patterns for both are consistent, with only the peaks and valley of the plots showing slight differences. This confirms that similar synoptic patterns are present in both cases, but the depth of low and strength of high are changed in accordance to the large-scale climate change forcing of the PGW perturbation.

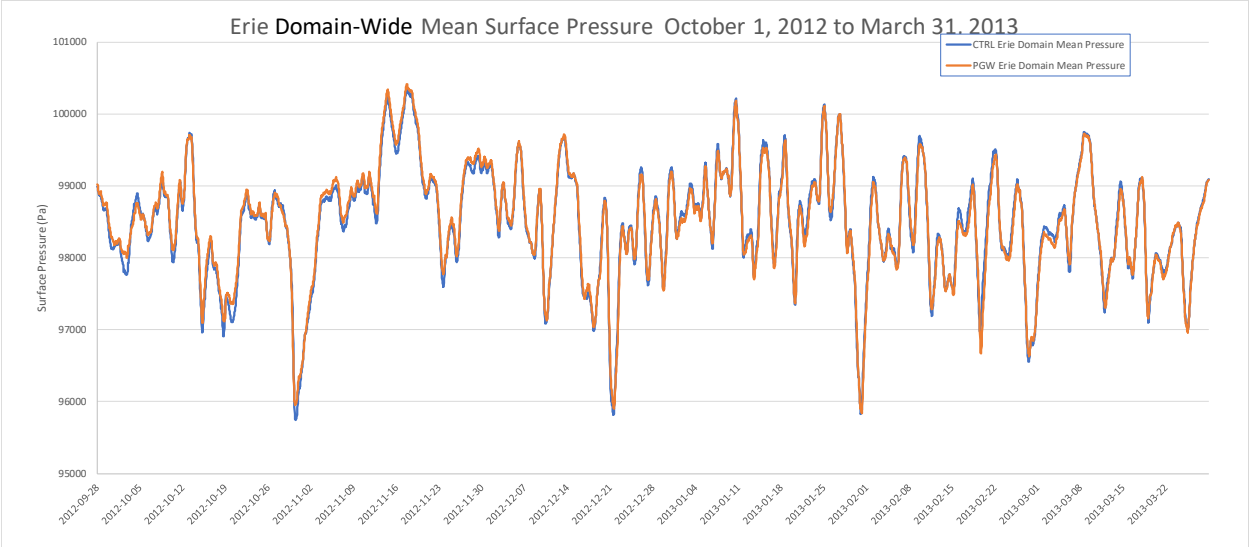

Figure 9: Time series of Lake Erie domain-wide average pressure of the historic and PGW cases for the 2012-2013 winter period.

4.4.3 Changes in Future Ice Cover over Lake Erie and Lake Ontario

Changes ice cover will affect the distance of open water wind fetch and thus affect wave heights. More specifically, reduced ice cover could result in increased open water fetch and increased wave heights, even if overall wind speed is unchanged. Thus, estimates of change in ice cover have a large bearing in determining the affect of future wind on wave heights in the Great Lakes.

However, ice cover is not explicitly available from the NCAR WRF downloads. Instead the sea surface skin temperature (SSTSK) was used as a proxy for prediction of ice cover in the NCAR simulations. Specifically, SSTSK less than or equal to zero was deemed to be indicative of potential ice cover, while SSTSK greater than zero was deemed to most likely be open water.

Model predicted SSTSK was extracted from the NCAR WRF outputs over the Lake Erie and Lake Ontario model domains. For specific storms of interest as identified by the storm surge and wave analysis, hourly snapshots of SSTSK for the historical and PGW cases were extracted. An example over each lake is described in the figures below.

Figure 10 shows a snapshot of hourly NCAR WRF predicted SSTSK during a storm event that occurred January 31, 2011 over Lake Erie alongside the historical ice cover from the NOAA - Great Lakes Environmental Research Laboratory (GLERL) for the same period. The historical ice chart from GLERL (right panel) show Lake Erie almost entirely covered in ice (shading for purple bin, 80% ice cover concentration). The WRF predicted SSTSK (left panel) shows all of the Lake Erie with a surface temperature less than 0° Celsius, which is consistent with a frozen ice surface.

NCAR WRF Predicted SSTSK as proxy for Ice 2011-01-31 Event

Lake Erie WRF Predicted Historical SSTSK

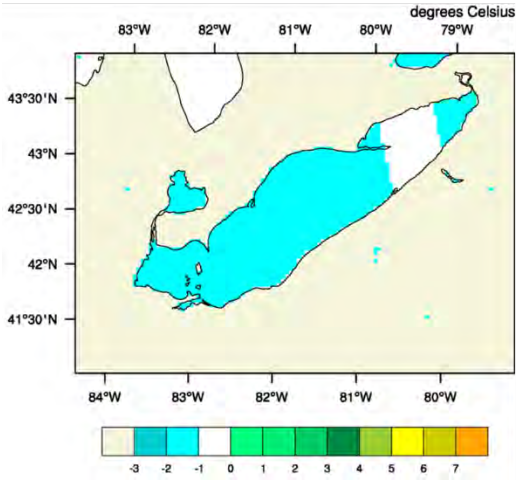

Historical GLERL Ice Chart

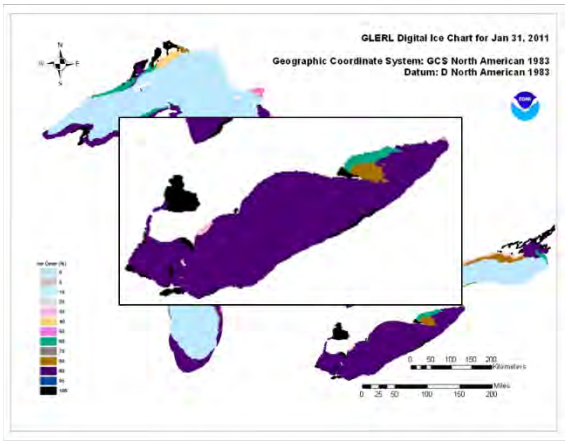

Figure 10: Example of NCAR WRF predicted SSTSK versus GLERL historical ice cover over Lake Erie.

In Figure 11, a snapshot of hourly NCAR WRF predicted SSTSK during a storm event that occurred March 2 of 2007 over Lake Ontario is shown again with the historical ice cover from GLERL alongside. In this case the historical ice chart from GLERL shows Lake Ontario mostly ice free, with notable ice cover only in the eastern portion of the Lake. This time the WRF predicted SSTSK shows most of Lake Erie with temperatures above 0° Celsius consistent with a liquid water surface, with a smaller region of temperature below 0° to the east where the GLERC chart also shows ice. Note that the NCAR WRF does also show a smaller region in the west end as potentially frozen that is not frozen in the historic charts, but overall WRF does predict a mostly open water lake surface consistent with the GLERC chart.

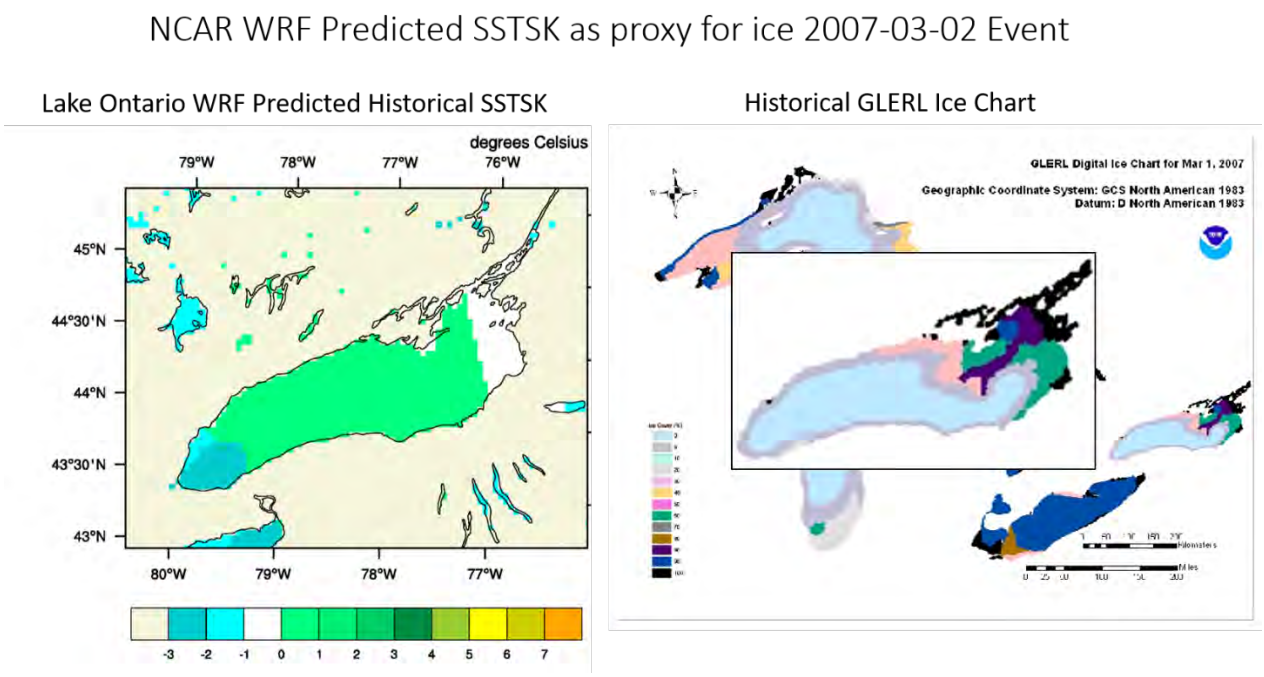

Figure 11: Example of NCAR WRF predicted SSTSK versus GLERL historical ice cover over Lake Ontario.

The two examples above are shown again along side the WRF predicted future SSTSK from the PGW case in Figure 12 and Figure 13. In both examples, the ice and or water surface has warmed several degrees, suggesting that ice cover in the future will be greatly reduced from present day.

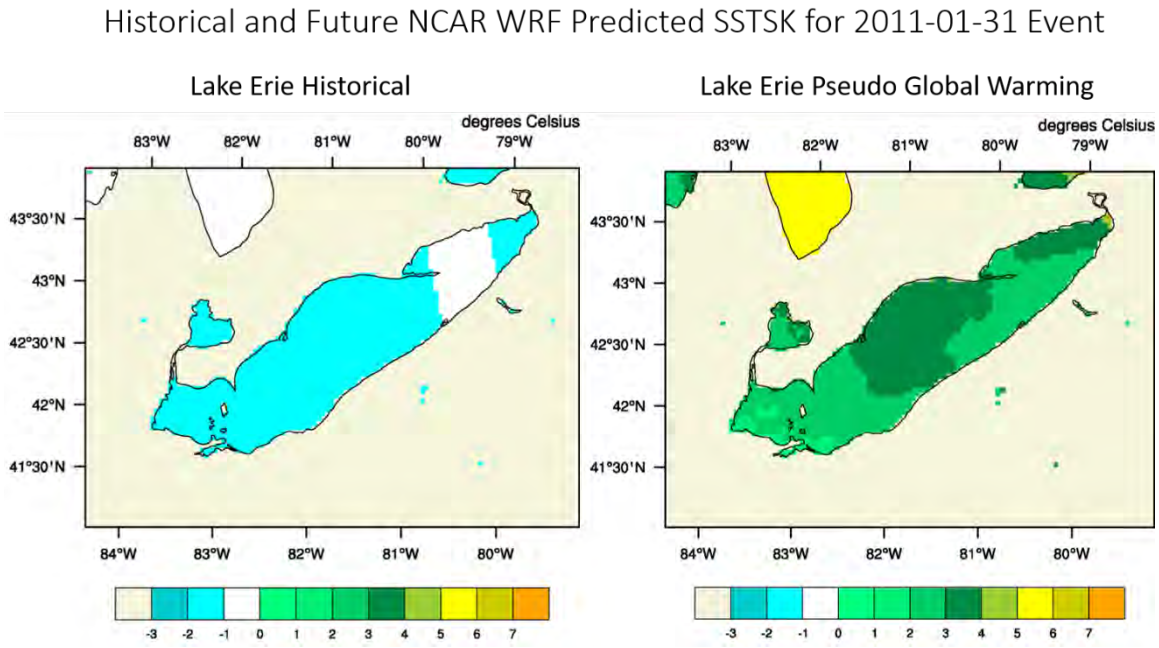

Figure 12: Example of NCAR WRF predicted changes in SSTSK as a proxy for potential changes in ice cover over Lake Erie.

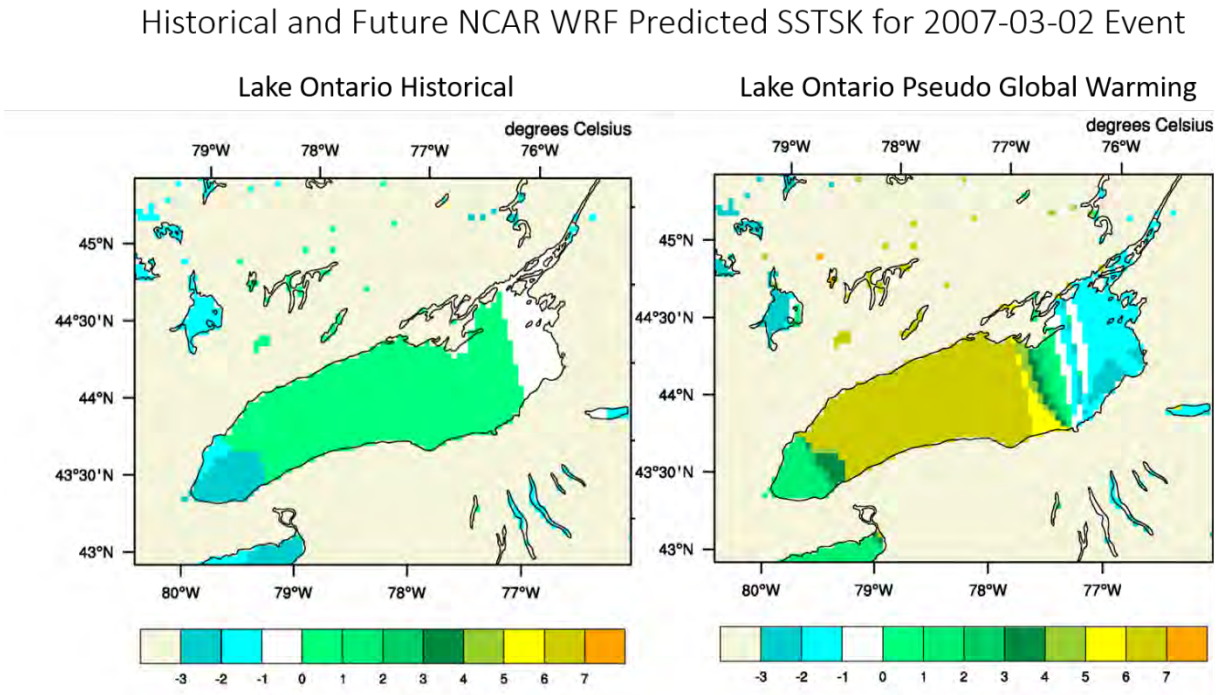

Figure 13: Example of NCAR WRF predicted changes in SSTSK as a proxy for potential changes in ice cover over Lake Ontario.

5 RESULTS AND DISCUSSION

In this section, results on the analysis in frequency changes in future storms on Lake Erie and Lake Ontario are presented and discussed. The results are presented from three independent analyses that considered changes in the frequency of storms as they could arise from: changes in synoptic weather patterns if storms are more likely to occur under some patterns than others (section 5.1); changes in SLP gradients across the lakes, which is the main physical parameter driving the generation of large waves (5.2); and changes in ice cover, for example if ice cover historically suppressed waves under storm conditions (5.3). Details of the analysis performed can be found in the Appendix.

RWDI downloaded and pre-processed high resolution WRF modelling output primarily for two purposes. First, the historical relationship between WRF surface temperatures and ice cover on Lake Erie and Lake Ontario was analyzed and the probability of ice cover under RCP8.5 by the end of the century assessed. These results are included in section 5.3 on changes in ice cover. Second, RWDI provided the required input parameters into the storm surge and wave modelling to Baird, who present their results in a separate report.

5.1 Changes in Synoptic Weather Types

Tables 2 and 3 show the calculated changes in the frequencies of storms over Lake Erie and Lake Ontario, respectively, for a range of storm ranking bins from the top 15, top 30, top 50, and top 100 top storm events. All analyses agree on a small decline of the future frequency of storms over both lakes by roughly 2%. However, the standard deviations across the five GCMs and four storm ranking are of similar size, 2% for Lake Erie and 3% for Lake Ontario.

Table 2: Mean change and its standard deviation (in percent) of the frequency of storms by the end of century under the RCP8.5 scenario based on changes in the frequency of synoptic weather types over Lake Erie.

Storm Ranking	GFDL-CM3	CMCC-CM	CanESM2	MRI-CGCM3	HadGEM2-CC	Mean	Standard Deviation
15	-1.4	-2.1	2.4	-0.8	-3.3	**-1.0**	**2.2**
30	-1.7	-4.2	0.6	-3.4	-3.3	**-2.4**	**1.9**
50	-1.4	-4.2	0.2	-2.8	-2.4	**-2.1**	**1.6**
100	-1.8	-3.6	-0.3	-2.1	-2.2	**-2.0**	**1.2**
Average	-1.6	-3.5	0.7	-2.3	-2.8	**-2**	**2**

Table 3: Mean change and its standard deviation (in percent) of the frequency of storms by the end of century under the RCP8.5 scenario based on changes in the frequency of synoptic weather types over Lake Ontario.

Storm Ranking	GFDL-CM3	CMCC-CM	CanESM2	MRI-CGCM3	HadGEM2-CC	Mean	Standard Deviation
15	3.6	-5.9	1.3	-7.4	1.4	**-1.4**	**4.9**
30	1.4	-3.8	1.3	-5.7	-0.7	**-1.5**	**3.2**
50	1.1	-4.3	0.8	-6.2	-0.6	**-1.9**	**3.2**
100	-0.3	-4	-0.7	-6.9	-0.5	**-2.5**	**2.9**
Average	1.5	-4.5	0.7	-6.6	-0.1	**-2**	**3**

5.2 Changes in SLP Gradients

Table 4 below summarizes the change in the frequency of storms based on future changes of pressure gradients across Lake Erie and Lake Ontario for all five GCMs. A decrease of approximately 8% is predicted for Lake Erie with an uncertainty (standard deviation) of 6%. For Lake Ontario, a lower decrease of 5% is predicted with substantial uncertainty (standard deviation of 12%).

Table 4: Mean change and its standard deviation (in percent) of the frequency of storms until the end of century under the RCP8.5 scenario based on SLP differences over Lake Erie and Lake Ontario.

	GFDL-CM3	CMCC-CM	CanESM2	MRI-CGCM3	HadGEM2-CC	Mean	Standard Deviation
Lake Erie	-3.9	-11.7	-11.8	2.2	-6.4	**-8**	**6**
Lake Ontario	-16.4	-15.0	-4.0	3.4	8.6	**-5**	**12**

5.3 Changes in Ice Cover

Ice cover on the Great Lakes has a potentially very influential role in the frequency and strength of storms. When other driving mechanisms are conducive to large wave height events, the presence of enough ice cover serves as an off-switch. A detailed analysis of historical and future ice cover on Lake Erie and Lake Ontario was beyond the scope of this study. However, acknowledging the potentially important changes to storm frequencies and strengths, a simplified manual analysis of ice cover was performed to provide a high-level assessment of the importance that rising temperatures under RCP8.5 by the end of this century might have for future storm events via reduced ice cover. Details of this analysis are presented in the appendix and the results summarized in Table 5. The simple approach did not provide a measure of uncertainty.

Table 5: Change (in percent) of the frequency of storms due to lack of ice cover on Lake Erie and Lake Ontario by the end of the century under the RCP8.5 scenario.

	Change
Lake Erie	25
Lake Ontario	13

Historically, ice cover has been less frequent on Lake Ontario than on Lake Erie. Therefore, total elimination of ice cover does not increase the number of storms as much over Lake Ontario as over Lake Erie. A more detailed analysis on the role of reduced future ice cover and associated wave energy was completed in the Baird (2019) report.

5.4 Discussion

Table 6 shows the combined results of changes in the frequency of storms over Lake Erie and Lake Ontario by the end of century under the RCP8.5 scenario due to changes in synoptic weather patterns, SLP differences, and ice cover. The true standard deviations are larger, because the estimates in the table do not include the (unknown) uncertainties in the estimated changes due to lack of ice cover.

Table 6: Combined mean change and its standard deviation (StDev (in percent) of the frequency of storms due to changes in synoptic weather patterns, on SLP differences, and lack of ice cover by the end of the century under the RCP8.5 scenario over Lake Erie and Lake Ontario.

	Mean	Standard Deviation
Lake Erie	15	6
Lake Ontario	6	12

The overall balance between the three factors (changes in synoptic weather patterns, SLP differences, and ice cover) is estimated to be an increase of 15% for Lake Erie and 6% for Lake Ontario. The greater increase for Lake Erie is primarily related to more frequent ice coverage than over Lake Ontario during the historical period. It is very likely that both lakes will remain ice free all year by the end of century under the RCP8.5 scenario. The increase in the frequency of storms is therefore greater on Lake Erie than Lake Ontario.

6 ASSUMPTIONS AND LIMITATIONS

This study was limited by several factors such as scope, knowledge gaps, and data availability. This section provides an overview of assumptions and limitations of the study, some leading to future recommendations, which are provided in the next section.

The results presented in this study are based on five GCMs, two more than in the original scope.

RWDI was unable to use 6-hourly weather patterns, because public access to GCM output of 500-hPa GPH was limited to daily time steps. A 6-hourly resolution would likely have improved the matching of storm events with the specific characteristics of synoptic weather patterns, particularly during times of fast-moving weather systems and short storms.

Ideally, an analysis would be performed over a thirty-year historical and future period, but the overlapping periods were shorter, which was a compromise RWDI accepted for the benefit of using a higher-resolution and generally better-performing reanalysis data set compared to alternatives with longer periods. A thirty-year high-resolution WRF simulation for the historical and future period was computationally not feasible for this study and is currently not publicly available.

Consideration of more than just the RCP8.5 would have been desirable. However, the NCAR WRF runs are perturbed by an ensemble of CMIP5 GCMs representing a single realization of the RCP8.5 by the end of the century. The analysis of the frequency of future storms was therefore also limited to the end-of-century period and the RCP8.5 scenario.

The PGW perturbation method does provide a future climate realization with the same synoptic patterns as the historical record. However, there remains a limited possibility that the future reality could provide differing regional climate than is predicted by the GCM or the PGW scenario.

Ice cover was not explicitly included in the NCAR model outputs. The sea surface temperature is a useful proxy, but in reality, the water surface will have greater variance in ice cover around the zero degrees point than is indicated simply by surface temp above or below zero. For example, winds could drive ice cover into the area of interest, or because of lower temperatures on previous days ice could still be present even if sea surface temperatures suggest otherwise. It is expected that using sea surface temperatures as a simple proxy would lead to even more uncertainties.

Some of the limitation associated with the NCAR WRF data set could have been overcome by running WRF specifically for this study. For example, ice cover could have been treated explicitly and extracted from WRF or a range of future climate scenarios been used as boundary conditions. NCAR performed the WRF runs to improve hydrological climate predictions, particularly for convectively driven precipitation. While an emphasis on precipitation requires suitable WRF setup for winter storms, some aspects of the NCAR WRF setup such as ice cover potentially received less attention. Within the computational and other resource limitations of this study, however, RWDI could only have run WRF for individual storm events and would have been unable to scrutinize its WRF runs as much as NCAR.

The k-means clustering approach in this study produced some weather types that appeared familiar to an operational forecaster while others were hard to interpret. However, k-means clustering could still be used to characterize the full range of historical and future weather patterns.

Future GCM output was mapped onto the same weather types as historical GCM output and ERA-Interim. It is possible that future climate generates entirely new weather patterns, which could not be represented well by historical weather types. If any of the five GCMs did indeed produce new weather patterns, the results suggest that they are rather rare events and do not affect averages.

The simple SLP difference (positive and negative), proved exceptionally effective in separating storm events from non-storm days. Alternative criteria were tested and found to be less effective. Since there are effectively unlimited alternative criteria, it is possible that more effective criteria exist, which could have reduced uncertainties.

The ice cover analysis was of a preliminary nature. A longer analysis period than 13 years would have been highly desirable, but that would have required an automated criterion based on WRF output or much more extensive manual processing of ice maps. Uncertainties could have been estimated by repeating other SLP threshold values than 5 hPa and by calculating the impact of future ice losses for different bin sizes similar to the analysis of future changes in SLP differences. Finally, it was conservatively assumed that no ice cover would form on either lake by the end of the century, but the future reduction in ice cover could be smaller.

Lastly, there is inherent uncertainty in GCM's, future ice cover analysis, NCAR WRF and PGW NCAR WRF simulations and any decision or action implemented as a result of this study is and shall be deemed to be the sole and exclusive decision of the party using the information without any involvement of or assistance or guidance provided by RWDI and without any liability on the part of RWDI as hereinbefore provided.

7 CONCLUSIONS AND RECOMMENDATIONS

The main objective of this part of the project was to estimate the future frequency of storm events over Lake Erie and Lake Ontario. The task was broken down into assessing how future changes in synoptic weather patterns, SLP gradients, and ice cover might affect storm frequencies.

At this stage, the results are mostly indicative because of large or unknown uncertainties. Two percent decreases of storm frequencies over both lakes due to changes in synoptic weather were estimated. However, the standard deviations were 2-3% for the estimate change from the five GCMs and the results therefore, are not statistically significantly different from 0. Based on future changes of pressure gradients across Lake Erie and Lake Ontario, frequencies of storms were estimated to decrease by 8% for Lake Erie with a standard deviation in the results from the five GCMs of 6% and by 5% for Lake Ontario with a standard deviation of 12% in the results from the five GCMs. Predicted changes due to reduced ice cover were preliminary and conservative, but large with an estimated increase of 25% over Lake Erie and 13% over Lake Ontario but unknown uncertainty.

The overall balance was that storm conditions will occur less frequently in the future but that reduced ice cover more than offsets the decrease in storm conditions by suppressing far fewer storms. The combined changes in synoptic weather patterns, SLP differences, and ice cover are estimated to increase the frequency of storms by 15% over Lake Erie (standard deviation 6% plus additional uncertainties from changes in ice cover) and 6% for Lake Ontario (standard deviation 12% plus additional uncertainties from changes in ice cover). It is recommended that conservative planning assumes increases in storm frequencies up to 30% over the Lake Erie and Lake Ontario by the end of the century.

Some of the underlying uncertainties and the associated conservatism are inevitable. One large uncertainty is associated with the RCP8.5. An alternative RCP could not be considered within the scope of this study but would be of limited use since the real challenge is the unknown likelihood of the RCP8.5 scenario. On the other hand, several improvements in future studies would likely reduce uncertainties and narrow the broad window of potential future increases in storm frequencies.

The uncertainty of estimated changes in storm frequencies from ice-cover changes could not be determined, which could be the greatest contributor to overall uncertainties. The main recommendation for future work is to perform a thorough ice cover analysis, which would provide the greatest improvement in predictions.

Additional improvements could be achieved by refining the criteria to represent SLP gradients, for example by categorizing the storms based on wind direction and using different criteria for different wind direction categories. This could possibly reduce uncertainties and lead to statistically significant predictions of future storm frequencies.

As the IPCC is working towards their sixth assessment report, next generation (CMIP6) GCM output should become available in the next couple of years, which could reduce uncertainties caused by differences across GCMs.

8 REFERENCES

Baird (2019). Adapting to the Future Storm and Ice Regime in the Great Lakes: Lake Erie and Ontario Nearshore Wave and Surge Modelling.

D. P. Dee, S.M. Uppala, A.J. Simmons, P. Berrisford, P. Poli, S. Kobayashi, U. Andrae, M.A. Balmaseda, G. Balsamo, P. Bauer, P. Bechtold, A.C.M. Beljaars, L. van de Berg, J. Bidlot, N. Bormann, C. Delsol, R. Dragani, M. Fuentes, A.J. Geer, L. Haimberger, S.B. Healy, H. Hersbach, E.V. Hólm, L. Isaksen, P. Kållberg, M. Köhler, M. Matricardi, A.P. McNally, B.M. Monge-Sanz, J.-J. Morcrette, B.-K. Park, C. Peubey, P. de Rosnay, C. Tavolato, J.-N. Thépaut, and F. Vitarta, 2011: The ERA-Interim reanalysis: configuration and performance of the data assimilation system. Quarterly J. Royal Meteor. Soc., 137, 553-597.

IPCC, 2013: Climate Change 2013: The Physical Science Basis. Contribution of Working Group I to the Fifth Assessment Report of the Intergovernmental Panel on Climate Change [Stocker, T.F., D. Qin, G.-K. Plattner, M. Tignor, S.K. Allen, J. Boschung, A. Nauels, Y. Xia, V. Bex, and P.M. Midgley (eds.)]. Cambridge University Press, Cambridge, United Kingdom and New York, NY, USA, 1535 pp.

Liu, C., K. Ikeda, R. Rasmussen, M. Barlage, A.J. Newman, A.F. Prein, F. Chen, L. Chen, M. Clark, A. Dai, J. Dudhia, T. Eidhammer, D. Gochis, E. Gutmann, S. Kurkute, Y. Li, G. Thompson, and D. Yates, 2017: Continental-scale convection-permitting modeling of the current and future climate of North America. Clim. Dyn., 49, 71-95.

McKendry, I.G., 1994: Synoptic circulation and summertime ground-level ozone concentrations in Vancouver, British Columbia. J. Appl. Meteorol., 33, 627-641.

Rasmussen, R., and C. Liu. 2017: High Resolution WRF Simulations of the Current and Future Climate of North America. Research Data Archive at the National Center for Atmospheric Research, Computational and Information Systems Laboratory. https://doi.org/10.5065/D6V40SXP. Accessed 27 March 2019.

Reuten C., B. Ainslie, D.G. Steyn, P.L. Jackson, I. McKendry, 2011: Impact of climate change on ozone pollution in the Lower Fraser Valley, Canada. Atmosphere-Ocean, 50, 42-53.

RWDI aims to accommodate. If you require this document in a different format in order to aid accessibility, please contact the sender of this document, email solutions@rwdi.com or call +1.519.823.13

APPENDIX A – Detailed Methods

APPENDIX A: DETAILED METHODS

A.1 CHANGES IN SYNOPTIC WEATHER TYPES

This section presents the results of intermediate steps and various tests in the weather typing process. In particular, several parameters needed to be chosen to perform the synoptic weather typing, which could possibly alter the results: seasonal constraints; domain boundaries; spatial resolution; temporal resolution; choice of physical parameters; the number of EOFs in the PCA; analysis period and storm rankings; and the number of centroids in the k-means clustering.

A.1.1 Seasonal Constraints

Various records of storms were used throughout the analysis for the different time periods and different number of top storms. None of them contained storms over the summer months. Including these months in the synoptic typing analysis would add noise, without adding any signal (i.e. storm occurrences). It is desirable to try to maximize the signal-to-noise ratio by curtailing the data sets to the fraction of the calendar year that contains most of the storms. The choice was to limit the analysis to a 'storm season' from Oct. 2 to April 15 every year (including leap years). That removed a few occurrences of the top 100 storms over either lake but did not remove any of the strongest ten to twenty storms.

A.1.2 Domain Boundaries

Synoptic weather typing is relatively robust against variations in domain boundary. Distributions of SLP and GPH outside of the domain are not captured in the weather types. If the weather-typing domain is too small, differences of SLP and GPH outside of the domain could, for example, affect the persistence of a low-pressure system over the Great Lakes and therefore the time permitted for high waves to build up. If the domain is chosen too large, SLP and GPH characteristics are captured within the domain boundaries that have no noticeable impact on the weather over the Great Lakes, thereby creating redundancies in the weather types.

We performed the first typing exercises on a conservatively large weather-typing domain (from 30°N to 64N° and 60°W to 120°W) and then in two steps reduced the typing domain (from 36°N to 51°N and 65°W to 100°W). For the two larger domains, some weather types differed near the domain boundaries but not over the Great Lakes. For the smallest domain size (from 36°N to 51°N and 65°W to 100°W) different weather types were associated with different weather pattern over the Great Lakes, as desired. The robustness of the result was confirmed in an additional test run with an even smaller typing domain, which showed practically the same centroid patterns within the smaller domain boundaries in both small and final typing domain.

A.1.3 Spatial Resolution

The synoptic weather typing via PCA and k-means clustering required a common grid across ERA-Interim and all five GCMs. Three different spatial resolutions were tested, from the highest resolution of ERA-Interim at 0.75° (in latitude and longitude) to the coarsest GCM output at 2.81°. The test showed that it was most desirable to capitalize on the high spatial resolution of ERA-Interim, which allows to establish strong statistical relationships between historical storm occurrences and associated synoptic weather patterns. As a minor modification, the final grid was spaced at 0.75° in latitudes and 1° in longitudes, which resulted in more square grid cells and therefore, in a similar spatial resolution in north-south and east-west direction.

A.1.4 Temporal Resolution

Originally, an improvement over the study reported by Reuten et al. (2011) was planned by increasing the temporal resolution from daily to 6-hourly, but for GCM output, 6-hourly output of GPH was unavailable. A 6-hourly resolution would likely have improved the matching of storm events with the specific characteristics of synoptic weather patterns, particularly during times of fast-moving weather systems and short storms. This compromise likely increased uncertainties in the statistical analyses but was inevitable since the use of GPH was necessary.

A.1.5 Choice of Physical Parameters

The choice of SLP and GPH followed recommendations and common practice in other studies such as McKendry (1994). As in Reuten et al. (2011), PCA and k-means clustering are applied to the standardized and equally weighted SLP and GPH field. Standardization is commonly applied in statistics to non-dimensionalize physical parameters, put different parameters on a similar scale, and avoid numerical issues: For each parameter at each grid point, the temporal mean over all daily parameter values over the entire period is subtracted; then, the result is divided by the standard deviation. After this process, the standardized data have a mean of 0 and a standard deviation of 1. Finally, the results are corrected for the increased spatial resolution at higher latitudes. That effectively puts SLP and GPH on equal footing at every grid point.

A.1.6 Number of Empirical Orthogonal Functions

SLP and GPH are strongly correlated in space, i.e. both parameters change in small increments over short distances. For example, when SLP is much higher than the temporal average at one location, SLP at nearby grid cells will also be higher than the average. While there are 1,512 parameter values in the combined spatial field of SLP and GPH, they do not vary independently of each other. Therefore, representation of most of the spatial detail of the SLP and GPH field on any given day requires substantially less points in space.

PCA is a commonly applied approach to represent a desired level of detail by a substantially reduced set of parameters, the EOFs. We performed PCA over a range from two to twenty EOFs and found that the output of the k-means clustering was no longer substantially affected by the choice of EOFs for more than approximately six EOFs. To err on the conservative side, eight EOFs were retained.

A.1.7 Analysis Period and Storm Rankings

The analysis period varied depending on the purposes. The full ERA-Interim data from 1979 to 2013 provided the richest data set for k-means clustering and association of storms with weather types. For the investigation of the changes from historical to future GCM weather types and the implied changes in storm frequencies, the historical period was limited to the overlapping period between ERA-Interim and historical GCM runs, i.e. from 1979 to 2005. Finally, for selecting storms of interest for Baird's wave modelling, the period was limited to the WRF period from 2000-10-01 to 2013-09-30.

Each of the three analysis periods required its own list of ranked storms, which effectively defined a wave-height threshold for storm events. To test the robustness of conclusions against the choice of threshold, all analyses were repeated for the 15, 30, 50, and 100 highest-ranked storms for each of the three historical periods. For a very small number of top events, derived statistics are more sensitive to minor changes in the threshold. For a very large number, weaker storms are included which tend to be more ubiquitous across a broader range of weather types and are of less relevance to the overall purpose of this study. As with other parameter choices, the conclusions were robust over a wide range of storm thresholds and over all three analysis periods.

A.1.8 Association of Storms with Synoptic Weather Types

The number of cluster centroids in k-means clustering can be a critical choice, particularly if data is clearly clustering in space. For example, if there was a clear underlying mechanism for data to cluster around three centroids, choosing two centroids or four centroids would lead to wrong conclusions with respect to the underlying mechanism. It is particularly difficult to infer the correct number of centroids if the data contain substantial noise and are represented in more than two dimensions and therefore, difficult to visualize.

Figure A.1 shows the distribution of weather patterns and their relationship to the centroids produced by the k-means clustering in the two-dimensional space of only two EOFs. This is an oversimplification of the complexity in the spatial SLP and GPH patterns, for which we used eight EOF to capture important day-to-day variability. However, if there was substantial spatial clustering in eight dimensions at least some spatial heterogeneities would be expected from a projection of the eight-dimensional EOF space to the two dimensions in Figure A.1. That, however, is not the case. The two frequency distributions in the middle and right panels of Figure A.1 show the 'marginal' distributions of weather patterns in each dimension. They are calculated by summing, for each EOF, over the other EOF. Both distributions are approximately normal with no noticeable structure. Furthermore, the rather regular distribution of cluster centroids over the 2-dimensional plane in the left panel of Figure A.1 suggests that the centroids are simply a least-squares fit to a two-dimensional normal distribution. The marginal distributions, which were also calculated for each of the eight EOFs that were retained for this study, are approximately normal as well (not shown).

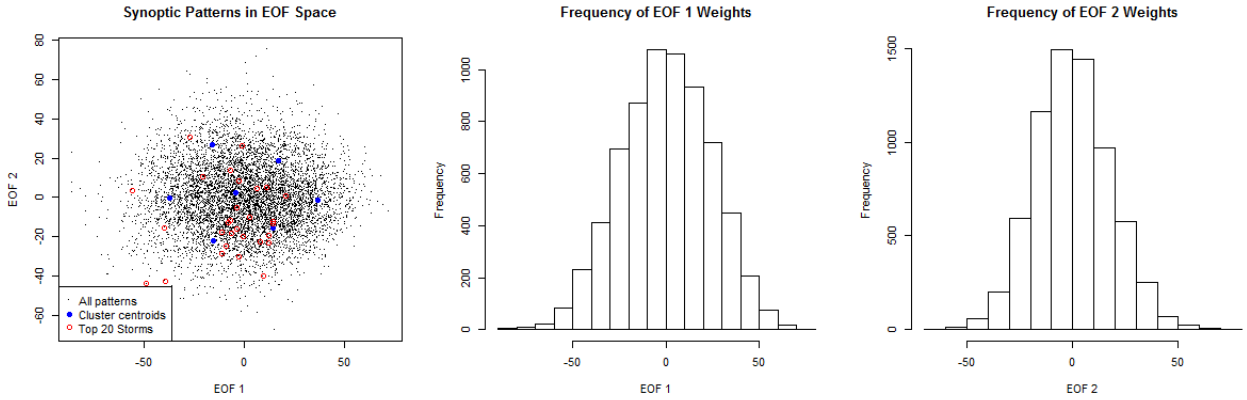

Figure A.1: Left: Distribution of synoptic weather patterns from ERA-Interim over the period from 1979 to 2013 in two-dimensional EOF space; locations of eight cluster centroids determined with k-means clustering; and locations of the weather patterns associated with the top 20 storms. Middle and right: Marginal frequency distributions of the synoptic weather patterns in the two EOF dimensions.

The physical explanation for a lack of clustering of the weather patterns is that winter weather in the region encompassing the Great Lakes is transient in both space and time and does not repeatedly lock into specific weather patterns for durations substantially exceeding one day.

In the absence of any apparent clustering of the weather pattern, the main criterion for choosing the number of cluster centroids is that storms stratify well across different clusters of weather patterns, i.e. that there is a large difference in storm frequencies between different clusters. Such stratification ensures that a shift in the cluster frequencies in the future could predict changes in the occurrence of storms. In this study, the top 20 storms tend to occur more frequently near some centroids than others. This can be seen by visual inspection in the left panel of Figure A.1 for only two EOFs.

To quantify the stratification, note that each daily weather pattern, including those associated with storms, belongs to one of the centroids. For each centroid, the ratio of the number of storm events and the total number of weather patterns is the storm frequency associated with that centroid. Figure A.2 shows results using eight EOFs to represent each daily weather pattern and associating the patterns with seven cluster centroids. The first seven panels show the weather patterns associated with each cluster centroid. To an operational weather forecaster, the seven weather types look sufficiently distinct and plausible, but they are primarily mathematical constructs that cannot be obviously associated with storm or non-storm weather patterns.

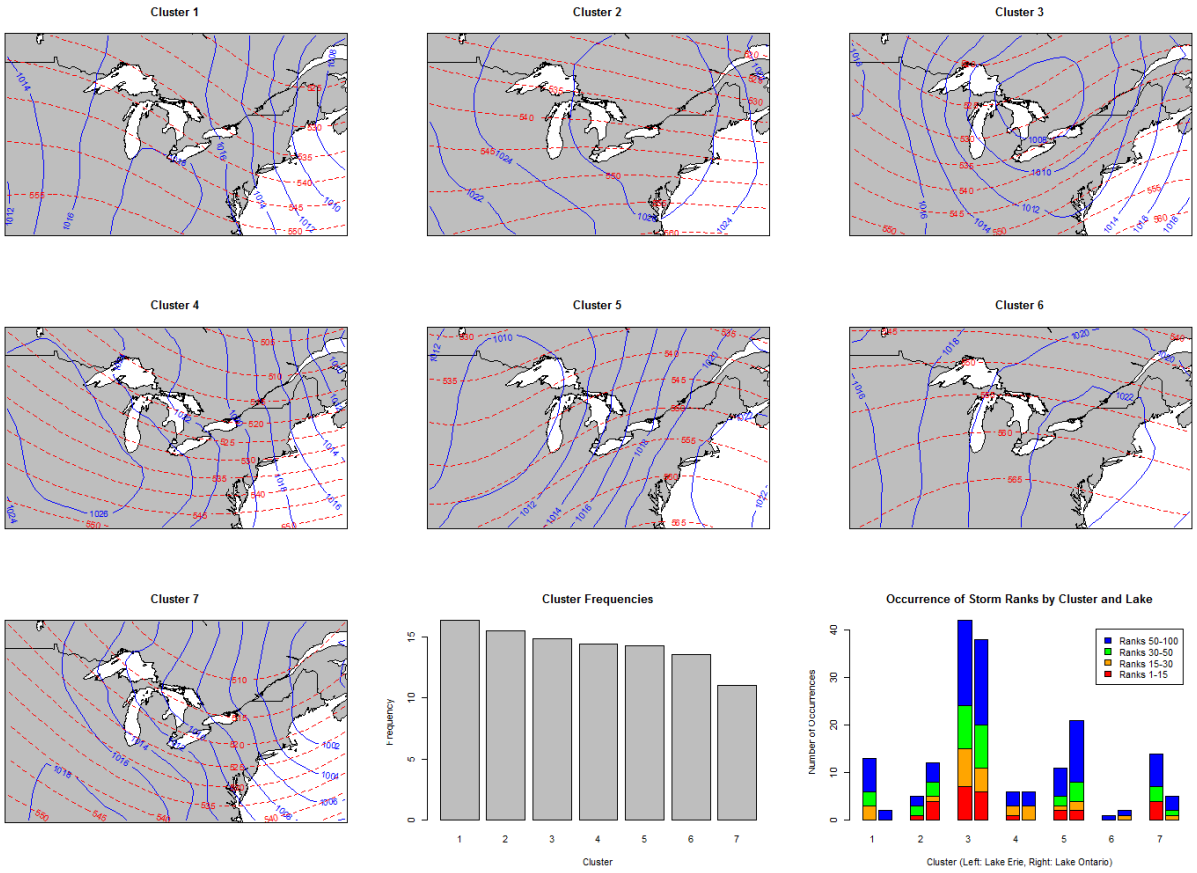

Figure A.2: (From left to right and top to bottom.) First seven panels as labelled: ERA-Interim synoptic weather types associated with seven cluster centroids in the k-means clustering based on daily SLP and GPH over the period from 1979 to 2005; blue solid contours are SLP with labels in units of hPa; red dashed contours are 500-hPa GPH in units of dm (decametres or 10 metres). Centre bottom: Cluster frequencies (percentage of synoptic weather types in each cluster) for the seven weather types. Right bottom: Number of storms associated with each cluster stacked by ranks as labelled for Lake Erie and Lake Ontario (left and right stacked columns in each pair, respectively).

The centre bottom panel in Figure A.2 shows the 'cluster frequencies' (percentage of weather types in each cluster) corresponding to the seven cluster centroids. The bottom right panel shows the number of storms associated with each cluster from the lists of strongest 15, 30, 50, and 100 storms over Lake Erie and Lake Ontario over the 1979-2005 period. While the cluster frequencies are relatively similar, storms occur preferentially in a subset of clusters. The stratification for the 15 highest-ranked storms (red) is clearer than for the lowest-ranked storms (blue). The lowest-ranked storms tend to occur more evenly spread across all seven clusters and for both lakes. In contrast, the 15 top storms over Lake Ontario all occurred during synoptic weather conditions associated with clusters 2, 3, and 4. If the same centroids are used to assess the historical and future GCM output, a shift in the frequency of patterns associated with each centroid from historical to future GCM output can be used to calculate the change in the total number of storm events. For example, over Lake Ontario a future shift in the frequency of clusters for example from clusters 1, 5, 6, and 7 to clusters 2, 3, and 4 would imply an increase in the frequency of the 15 top storms. For Lake Erie, the vast majority of the top 15 storms occurred under synoptic weather patterns associated with centroids 2 and 7.

A.1.9 Synoptic Weather Typing of Historical GCM Output

Synoptic typing was repeated for output from each of the five GCMs over the 1979-2005 period. For each GCM, a PCA was performed on the daily SLP and GPH fields; eight EOFs were retained; and k-mean clustering was performed for five to nine cluster centroids. The agreement between ERA-Interim and GCM weather types was assessed qualitatively. Given the substantially lower resolution of GCM output compared to ERA-Interim, the depth of low-pressure systems might not be fully captured in GCM output. However, for a GCM output to be considered an acceptable representation of historical weather patterns we required the distributions of high- and low-pressure systems to be more similar between matching pair of GCM output and ERA-Interim than between any pairs of weather types.

Figure A.3 shows the synoptic typing results for GFDL-CM3 output for 1979-2005. This can be compared with Figure A.2 above. Clusters agree well qualitatively between Figures A.3 and A.2, when the following clusters are compared between Figure A.3 and Figure A.2: 1 to 1, 2 to 4, 3 to 5, 4 to 3, 5 to 2, 6 to 6, and 7 to 7.

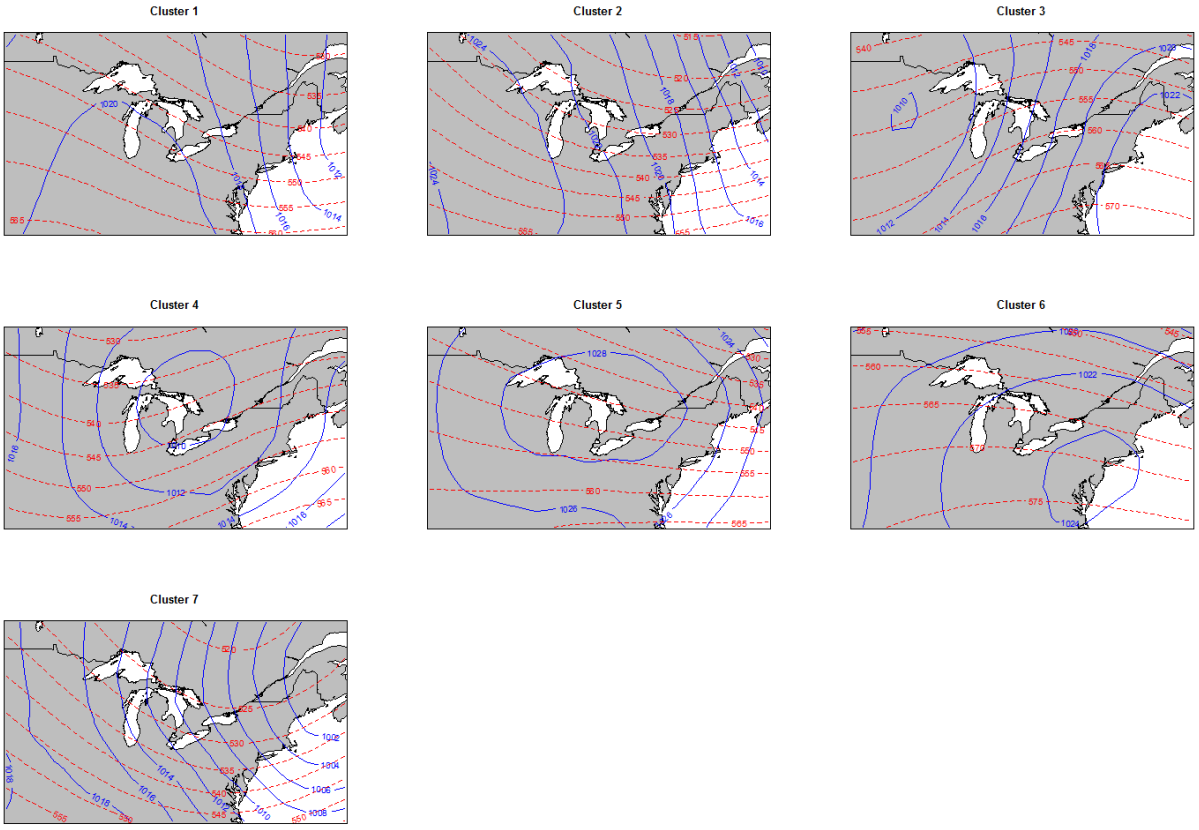

Figure A.3: GFDL-CM3 synoptic weather types associated with seven cluster centroids in the k-means clustering based on daily SLP and GPH over the period from 1979 to 2005. Blue solid contours are SLP with labels in units of hPa; red dashed contours are 500-hPa GPH in units of dm (decametres or 10 metres).

Weather typing for GFDL-CM3 (resolution: 2.0° latitude by 2.5° longitude), CMCC-CM3 (0.75° x 0.75°), and CanESM2 (2.79° x 2.81°) showed very good agreement with ERA-Interim. For MRI-CGCM3 (1.12° x 1.12°), the weather types could be matched with ERA-Interim, although not all patterns agreed well. Finally, for HadGEM-CC (1.2° x 1.875°), the weather types could not be matched with ERA-Interim. The three best performing GCMs span the full range of grid resolutions across the five GCMs. Hence, grid resolution is unlikely responsible for the difference in synoptic weather typing between the GCMs.

Based on this analysis, at least three of the five GCMs were considered suitable for the subsequent steps. In line with previous IPCC assessments, it was decided to continue the analysis with all five GCMs (and to not apply any weighting between the GCMs based on the analysis above) to use the variation across several models as a substitute for model uncertainty.

A.1.10 Future Changes in Storm Frequencies based on Weather Types

In the next step, the 1979-2005 ERA-Interim weather types were used as a common baseline. 1979-2005 GCM daily weather patterns were matched with their closest ERA-Interim weather types (based on squared distances in EOF space) to determine historical cluster frequencies. This was followed by the same analysis for future GCM output, i.e. the RCP8.5 2071-2100 daily SLP and GPH fields for each of the five GCMs were matched with the historical ERA-Interim weather types to determine future cluster frequencies. Each ERA-Interim weather type has an associated frequency of storms such as shown in Figure A.2 above. In the final step, the cluster frequencies and total number of storm occurrence were calculated for each GCM for the historical and the future period and the relative change in storm frequency estimated. These three steps were repeated for five to nine cluster centroids which confirmed that the conclusions are independent of the choice of seven clusters.

Full quantitative results for seven clusters for Lake Erie and Lake Ontario are presented in the main body of the report in Tables 2 and 3, respectively. Cluster frequencies of the seven ERA-Interim clusters are shown in the left top panel in Figure A.4. The cluster results for the five GCMs are shown in the remaining five panels in Figure A.4 sorted by decreasing qualitative agreement of their weather types with those from ERA-interim (from left to right and top to bottom). In the pairs of bars for the GCMs, the left bars show cluster frequencies for the historical period (1979-2005) and the right bars for the future period (2071-2100).

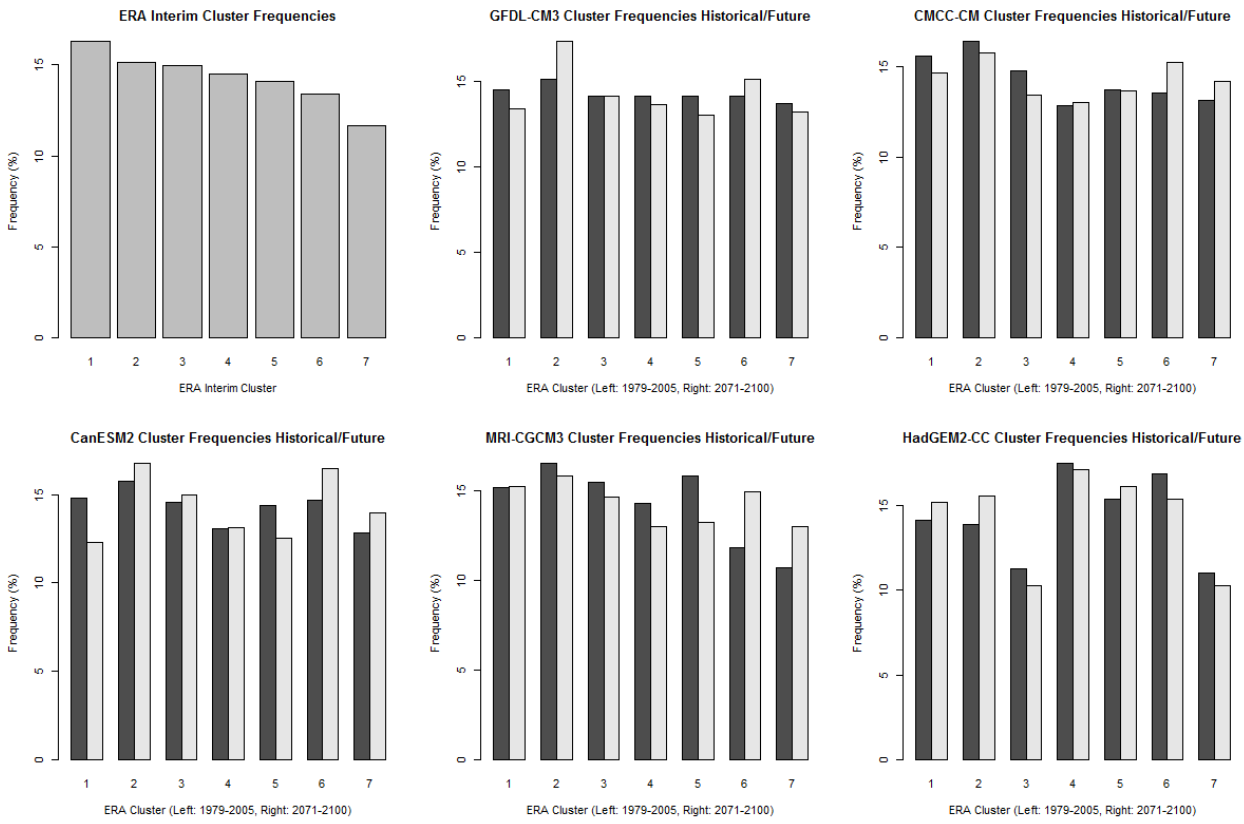

Figure A.4: Cluster frequencies of daily synoptic weather types for ERA-Interim for 1979-2005 (top left) and for five GCMs for 1979-2005 (left dark grey bars) and 2071-2100 (right light grey bars).

With decreasing agreement of weather types between the historical GCM output and ERA-Interim, the cluster frequencies of the GCMs shown in Figure A.4 also tend to deviate more from ERA-Interim. Visually, it is difficult to infer systematic changes from historical to future GCM output across all five models, and the quantitative results presented in the main body of this report showed only small decreases across all five GCMs.

A.2 CHANGES IN SLP GRADIENTS

It is plausible that SLP gradients over the Great Lakes change in the future without substantial changes in synoptic weather patterns. Several criteria were investigated to quantify SLP gradients near the two modelled wave locations over Lake Erie and Lake Ontario. One set of criteria involved statistics such as standard deviation and the maximum range of SLPs over a small grid of grid cells covering each lake. The second set considered the SLP difference between different pairs of reference points near the modelled wave locations, which also permitted directional considerations. For example, for a pair of reference points, winds blow approximately counterclockwise around the point with the lower SLP.

These criteria were applied to daily SLP fields from ERA-Interim over the period from 1979 to 2005. The 100 highest ranked storm events for the period 1979-2005 were then binned according to their associated SLP metrics. Histograms were generated for the number of weather patterns within each bin, the number of storms in each bin, and the ratio of those two as a measure of probability of storms for each bin. The best separation between bins was achieved with the SLP difference between two reference points north and south of each lake near the modelled wave locations (see Figure 2).

After the criteria were established, two refinements following Reuten et al. (2011) were applied. First, the binning was performed with a constant number of weather patterns per bin resulting in variable bin widths. This ensured equal uncertainties between bins. Since the choice of bin boundaries can affect the results, the analysis was repeated for 50 to 200 weather patterns per bin and the results presented as the mean and standard deviation (as a measure of the noise in the statistics) across the range of weather patterns per bin. Second, the total number of weather patterns across the storm season for the period from 1979 to 2005 exceeded 5000 with most weather patterns being associated with weak SLP differences and low probabilities of storms. To reduce the noise in the statistics, only a subset of the greatest absolute SLP differences was retained. Among retaining the top 500, 1000, 2000, and 5000 SLP differences, 2000 produced the lowest standard deviations.

The histograms for GCM output over the 1979-2005 period differ from ERA-Interim histograms and required a bias correction before storm occurrences could be matched with historical GCM output. For each number of weather patterns per bin, the bin boundaries were matched. For example, for 130 weather patterns per bin, the bin boundaries for the 130 highest SLP differences from GCM output were matched with the bin boundaries of the 130 highest SLP differences from ERA-Interim, and the associated storm probabilities were applied to the GCM output. The future GCM output was then binned within the same historical GCM bin boundaries. If the future number of weather patterns in that bin for example increases from 130 to 140 weather patterns the occurrence of storms from that bin increases by a factor of 140/130. To ensure equal statistical properties between historical and future GCM output, the first three years of the 2071-2100 end-of-century data set were removed to have the same number of years as the historical 1979-2005 period.

The top row in Figure A.5 shows the storm probabilities for 1979-2005 ERA-Interim weather patterns as a function of the SLP differences between the northerly and southerly reference points over Lake Erie and Lake Ontario shown in Figure 2. These histograms were generated for 130 daily patterns per bin for the 1950 highest SLP differences (the largest number below 2000 that is dividable by 130) for a total of 15 bins. Storm probabilities were normalized to sum to 1 across all bins. Note that the histograms for the GCM output over the same 1979-2005 are identical to the ones shown after applying the bias correction. The bottom row shows the predicted changes from the GFDL-CM3 model output for RCP8.5 for the period from 2074 to 2100 (after the bias correction was applied to the bin boundaries). Note that the bin boundaries are equal between historical and future histograms but that the vertical axes differ slightly.

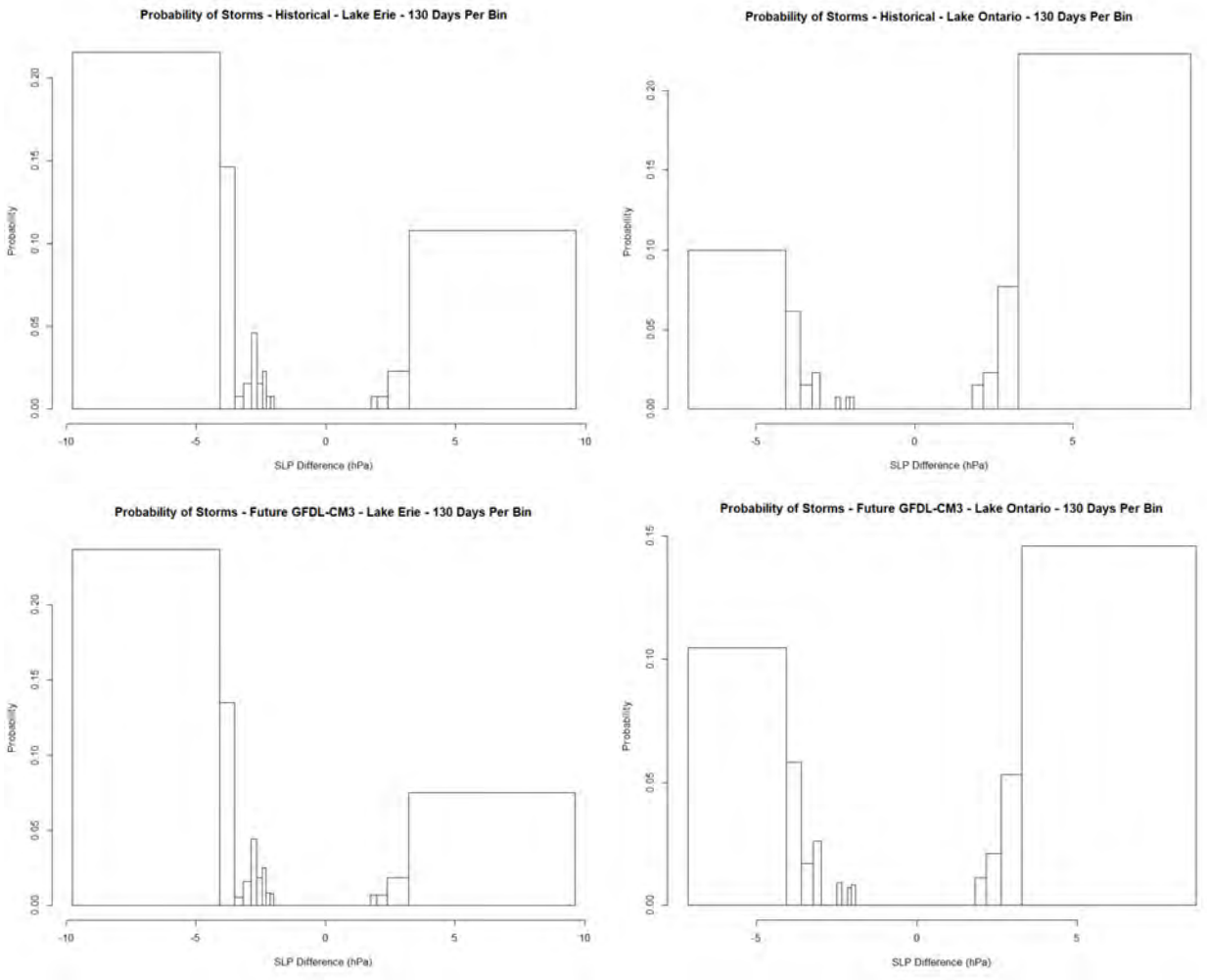

Figure A.5: Normalized probabilities of storms as a function of SLP differences between the two reference points in Figure 2 for Lake Erie (left panels) and Lake Ontario (right panels) over the 1979-2005 historical period (top panels) and 2074-2100 future period (bottom panels) as predicted by GFDL-CM3 for RCP8.5.

Over both lakes, the differences between historical and future storm probabilities are similar. There is a noticeable decline in the storm probabilities for positive SLP differences and a corresponding increase for negative SLP differences. The differences were defined to be positive for higher pressures at the northern reference points. Therefore, the trends suggest an overall decrease of SLP in the north and are in line with an observed northward trend of the storm tracks in the northern hemisphere (section TS.2.4 in IPCC, 2013), which causes a decrease in the overall pressure further north.

Table 4 in the main body of the report summarizes the total shift in the number of storms for all five GCM. For each GCM, the standard deviation was calculated based on the spread of predicted changes over the range of bin sizes from 50 to 200 weather patterns. These standard deviations were used to calculate the total weighted mean and standard deviations across all five GCM predictions, which are shown in the two right-most columns in Table 4.

A.3 CHANGES IN ICE COVER

Synoptic weather patterns and SLP differences move along a continuous spectrum for which regular, once-daily snapshots were available and could be subjected to automated processing. A similarly systematic and thorough treatment of ice cover was not possible within the scope of this project. Ice cover is neither available at daily resolution, nor is there a simple continuous parameter to quantify the role of ice cover in storm events. Furthermore, ice cover on the Great Lakes is rarely ever complete. Both the percentage and the spatial distribution of ice cover relative to the impacted location and wind direction are important determinants or moderators for the occurrence or strength of a high-wave event.

To remain roughly in line with the previous analyses using synoptic weather typing and SLP gradients, the 100 highest ranking storms over the period from 1979-2013 were considered. 'Candidate days' were defined as days when the absolute value of the SLP difference between the two reference points over each lake exceeded 5 hPa. To keep the manual processing manageable and to serve Baird's wave modelling, the analysis was limited to the WRF period from 2000-10-01 to 2013-09-30. The calculations in the following paragraph are summarized in Table A.1.

Table A.1: Calculation of changes in number of storm days based on candidate days defined by absolute SLP differences of at least 5 hPa between the two reference points over Lake Erie and Lake Ontario shown in Figure 2.

	Total Candidate Days	Candidate Days without Ice (Hist.)	Storm Days (Hist.)	Probability of Storm on Days without Ice	Candidate Days without Ice (Fut.)	Storm Days (Fut.)	Change Storm Days (%)
Lake Erie	25	20	13	13/20 = 0.65	25	0.65x25 = 16.25	**25**
Lake Ontario	26	23	8	8/23 = 0.35	26	0.35x26 = 9.0	**13**

For Lake Erie, a total of 25 candidate days were determined for the WRF period (Table A.1). Of these, 13 days were on the list of the 100 top ranked storms over the period from 1979-2013 and did not have any substantial ice cover. For the remaining 12 candidate days, the closest available ice maps were downloaded and manually assessed for substantial ice cover that would be expected to suppress storms. For Lake Erie, five days showed substantial ice cover. Therefore, among the 25 total candidate days, there were 20 candidate days without ice cover. Hence, the probability of a storm, given that there is no ice cover, is 13/20 = 0.65.

A detailed study of potential future ice cover by the end of the century for RCP8.5 was not performed. However, several examples of WRF output during candidate days were assessed suggesting warming of skin surface temperature of several degrees making it highly unlikely that future lake surface temperatures could be sustained long enough below the threshold to form substantial ice cover either on Lake Erie or Lake Ontario. A more thorough analysis of ice cover against several possible metrics for ice formation from WRF would be necessary to support more comprehensive calculations. For the purpose of this study, it was assumed that there would be no ice cover in the future during candidate days.

For Lake Erie, this implies 25 candidate days without ice cover in the future (Table A.1). That would increase the number of storm days by the probability of storm days, given that there is no ice cover, (0.65) multiplied by the number of candidate days without ice cover in the future (25) which is 16.25 days. This corresponds to an increase of the number of storm days by 25% over Lake Erie by the end of the century under RCP8.5. A similar calculation for Lake Ontario in Table A.1 suggests an increase of approximately 13%.

A.4 COMBINED STATISTICS

An estimate of the combined effect of changes in synoptic weather patterns, pressure gradients, and ice cover was derived by adding the three mean values for each lake. Uncertainties, expressed as standard deviations, were only available for the mean changes in the frequency of storms due to changes in synoptic weather patterns and pressure gradients. The combined uncertainty was calculated using error propagation but is missing the contribution from uncertainties in the estimation of changes in storm frequencies from reduced ice cover.

APPENDIX B

Lake Erie and Ontario Nearshore Wave and Surge Modeling

Adapting to the Future Storm and Ice Regime in the Great Lakes

Lake Erie and Ontario Nearshore Wave and Surge Modelling

April 30 2019 | 12880.101

Baird.
Innovation Engineered.

baird.com

Adapting to the Future Storm and Ice Regime in the Great Lakes

Lake Erie and Ontario Nearshore Wave and Surge Modelling

Prepared for:

Prepared by:

Zuzek Inc.
125 Wimberly Avenue
Waterdown, Ontario
Canada L8B 0S2

W.F. Baird & Associates Coastal Engineers Ltd.

For further information, please contact
Mike Fullarton at +1 905 845 5385
mfullarton@baird.com
www.baird.com

12880.101

Z:\Shared With Me\QMS\2020\Reports_2020\12880.101.R1.Rev0_NRCAN_GL_Report.docx

Revision	Date	Status	Comments	Prepared	Reviewed	Approved
Rev A	April 23 2019	Draft	Client review	AM/KH/MF	FD	MF
Rev 0	April 30 2019	Final		AM/KH/MF	FD	MF

Table of Contents

Tables

Figures

1. Introduction

The overall objective of this project, which is entitled “Adapting to the Future Storm and Ice Regime in the Great Lakes” is to advance the knowledge base and enhance the adaptive capacity of practitioners managing the coastal zone in the Great Lakes Basin. The project is broken out into two Streams:

- Stream 1.0 – Storm characterization and numerical modelling to define wave and water level conditions in Lake Erie and Lake Ontario for fifteen storm events under baseline and future wind and ice conditions.
- Stream 2.0 – Integrate the findings from Stream 1.0 into case studies on each lake to assess future hazards and vulnerability and develop appropriate adaptation strategies to inform coastal zone management and planning in the lower Great Lakes.

This report describes the wave and surge modelling that was completed on Lake Ontario and Lake Erie as part of Stream 1.0. Specific objectives of Stream 1.0 include:

- Identification of the top 15 storms on each lake using the Wave Information Studies (WIS) data. The storm listing was used to support a storm typing exercise for extreme events. (RWDI, 2020)
- Development of two-dimensional wave and hydrodynamic models for both lakes. Simulate the top fifteen storms under baseline conditions and a future climate scenario to assess the relative change in wave height and water level (surge). The Danish Hydraulic Institute’s (DHI) MIKE modelling system was used to complete this task.
- Development of deepwater wave models to simulate wave conditions on both lakes from 2000 to 2013. This was an addendum to the original scope and provides a more detailed assessment of the impact of wind and ice on wave climatology as the model can capture all storms over the thirteen-year period. The wave model WAVAD was used to complete this task.
- Provide wave and water level information offshore of the case study sites to support work to be completed as part of Stream 2.0.

The baseline and future climate conditions used in this study were generated by the National Center for Atmospheric Research (NCAR). The data is from a high-resolution climate change simulation using the Weather Research and Forecasting (WRF) model. Two thirteen-year simulations were completed using October 2000 to September 2013 as a baseline condition and then re-running the simulation by adding the CMIP5 ensemble mean of the high emission scenario for climate change (Rasmussen, R., and C. Liu, 2017).

The case study sites on Lake Ontario are shown in Figure 1.1 and include the Burlington waterfront and Credit Valley Conservation Authority waterfront. Figure 1.2 shows the Chatham-Kent waterfront on Lake Erie.

The report is broken out into the following sections: Section 2.0 provides an overview of the key physical datasets used in the project to define the storm listings and support model development; an analysis of wave and water level conditions near the case study sites along with the storm listings for the top fifteen events are summarized in Section 3.0; MIKE21 model development and simulation of the top fifteen storms under baseline and future conditions are discussed in Section 4.0; WAVAD model development and simulation of baseline and future conditions from 2000 to 2013 are discussed in Section 5.0; conclusions from the report are presented in Section 6.0.

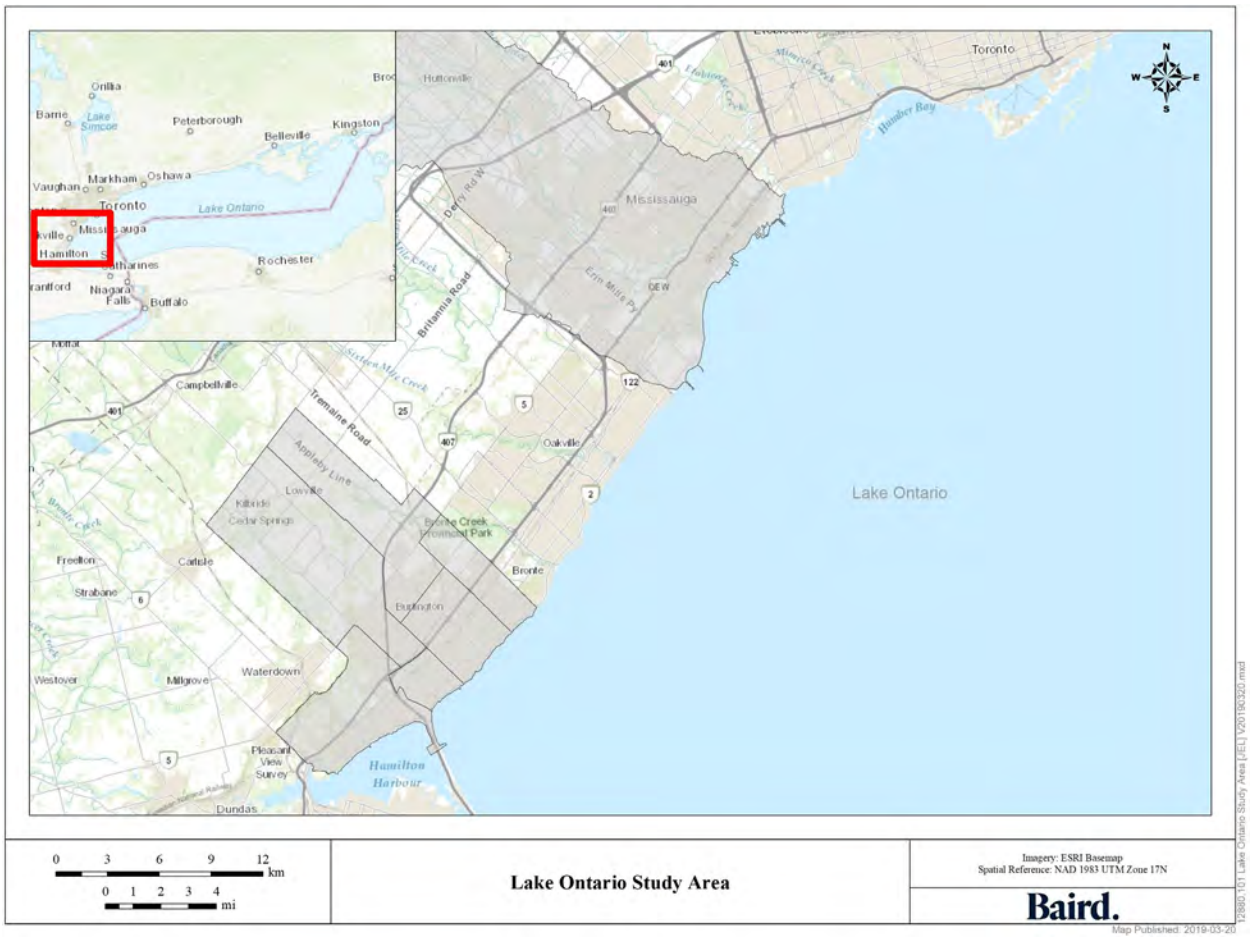

Figure 1.1: Case study sites on Lake Ontario: Burlington and Credit Valley Conservation Authority waterfronts.

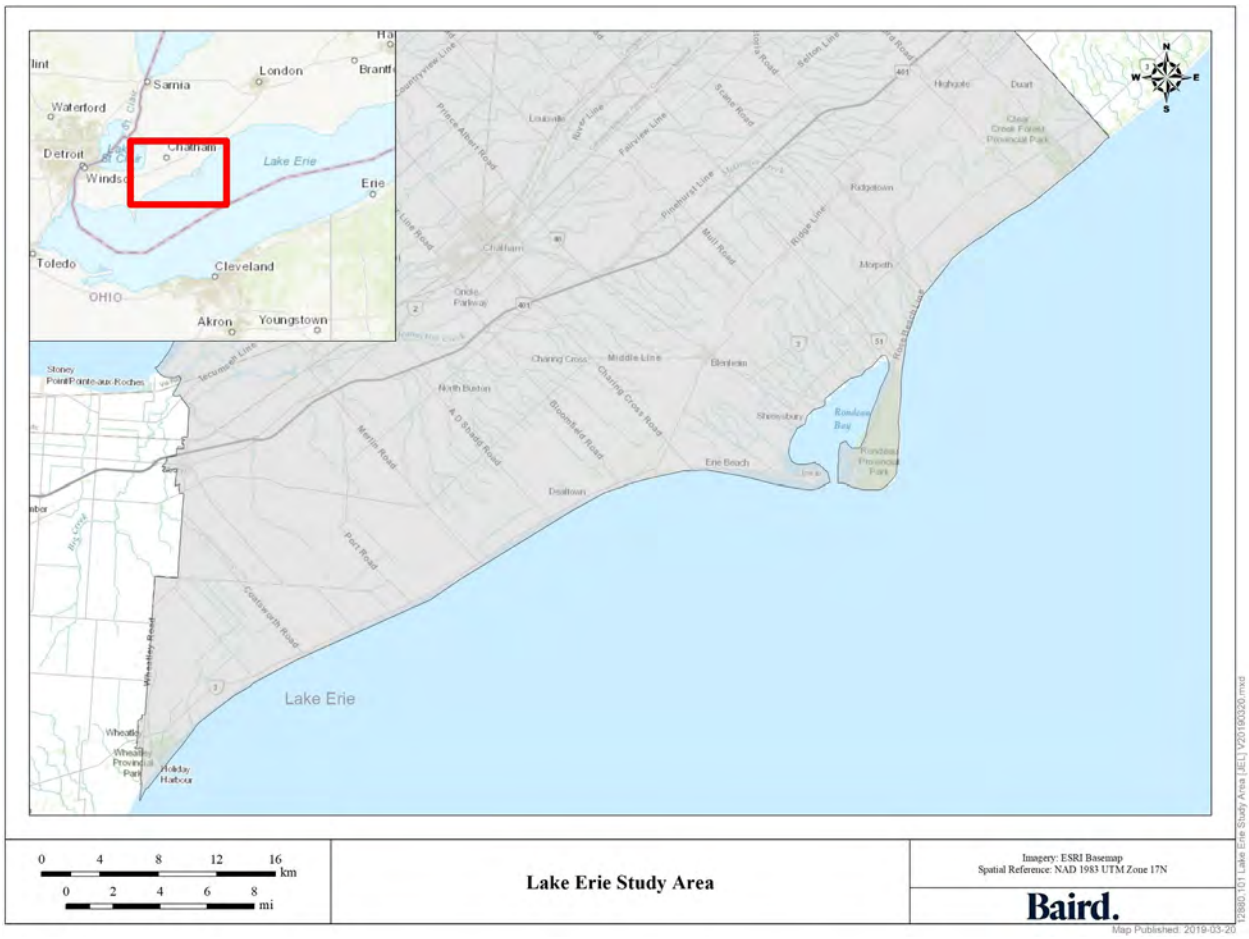

Figure 1.2: Case study site on Lake Erie: Chatham-Kent waterfront.

2. Datasets used in Project

Several datasets were assembled and used to support this study; these include both physical measurements and model results. Key datasets include lake bathymetry and shoreline data, historical ice charts, spatial wind and pressure fields, wave hindcast data, and measured water level and wave buoy data at select locations. Figure 2.1 and Figure 2.2 provide an overview of the bathymetry, water level and wave data used on each lake to support the objectives of the study.

2.1 Lake Bathymetry

Lake bathymetry was required for both lakes to support the development of the numerical models. The bathymetric datasets were obtained from NOAA's National Geophysical Data Center, which is now the National Centers for Environmental Information (NCEI). The hydrographic data compiled on the Great Lakes is based on all hydrographic sounding datasets collected by the Canadian Hydrographic Services (CHS), the U.S. National Ocean Service (NOS) and the U.S. Army Corps of Engineers.

The data, which were provided in metres in the WGS84 geographic coordinate system, was transformed to UTM Zone 17 for both lakes. The bathymetric data for each lake is referenced to International Great Lakes Datum 1985 (IGLD85); for Lakes Ontario and Erie the vertical datums are 74.2 m and 173.5 m, respectively.

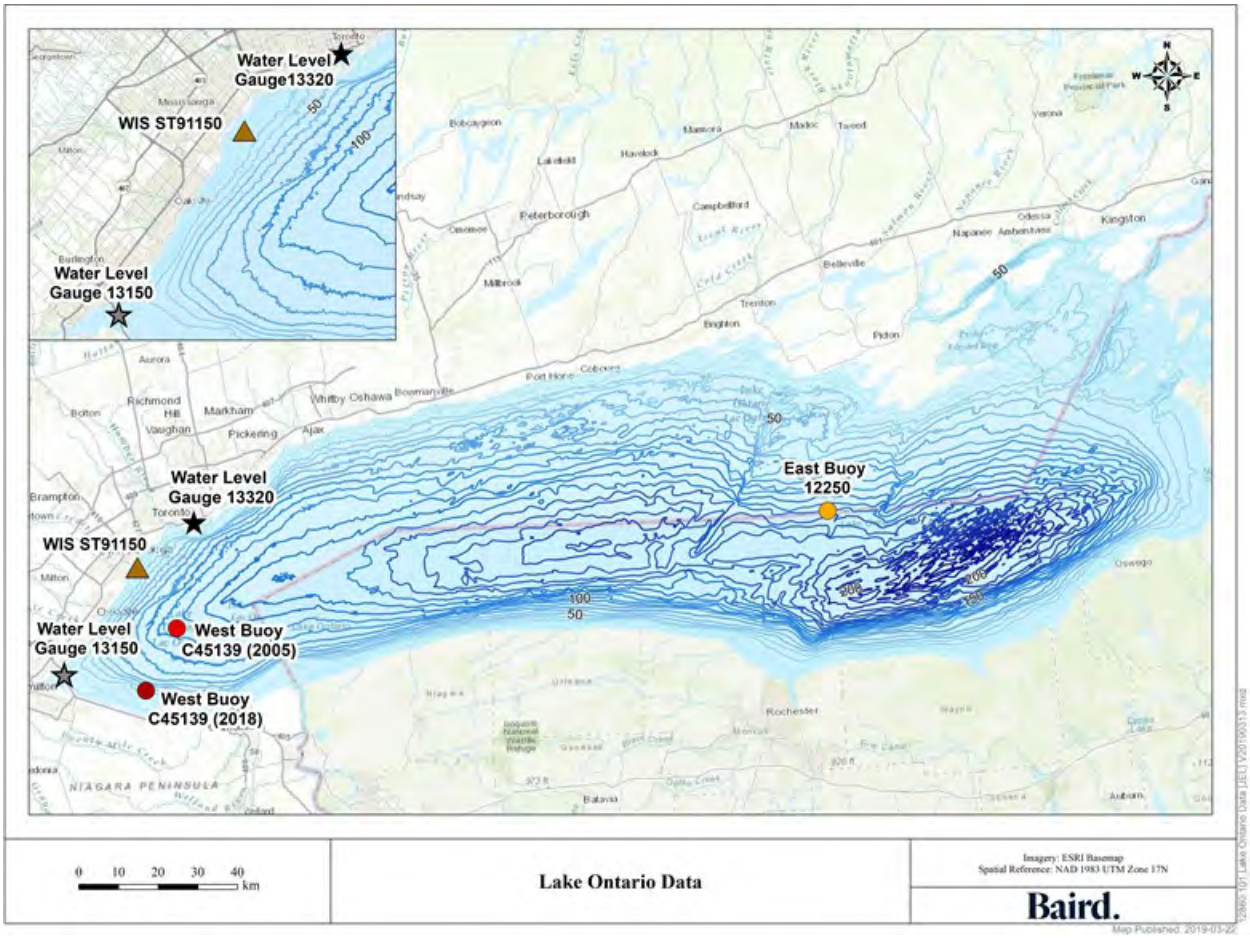

Figure 2.1: Overview of the bathymetry, water level and wave data used on Lake Ontario.

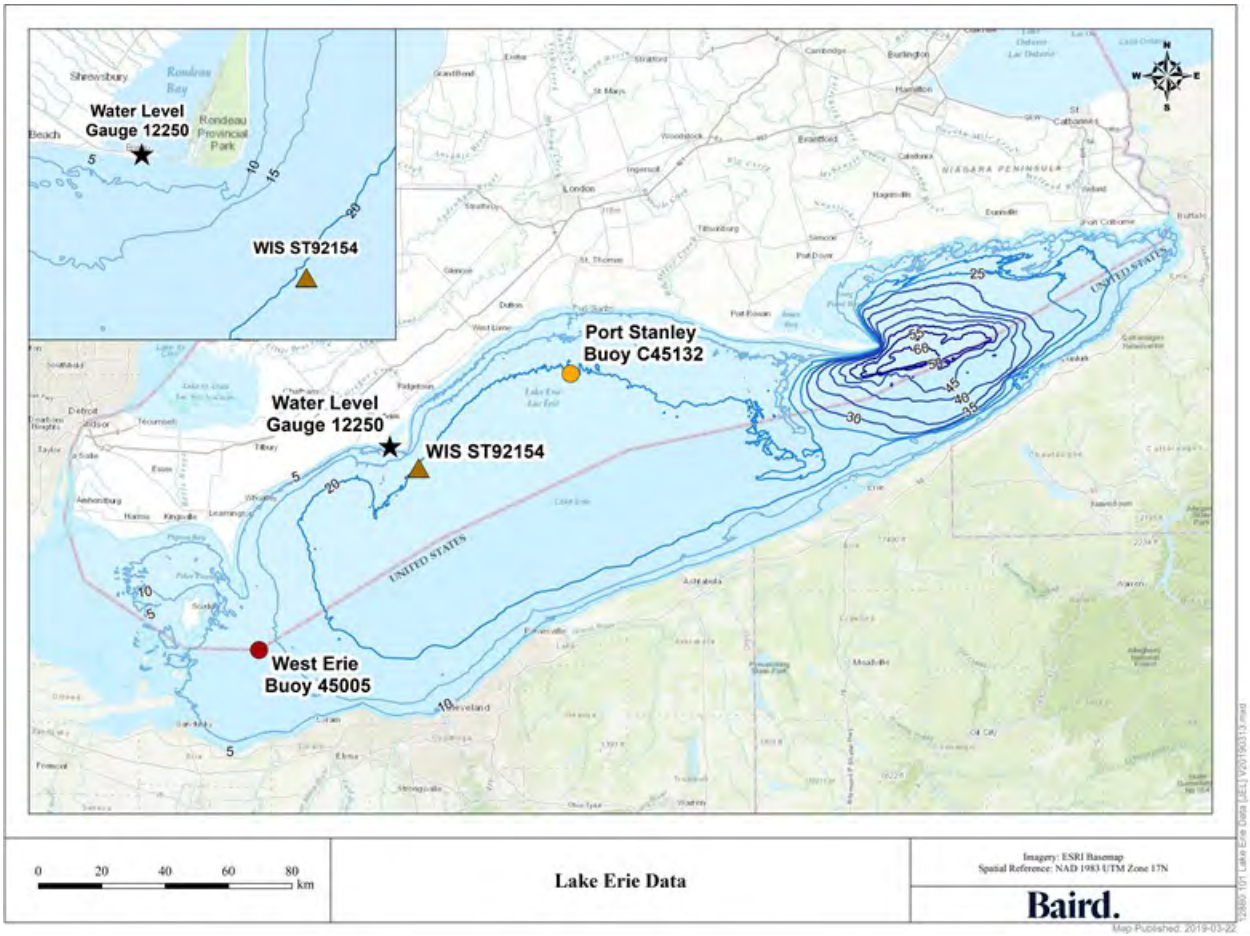

Figure 2.2: Overview of the bathymetry, water level and wave data used on Lake Erie.

2.2 Wave Data

There are several buoys deployed on both lakes that measure wave conditions during the ice-free season. These units are maintained by NOAA's National Data Buoy Center and ECCC Meteorological Service of Canada Marine Environment Data Section. The buoys used in this study are summarized in Table 2.1 and their locations are illustrated in Figure 2.1 and Figure 2.2. Data coverage is limited to the ice-free season as the units are removed in late fall and re-deployed in the spring. There are also time periods where data is missing or erroneous. The data is provided in an hourly format (UTC) and the units measure several parameters, however only significant wave height and period were considered in this study. The data were used to support a high-level calibration of the wave models.

Table 2.1: Summary of the buoy data used for Lake Ontario and Lake Erie.

Station	Station Name	Coordinates (DD)	Data Availability	Data Source	Time Step
		Lake Erie Buoys			
45005	West Erie	41.677 N, 82.398 W	1980-2017	NDBC	60 min
C45132	Port Stanley	42.460 N, 81.22 W	1989 - 2018	ECCC	60 min
		Lake Ontario Buoys			
45012	East Lake Ontario	43.621 N, 77.399 W	2002-2018	NBDC	60 min
C45139	West Lake Ontario	43.250 N, 79.53 W	1991-2018	ECCC	60 min

2.3 Water Level Data

Hourly water level data (UTC) was obtained for both lakes from the ECCC Meteorological Service of Canada Marine Environment Data Section. Table 2.2 provides a summary of the gauges used in this study; their locations are shown in Figure 2.1 and Figure 2.2. Only gauges near the case study sites were considered in this project.

The data were used to analyse surge levels and support a high-level calibration of the hydrodynamic models.

Table 2.2: Summary of the water level data used for Lake Ontario and Lake Erie (IGLD85 Datum).

Gauge Name	Station Number	Lake	Latitude N (dd)	Longitude W (dd)	Data Availability
Erieau	12250	Erie	42.26	-81.91	1962-2018
Burlington	13150	Ontario	42.30	-79.79	1971-2018
Toronto Island	13320	Ontario	43.64	-79.38	1962-2018

2.4 Ice Coverage Data

Ice coverage on the Great Lakes during the winter months impacts the amount of wave energy that reaches the shore as it can limit fetch lengths (reducing wave heights). It can also protect the shoreline from incoming waves; therefore, ice was a consideration in the model if it was present during the simulation period.

Gridded ice concentration data was obtained through NOAA's Great Lakes Environmental Research Laboratory. An example of an ice chart is shown in Figure 2.3 and additional details are provided in Table 2.3. These ice products were developed by the U.S. National Ice Center and the Canadian Ice Service. The data were available from 1973-2018 and typically had a daily timestep during periods with ice. The units indicate the percentage of the grid cell covered by ice. Figure 2.3 shows significant ice coverage across Lake Erie and in the east end of Lake Ontario and along the south shore.

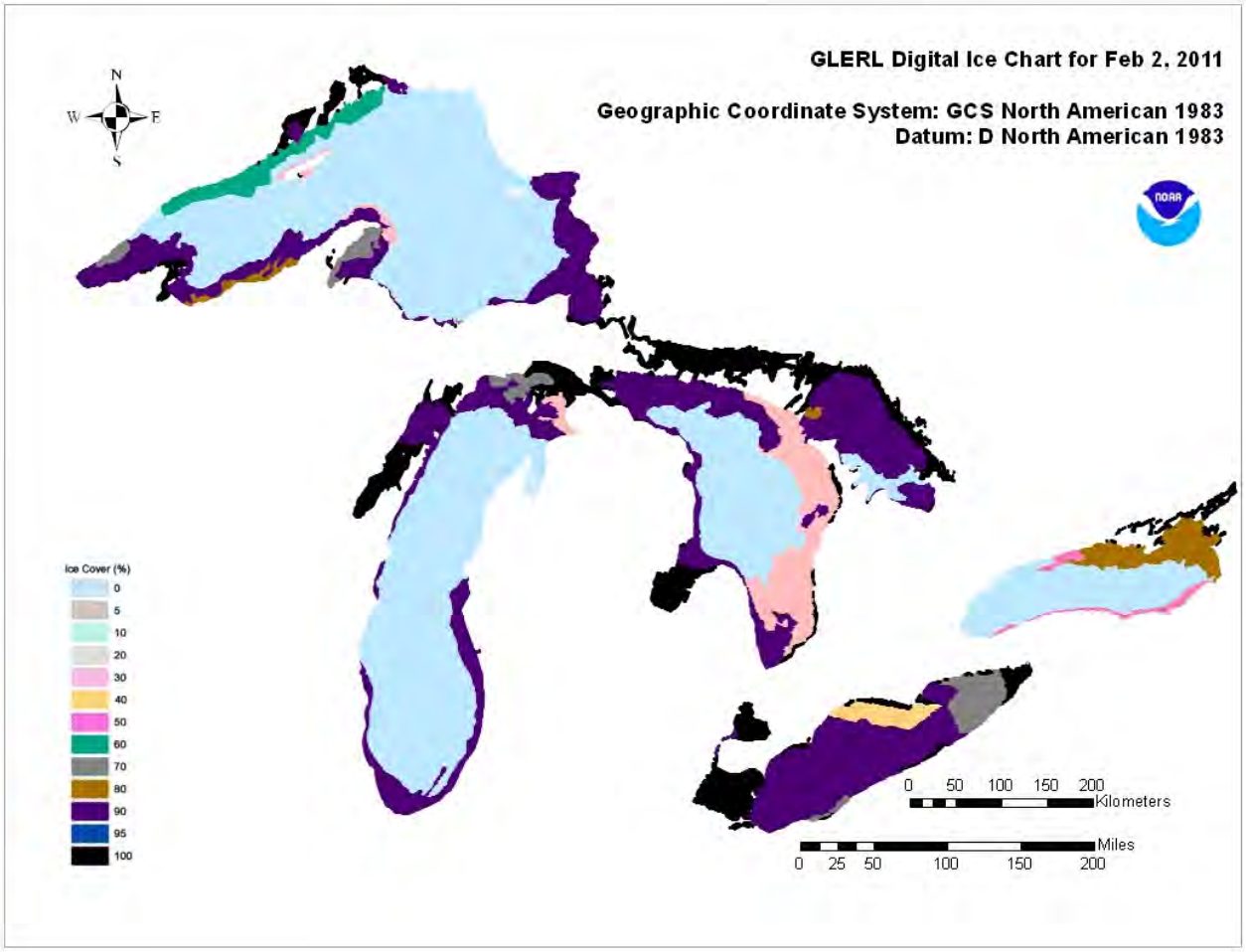

Figure 2.3: Example of a NOAA-GLERL ice chart for the Great Lakes.

Table 2.3: Summary of ice coverage grid resolution.

Years	Rows x Columns	Cell Size (meter)
1973-2006	510 x 516	2550
2007-2018	1024 x 1024	1275

2.5 Wind and Air Pressure Data

The spatially and temporally varying wind and pressure fields used in this study were developed by NCAR using a high resolution (4 km) WRF model over North America. Both a baseline condition and future climate scenario were produced using a thirteen-year period between October 2000 and September 2013. The baseline condition was completed with initial and boundary conditions from ERA-Interim and the future scenario was developed using CMIP5 ensemble mean of the high emission scenario. More information on the development of these wind fields can be found on the NCAR website (https://rda.ucar.edu/datasets/ds612.0/).

2.6 WIS Wave Data

The Wave Information Studies (WIS) is a U.S. Army Corps effort to provide high-quality continuous coastal wave hindcast model estimates for at least 20-30 years. The current dataset runs from 1979 to 2014. Hindcast datasets generated on the Great Lakes provide wave information for locations every few miles along the shoreline at a water depth of approximately 10 m. For Lake Ontario and Lake Erie the WIS hindcast was developed using the spectral wave model (WAM) and Coastal Forecast System Reanalysis (CFSR) wind fields developed by NCAR. Lake bathymetry were discretized on a spherical 0.02-degree resolution grid and the model included mean daily ice concentration maps derived from Assel's atlas. Wave data were extracted at the locations nearest the case study sites on each lake (refer to Figure 2.1 and Figure 2.2) and used to develop the storm listings for this study. This is discussed further in the following section.

3. Storm Event Selection

3.1 WIS Wave Analysis

The top fifteen wave events from 2000 to 2013 were generated for each lake using the WIS wave dataset summarized in Table 3.1. This period was considered as it matches the period of the WRF wind dataset used in the study. These storm events were used to assess the change in wave and water levels offshore of the case study sites under baseline and future climate scenarios. Measured water level data from local gauges were analysed to evaluate surge levels as a function of return period.

Table 3.1: Data used to generate storm listings on Lake Ontario and Lake Erie.

Great Lake	WIS Station ID	WL Station ID
Lake Ontario	91150 (1979-2014)	Toronto 13320 (1960-2018)
Lake Erie	92154 (1979-2014)	Erieau 12250 (1960-2018)

The wave climatology at each WIS location for the period 1979 to 2014 is summarized in the form of wave height roses in Figure 3.1 and exceedance curves in Figure 3.2. In general, the dominant wave directions at the case study sites on Lake Ontario and Lake Erie are from the east and south-west, respectively. The WIS data point on Lake Erie is exposed to larger waves as shown from the exceedance curve. The maximum predicted wave heights were 5.1 m on Lake Ontario and 5.9 m on Lake Erie; the average wave height was determined to be 0.47 m and 0.62 m, respectively.

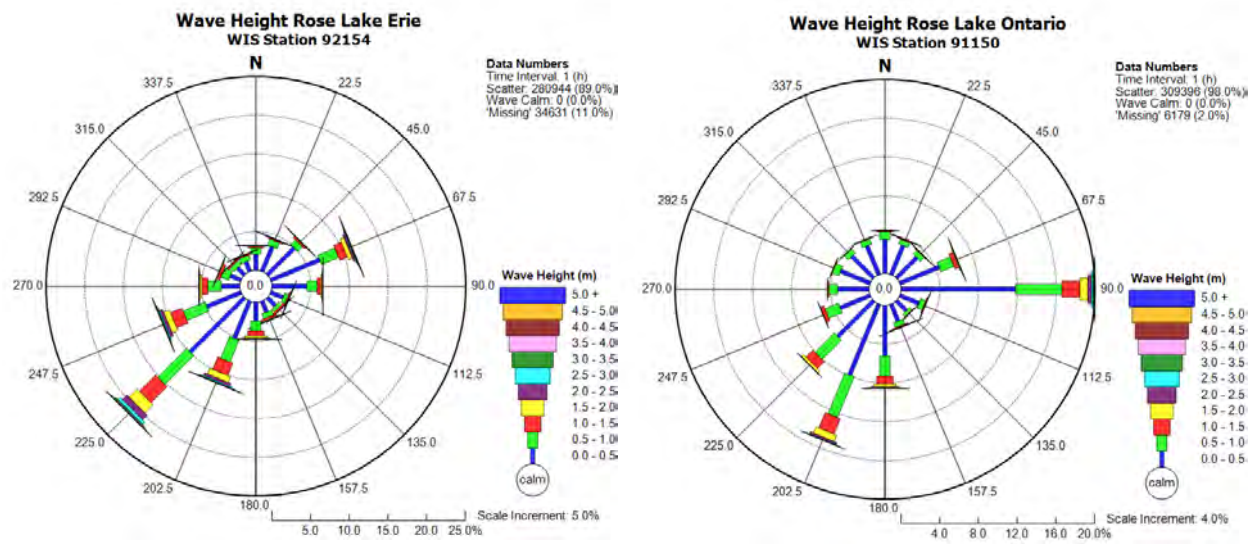

Figure 3.1: WIS data wave height roses.

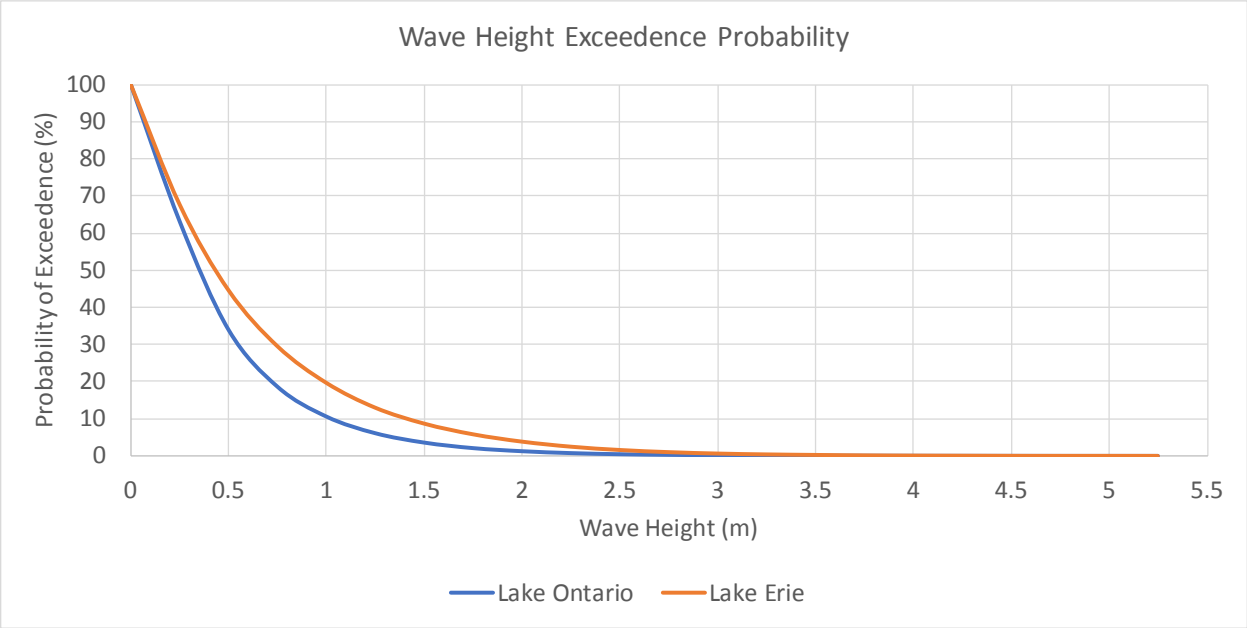

Figure 3.2: WIS data wave height exceedance probability.

A storm listing on each lake was developed using the hourly predicted wave conditions generated at the WIS output points presented in Table 3.1. The wave data were filtered using the Peak Over Threshold (POT) method to separate and identify extreme storm events that could then be sorted into a storm listing. The filters included a minimum wave height threshold of 2.0 m, minimum storm duration of 1 hour, and a 24-hour period between events. An extreme value analysis was completed on the top 60 storms between 1979-2014, the results are present in Figure 3.3. The data were filtered again to only include the top 60 events between October 1, 2000 and September 30, 2013 to examine how the wave heights differ between these two time periods, the findings from an extreme value analysis of that dataset are provided in Figure 3.4.

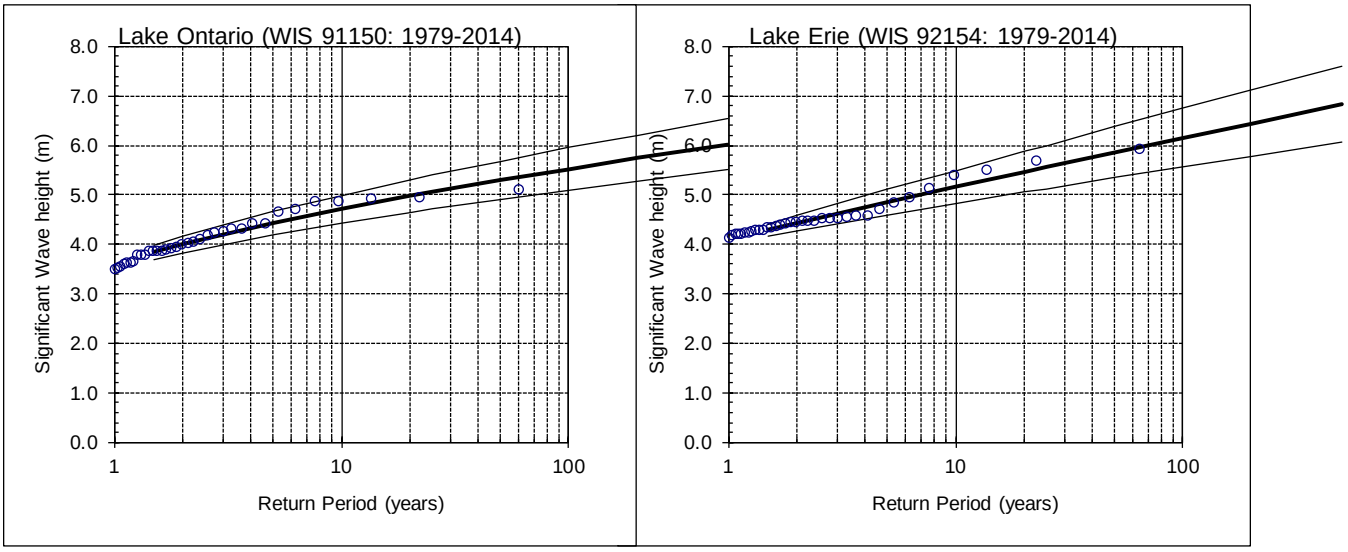

Figure 3.3: WIS wave height as a function of return period for Lake Ontario and Lake Erie (1979-2014).

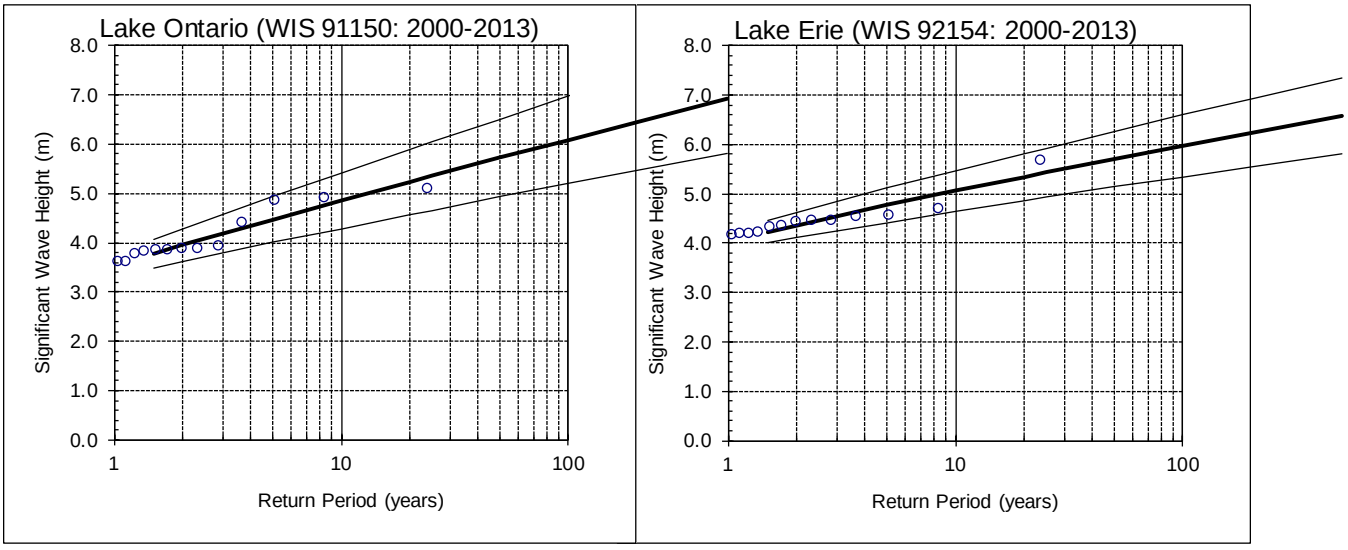

Figure 3.4: WIS wave height as a function of return period for Lake Ontario and Lake Erie (2000-2013).

The results of the EVA showed an increase in wave heights on Lake Ontario for the period 2000-2013 suggesting an increase in extreme storms during this period compared with 1979-2014. On Lake Erie the return period wave heights from 2000-2013 were more similar for both time periods.

3.2 Storm Surge Analysis

An assessment of water levels was completed using the Toronto gauge (13320) on Lake Ontario and the Erieau gauge (12250) on Lake Erie. The primary purpose of this task was to provide information on surge levels to support the Stream 2.0 work. The storm listings developed to support numerical modelling activities was based on wave events.

Measured water levels from 1962 to 2018 were assembled and analysed at both the Toronto and Erieau gauges. Surge estimates were calculated by subtracting the hourly water level measurements from a static water level represented by a 30-day average water level. All data presented is referenced to IGLD85.

The long-term average water levels on Lake Ontario and Lake Erie are 74.76 m and 174.15 m IGLD85, respectively. The maximum and minimum monthly mean water levels on Lake Ontario occurred in June 2017 (75.87 m) and January 1965 (73.82 m). The maximum and minimum water levels on Lake Erie occurred in June 1986 (175.04 m) and December 1964 (173.39 m).

An extreme value analysis was completed on the calculated surge levels, the results are presented in Figure 3.7 and Figure 3.8. The 10 year and 100-year surge levels were estimated to be 0.22 m and 0.28 m, respectively at Toronto, and 0.325 m and 0.42 m at Erieau.

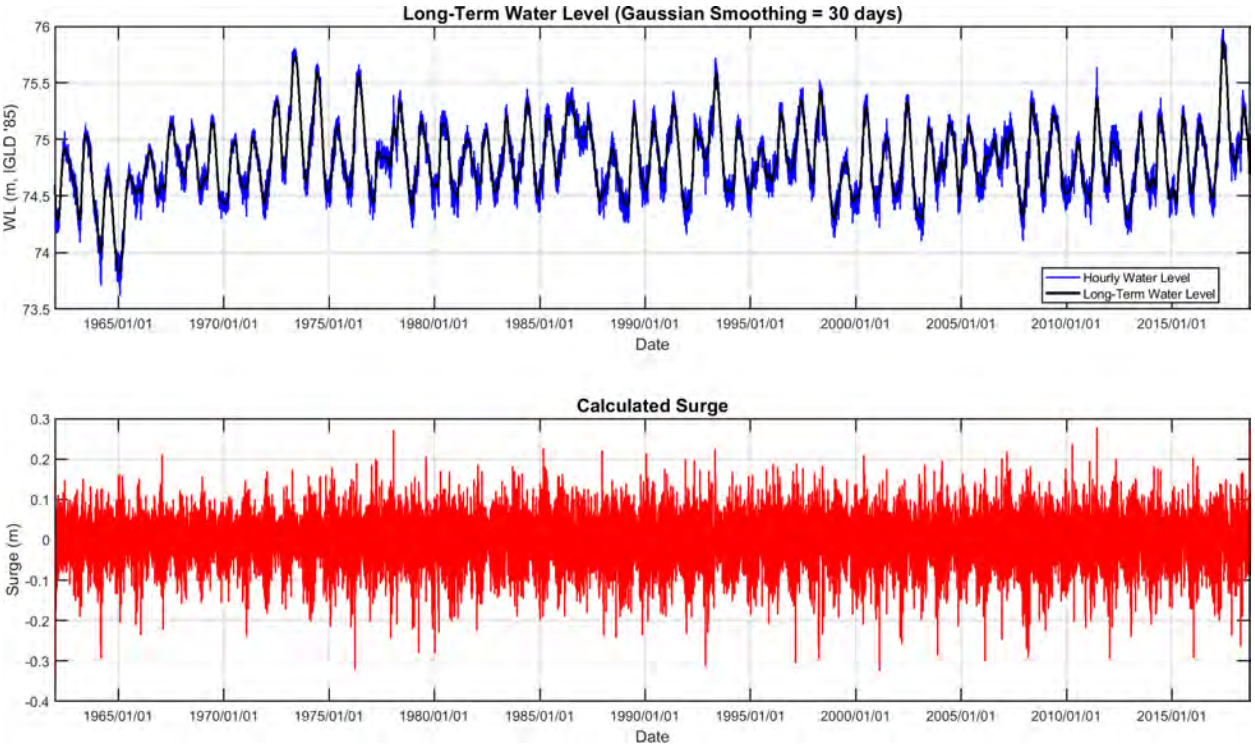

Figure 3.5: Measured water level and surge on Lake Ontario at Toronto gauge (ID: 13320).

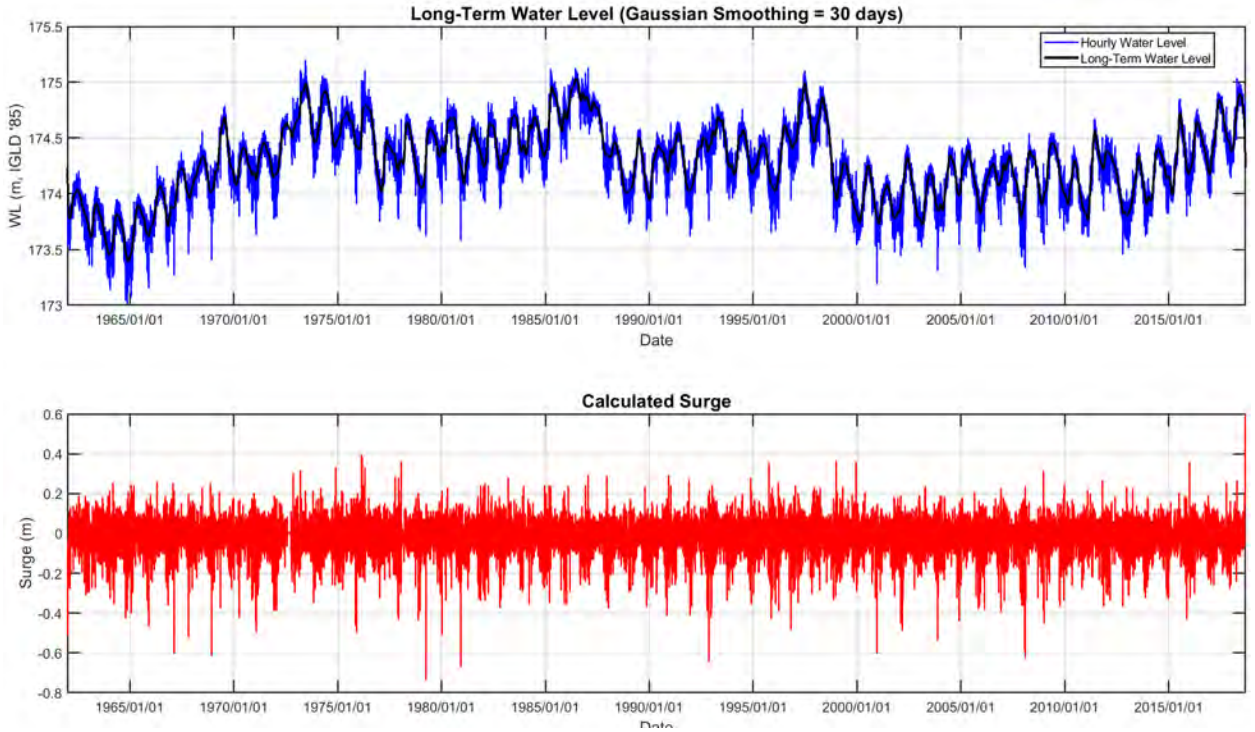

Figure 3.6: Measured water level and surge on Lake Erie at Erieau gauge (12250).

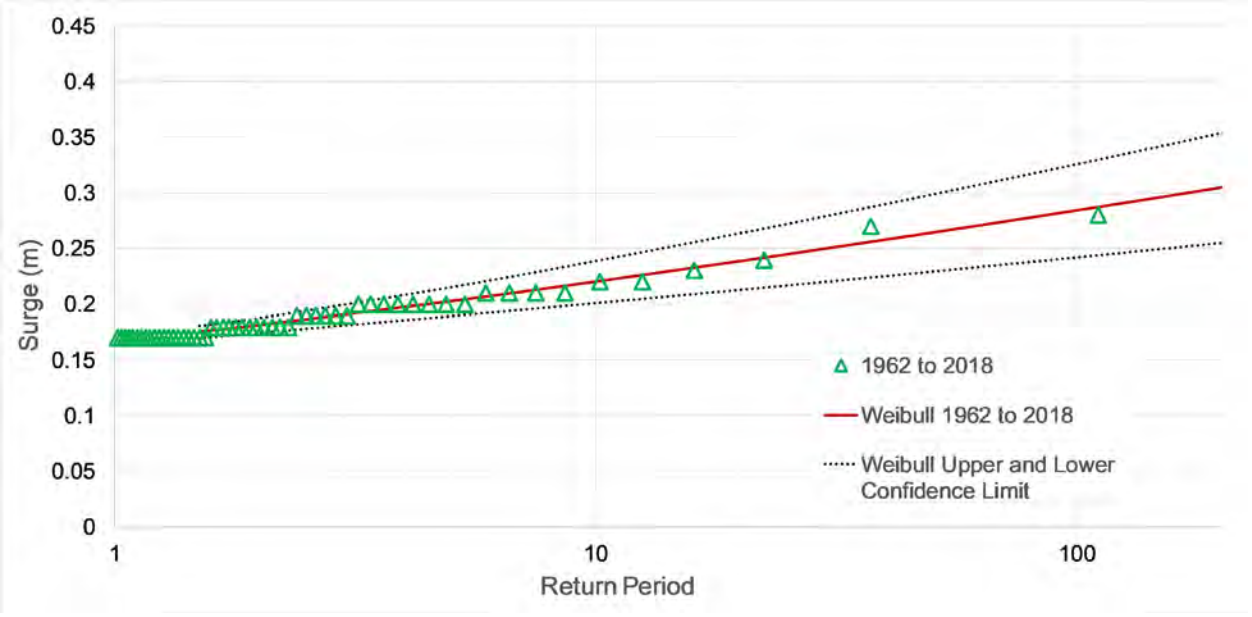

Figure 3.7: Surge as a function of return period at the Toronto gauge (13320) on Lake Ontario.

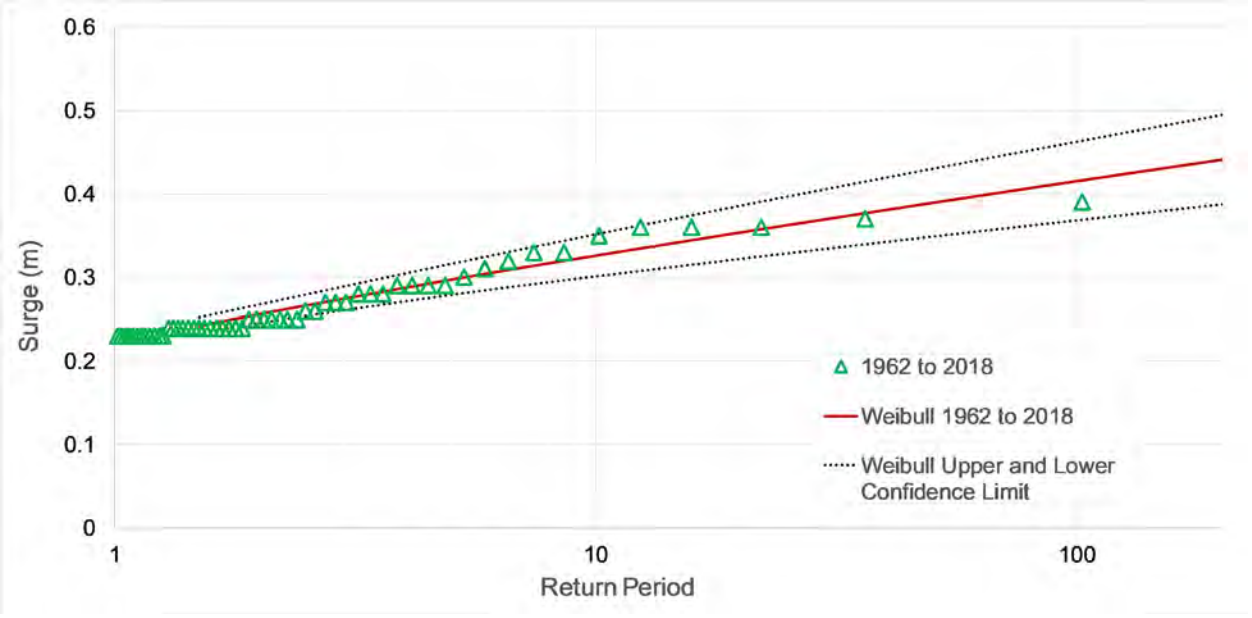

Figure 3.8: Surge as a function of return period at the Erieau gauge (12250) on Lake Erie.

3.3 Storm Listing for Lake Ontario and Lake Erie

The following fifteen storms were selected using the WIS data and summarized in Table 3.2. These events were then modelled using the MIKE models and the baseline and future WRF wind conditions.

Table 3.2: Storm listing for Lake Ontario (WIS Station 91150).

Storm	Peak Storm Date	Hm0 (m)	Tp (s)	Dir (deg)
1	2013/04/12	5.10	9.4	90
2 (Ice)	2011/02/02	4.92	9.1	90
3	2011/10/20	4.85	9.3	89
4	2007/03/02	4.41	8.6	88
5	2011/04/20	3.93	8.3	88
6	2007/12/16	3.89	8.8	88
7	2005/01/22	3.87	8.2	83
8	2006/12/01	3.86	7.6	88
9	2012/10/30	3.85	10.6	84
10	2008/12/19	3.84	8.2	82
11	2012/03/03	3.77	7.4	193
12	2012/02/29	3.63	7.9	91
13	2011/11/23	3.61	8.2	87
14	2010/03/14	3.51	8.4	84
15	2009/12/09	3.47	8.0	88

Table 3.3: Storm listing for Lake Erie (WIS Station 92154).

Storm	Peak Storm Date	Hm0 (m)	Tp (s)	Dir (deg)
1	2009/12/10	5.67	9.1	225
2	2002/03/10	4.69	8.4	230
3	2011/04/15	4.56	8.4	77
4	2011/11/23	4.53	8.4	77
5	2012/12/26	4.45	8.4	76
6	2002/11/29	4.45	7.9	215
7	2012/03/03	4.43	8.0	227
8	2007/12/24	4.35	7.8	228
9	2011/11/10	4.32	7.8	231
10	2009/09/28	4.23	7.8	228
11	2003/11/13	4.20	7.7	242
12	2006/12/01	4.19	7.7	236
13	2008/12/22	4.18	7.7	232
14	2011/04/28	4.11	7.6	226
15	2011/10/20	3.96	7.6	67

4. Model Development

The MIKE21 modelling system was used to evaluate the impact of future wind fields on wave climatology and hydrodynamics under an extreme-case that assumed ice-free conditions in the future. Developed by the Danish Hydraulic Institute (DHI), the MIKE models have been used extensively by Baird and others on coastal and hydraulic related projects around the world. For this study, wave and hydrodynamic conditions were predicted using the MIKE21 Spectral Wave (MIKE21 SW) and MIKE21 Hydrodynamic (MIKE21 HD) models. A brief description of each model is provided below.

MIKE21 Spectral Wave Model

MIKE21 SW is a spectral wind-wave model that uses an unstructured (flexible) mesh to simulate the growth, propagation, transformation and decay of wind generated waves and swell in offshore and coastal areas. The model is capable of simulating phenomena such as wave growth due to wind, dissipation due to white capping, breaking and friction, non-linear wave-wave interaction, shoaling and refraction. The model can also be coupled to the hydrodynamic model to simulate wave-current interactions, although this is computationally demanding. In this study, the wave radiation stresses from the MIKE21 SW model were defined as an input to the hydrodynamic model (uncoupled) in order to account for momentum generated from breaking waves.

MIKE21 Hydrodynamic Model

The MIKE21 hydrodynamic model is a two-dimensional modeling system capable of simulating free surface flows where stratification is not of concern. The model utilizes an unstructured (flexible) mesh and can be used to simulate a range of hydraulic conditions including tidal exchange, currents, storm surge, heat and recirculation, and water quality. The strength of the flexible mesh is that it allows for greater resolution and improved boundary fit in regions of interest and less resolution in less critical areas.

4.1 MIKE21 Model Setup

The mesh developed for each lake is presented in Figure 4.1. Note that the wave and hydrodynamic models utilize the same mesh file. Several variations of mesh resolution were tested to optimize run time and model predictions. The final resolution ranged from 1.6 km offshore down to 150 m at the case study sites. Inflows and outflows from connecting channels were not included in the model as they do not impact or influence the wave and hydrodynamic processes during extreme storm events which occur over a relatively short time period.

Temporally and spatially varying wind and ice fields were developed for the fifteen baseline storm events summarized in Table 3.2 and Table 3.3. For reference, Lake Ontario does not experience the same ice coverage patterns as Lake Erie, which tends to have more ice covering the lake during the winter months. The existence of ice can impact wave climatology. Ice sheets covering large regions of the lake can reduce fetch length (wave growth) and protect shorelines from incoming waves by damping out the wave energy before it reaches shore. This is illustrated in Figure 4.2 which compares wave predictions with and without ice on Lake Erie using Storm No. 13 which occurred on December 22, 2008. The results show no wave energy in the west end of the lake and along the Chatham-Kent shoreline where ice was present.

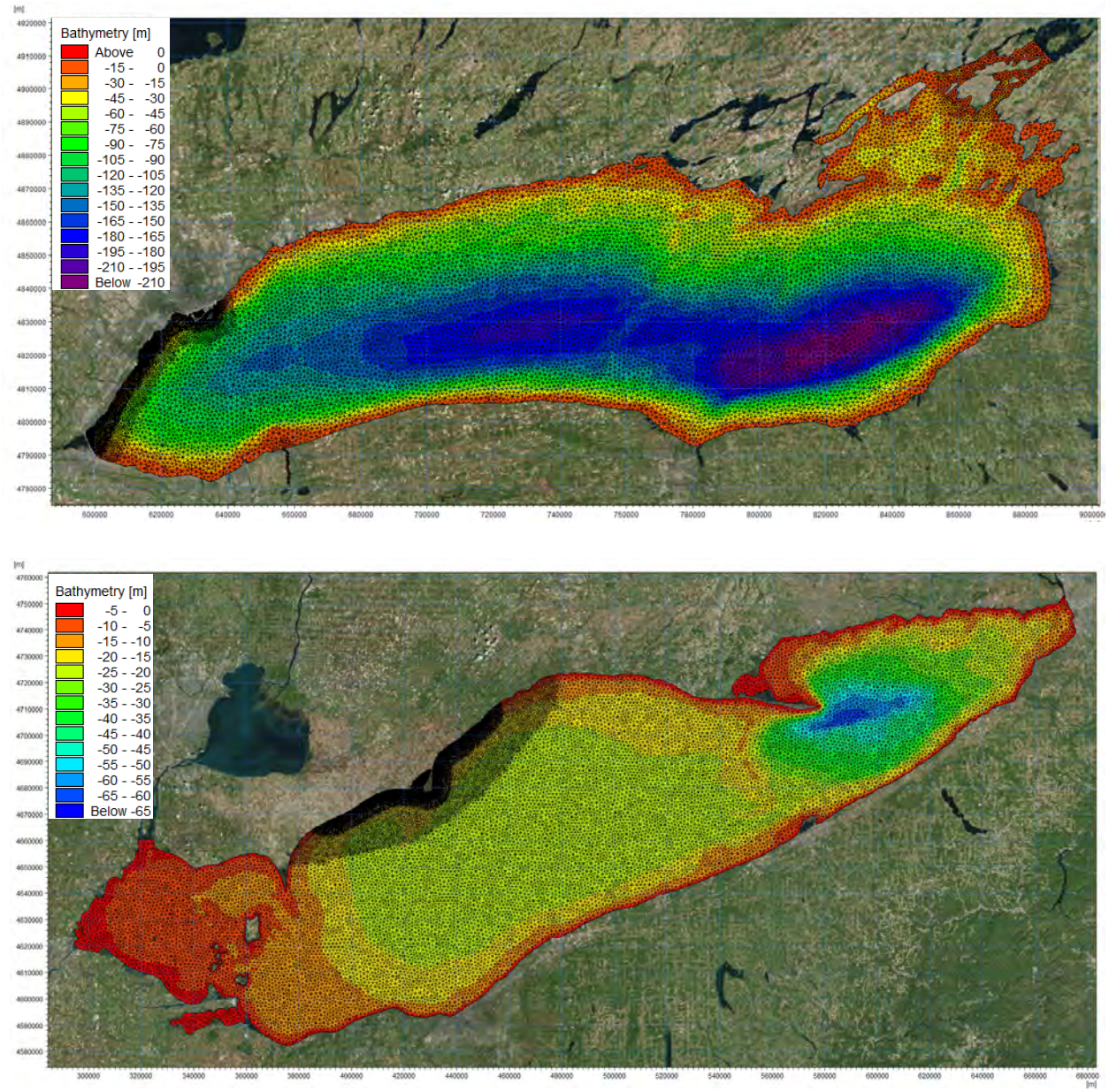

Figure 4.1: MIKE model mesh for Lake Ontario (top) and Lake Erie (bottom). The darker regions indicate the location of the case study sites.

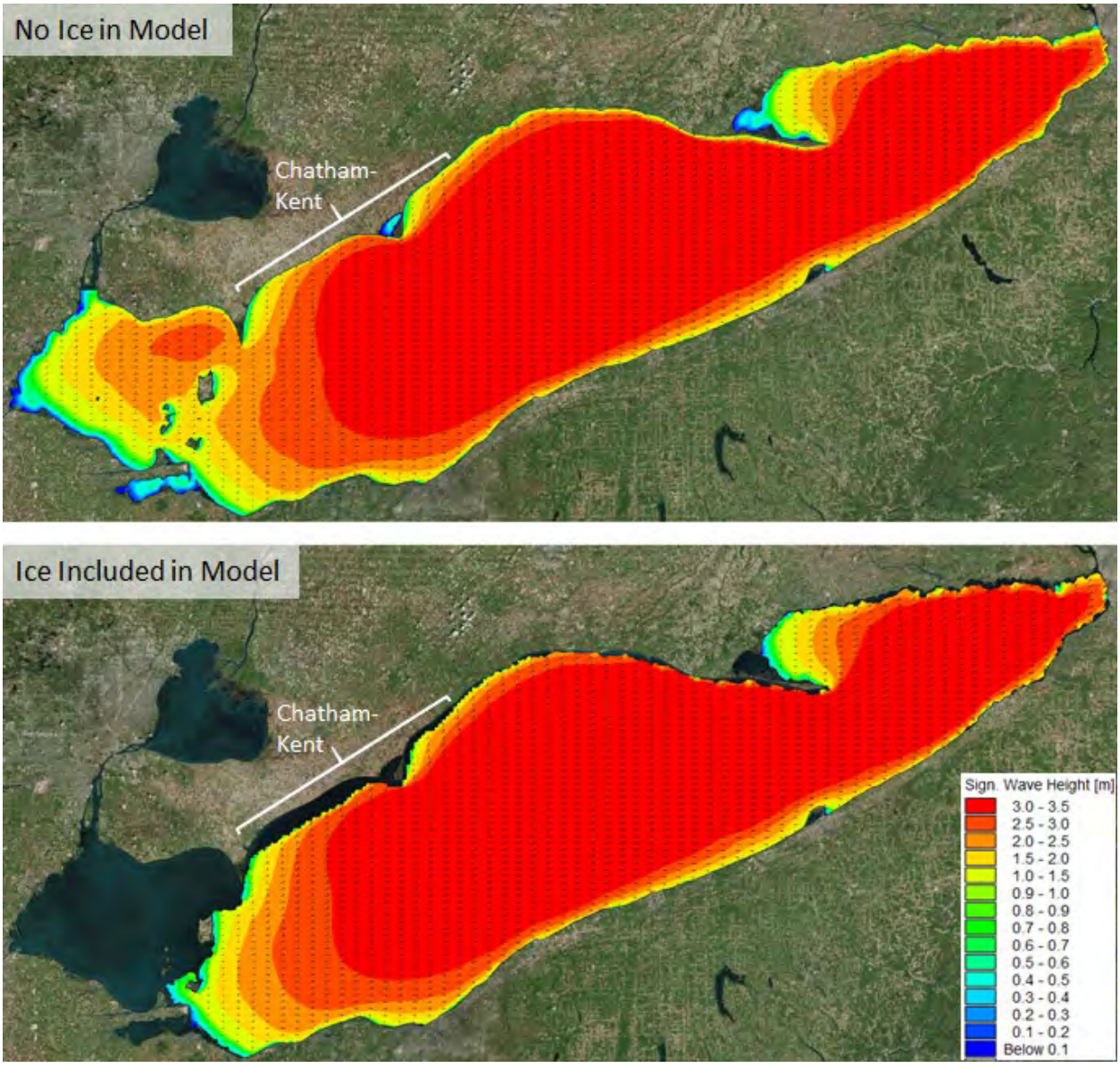

Figure 4.2: Influence of ice on wave climatology on Lake Erie (Storm 13: December 22, 2008).

4.2 Correct Wind Fields Over Water

The WRF wind dataset was used to drive the wave and hydrodynamic models. To improve the predictions of wind speed over water, the wind fields were compared with measured winds recorded at all buoy locations on the lake. Figure 4.3 shows the WRF output locations and the buoys used for comparison. Correction factors were applied to each grid location based on a comparative analysis of wind speed by directional quadrant (8 quadrants in total). The colours show which WRF points were corrected to each buoy.

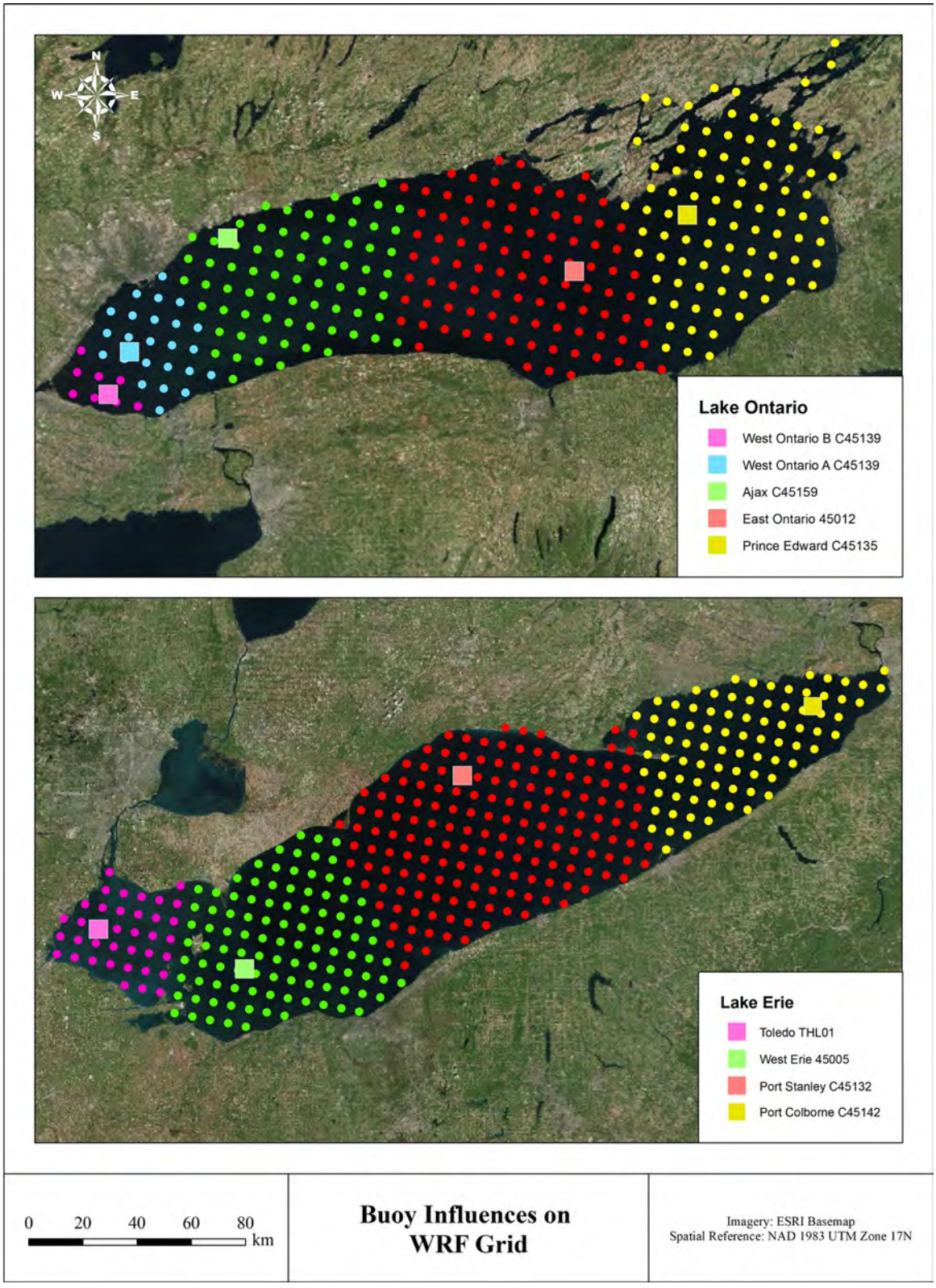

Figure 4.3: WRF data points and corresponding buoys used for wind speed corrections.

Figure 4.4 illustrates the correction process done on Lake Ontario by showing a comparison of the uncorrected and corrected wind speeds for all quadrants of the WRF grid point closest to Buoy C45139. A review of the uncorrected data showed that the WRF wind field underestimated the moderate to stronger wind speeds, which are important for the storm modelling completed for this study. The corrected data showed stronger statistical correlation with the measured data. This analysis was completed for each WRF grid point. The corrected WRF wind data was then interpolated to the model mesh in order to drive both the wave and hydrodynamic models. Note that wind speeds below 3 m/s were not included in the analysis as the study focused on strong wind events.

Note, Quantile-Quantile (Q-Q) plots were used to evaluate the data statistically. A Q-Q plot is a graphical technique for assessing whether two datasets are statistically equivalent. In this approach the quantiles (percentages of data points below a given wind speed value) were plotted against the quantiles of the second dataset. If equivalent quantiles provide equivalent wind speed, the datasets are statistically similar, as is the case in Figure 4.4.

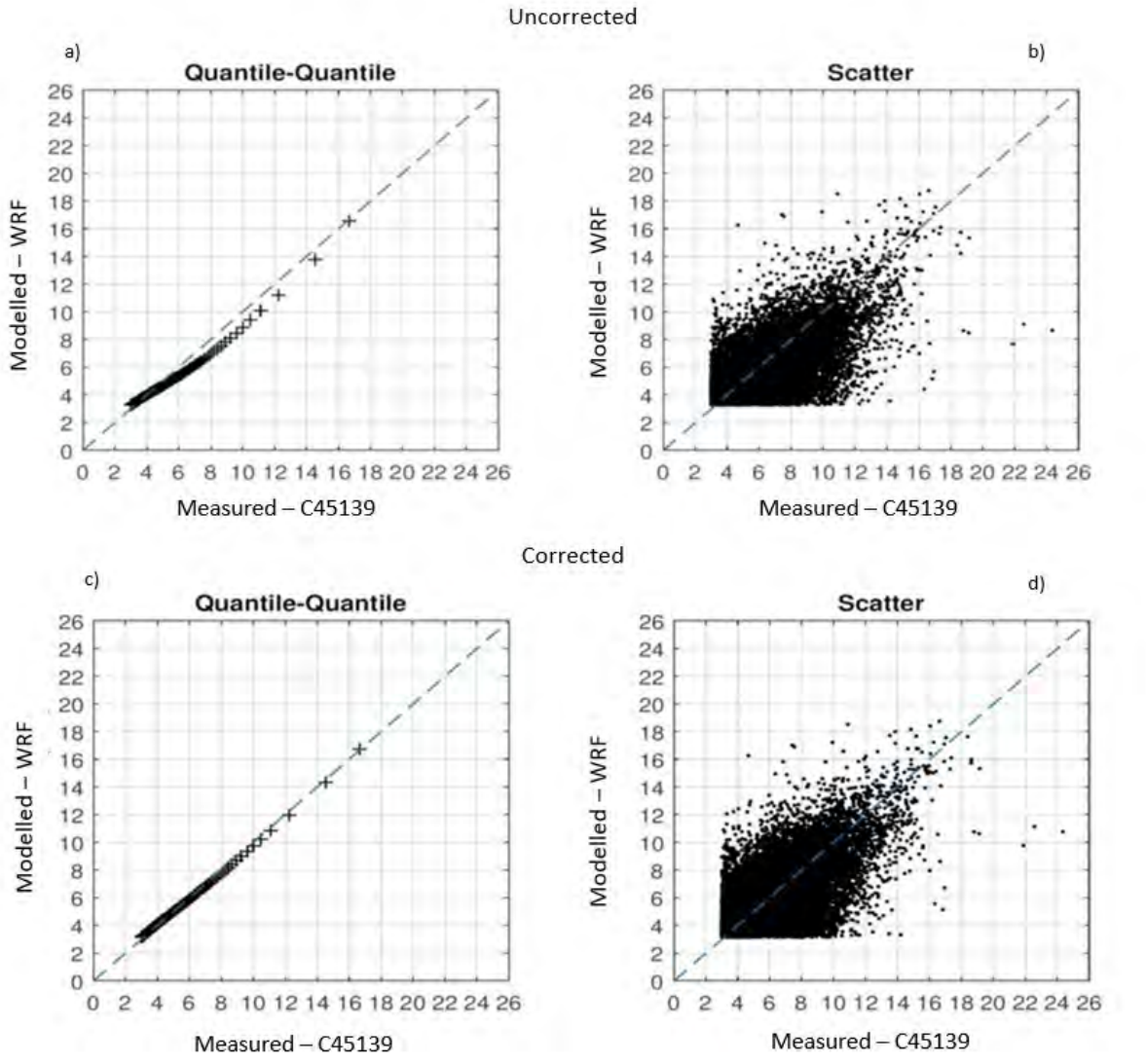

Figure 4.4: Example of WRF wind speed correction at one point near buoy C45139.

4.3 Comparison between Baseline and Future Winds

A comparison between baseline and future wind conditions was completed at one location on each lake in order to understand the difference in the wind fields. Figure 4.5 and Figure 4.6 summarize the results from the analysis in the form of a Q-Q analysis, scatter plots and directional frequency histogram rose.

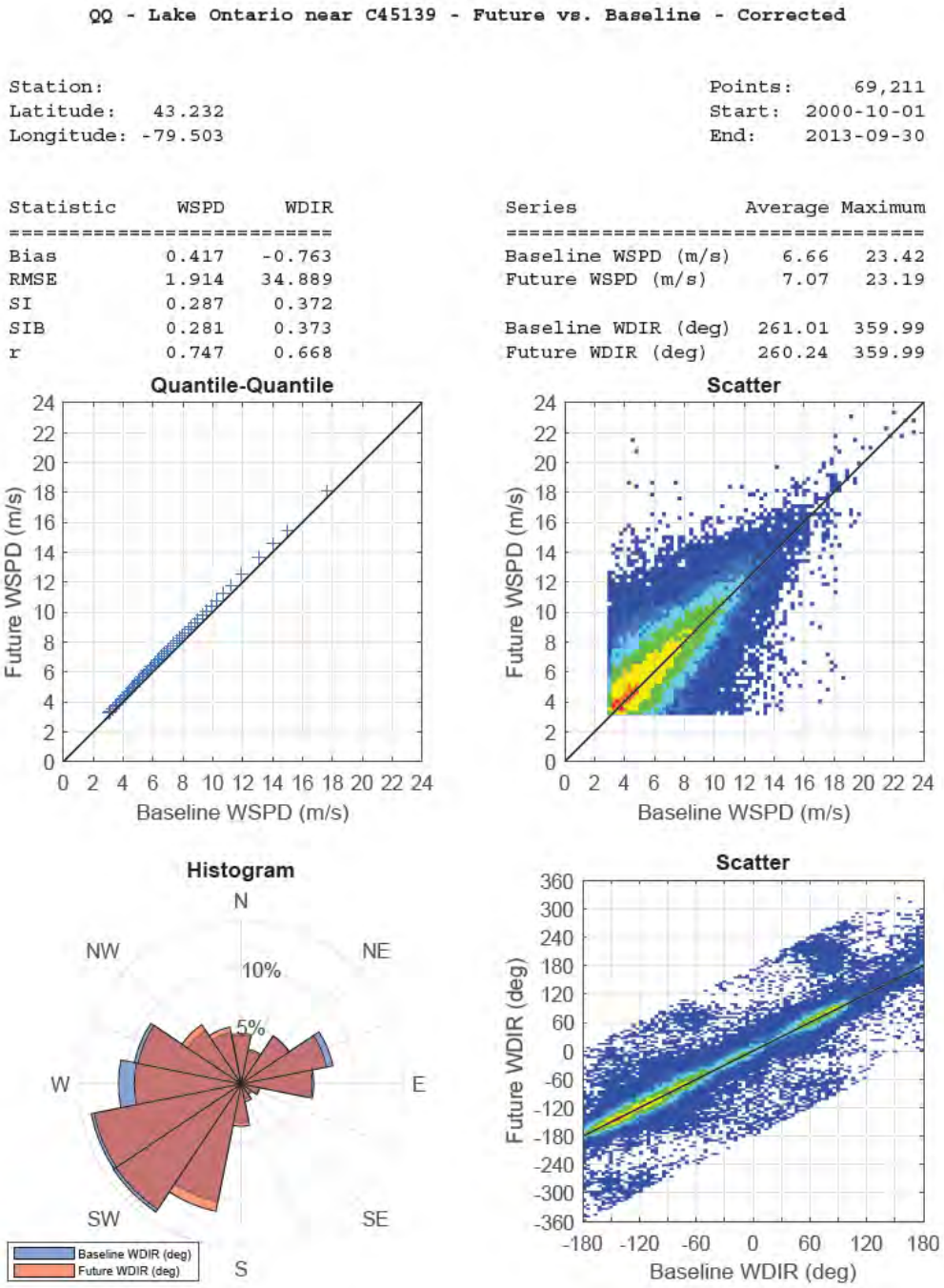

Figure 4.5: Comparison of baseline and future wind conditions near buoy C45139 on Lake Ontario.

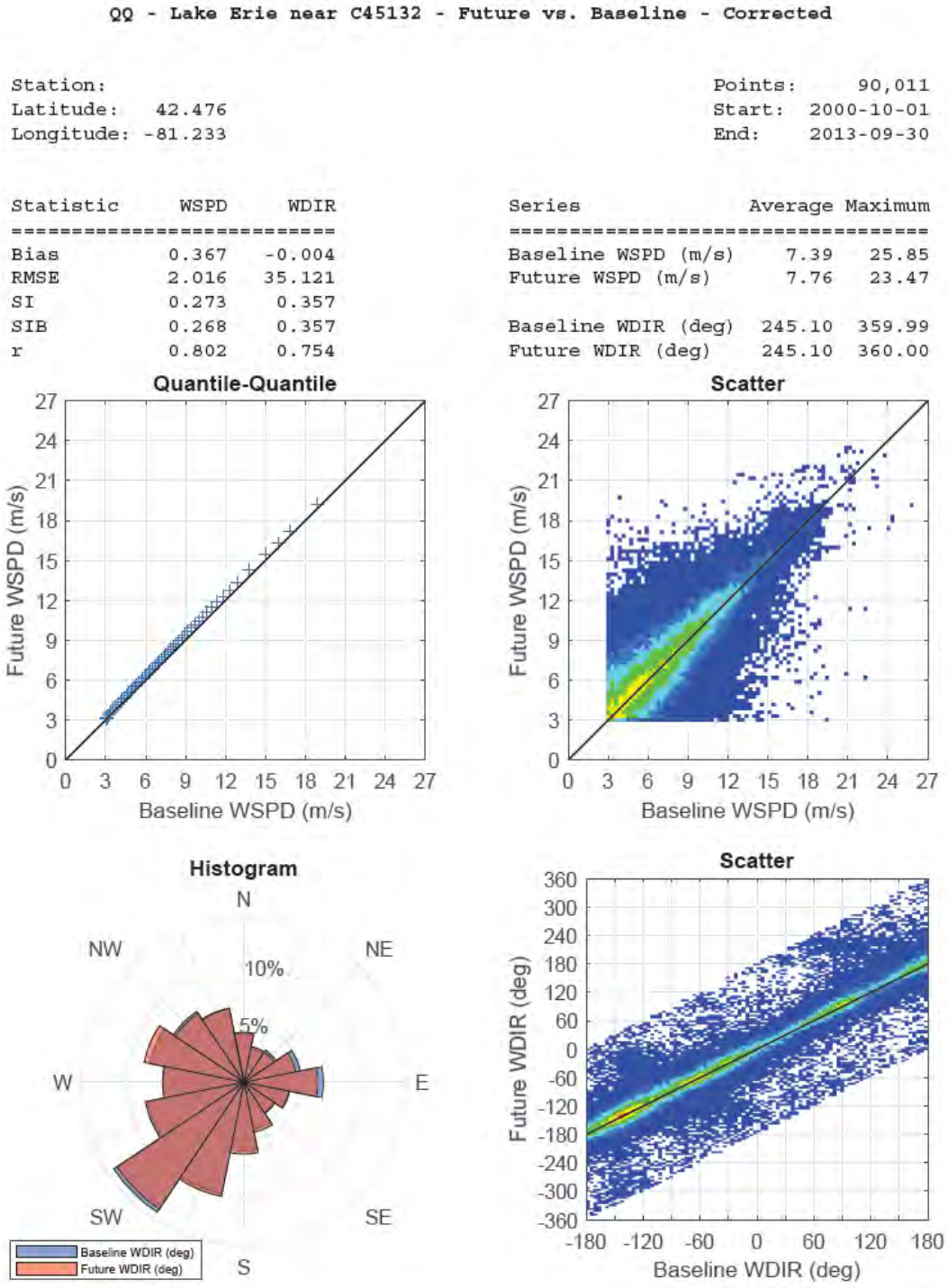

Figure 4.6: Comparison of baseline and future wind conditions near buoy C45132 on Lake Erie.

In general, the future winds are quite similar to baseline conditions as the speed and direction scatter plots show the highest concentration of points (shaded green, yellow and red) fall along the unity line. Correlation ('r') values for wind speed range from 0.74 to 0.80 and the RMSE is approximately 2.0 m/s. The Q-Q plot

showed a strong statistical similarity between wind speeds on both lakes with the future winds approximately 5% larger on average. Directionally, there is an increase in the frequency of winds from the south-southwest and northwest on Lake Ontario for the future condition, and an increase from the west-northwest and other southerly directions on Lake Erie. There are less frequent winds from the east, west and southwest compared with the baseline condition.

The findings from the comparative analysis suggests that the change in wave climatology will not be significant given how similar the future wind fields are to the baseline condition.

4.4 MIKE21 Model Calibration

The wave and hydrodynamic models were calibrated against select storms from the top fifteen events on each lake. Various model components such as, resolution, forcing inputs, and parameters were considered during model development, including, wind, friction, radiation stresses and ice. It should be noted however that this task was not intended to be comprehensive, but rather a high-level comparison with measured data to ensure the model was generating reasonable results for the purposes of this study, which was to examine the relative change in wave and water level conditions under one future wind and ice regime scenario.

A comparison of the measured and modelled peak wave height and surge levels on Lake Ontario and Lake Erie are presented in Table 4.1 and Table 4.2, respectively. The percent error was calculated by subtracting the predicted results from measured data and dividing the difference by the measured data. A negative value means the model overestimated the measured value. Timeseries of measured and modelled wave and surge results are presented in Appendix A.

Table 4.1: Comparison of measured and modelled peak wave height and surge on Lake Ontario.

Storm Rank	1	2	3	4	5	6	7	8	9	10	11	12	13	14	15	Mean
Wave Buoy C45139																
Hmo Modelled (m)	3.83	3.40	4.21	2.98	1.85	3.26	2.71	3.50	3.99	3.96	2.28	2.19	3.28	2.82	2.02	
Hmo Observed (m)	N/A	N/A	2.67	N/A	N/A	N/A	N/A	N/A	3.05	N/A	N/A	N/A	3.18	N/A	N/A	
Percent Error			**-58%**						**-31%**				**-3%**			**-30%**
Wave Buoy 45012																
Hmo Modelled (m)	2.70	2.55	2.89	1.97	2.75	2.96	2.50	5.05	4.55	3.65	4.10	4.10	2.91	2.38	5.51	
Hmo Observed (m)	N/A	N/A	2.55	N/A	N/A	N/A	N/A	N/A	3.69	N/A	N/A	N/A	N/A	N/A	N/A	
Percent Error			**-13%**						**-23%**							**-18%**
Toronto Gauge (13320)																
Surge Modelled (m)	0.16	0.13	0.12	0.15	0.09	0.12	0.10	0.15	0.05	0.12	0.14	0.13	0.09	0.08	0.15	
Surge Observed (m)	0.15	0.20	0.12	0.22	0.10	0.12	0.17	0.20	0.08	0.10	0.15	0.15	0.08	0.06	0.18	
Percent Error	**-5%**	**36%**	**1%**	**33%**	**6%**	**0%**	**41%**	**27%**	**38%**	**-19%**	**4%**	**11%**	**-14%**	**-32%**	**19%**	**10%**
Burlington Gauge (13150)																
Surge Modelled (m)	0.27	0.25	0.26	0.27	0.13	0.22	0.15	0.28	0.13	0.29	0.19	0.14	0.22	0.17	0.17	
Surge Observed (m)	0.29	0.43	0.26	0.26	0.07	0.57	0.21	0.26	0.20	0.40	0.16	0.16	0.16	0.25	0.21	
Percent Error	**7%**	**42%**	**0%**	**-4%**	**-84%**	**61%**	**29%**	**-9%**	**37%**	**27%**	**-20%**	**10%**	**-34%**	**34%**	**17%**	**8%**

Percent Error = (Observed-Modelled)/Observed *100

Table 4.2: Comparison of measured and modelled peak wave height and surge on Lake Erie.

Storm Rank	1	2	3	4	5	6	7	8	9	10	11	12	13	14	15	Mean
Wave Buoy C45132																
Hmo Modelled (m)	4.41	3.38	2.85	2.07	2.24	3.51	2.84	3.83	2.78	3.11	4.16	4.44	3.76	2.38	3.16	
Hmo Observed (m)	N/A	N/A	2.87	N/A	N/A	3.62	N/A	N/A	3.74	4.13	3.37	N/A	N/A	4.52	2.84	
Percent Error			**1%**			**3%**			**26%**	**25%**	**-23%**			**47%**	**-11%**	**10%**
Wave Buoy 45005																
Hmo Modelled (m)	2.83	2.49	2.31	2.16	2.79	2.32	1.50	2.59	2.01	2.32	2.92	2.92	2.47	1.73	2.74	
Hmo Observed (m)	N/A	N/A	N/A	3.14	N/A	2.06	N/A	N/A	1.76	2.70	3.08	N/A	N/A	3.23	3.23	
Percent Error				**31%**		**-13%**			**-14%**	**14%**	**5%**			**46%**	**15%**	**12%**
Erieau Gauge (12250)																
Surge Modelled (m)	0.21	0.09	0.19	0.12	0.17	0.06	0.16	0.13	0.17	0.11	0.08	0.24	0.23	0.13	0.31	
Surge Observed (m)	0.20	0.10	0.10	0.12	0.23	0.08	0.11	0.17	0.06	0.07	0.08	0.23	0.31	0.16	0.27	
Percent Error	**-5%**	**12%**	**-88%**	**3%**	**27%**	**23%**	**-49%**	**24%**	**-178%**	**-62%**	**5%**	**-4%**	**26%**	**16%**	**-14%**	**-18%**

Percent Error = (Observed-Modelled)/Observed *100

In general, the model overestimated wave heights and surge levels for some storm events and underestimated other events. The timeseries comparisons presented in Appendix A showed that the model does capture the trends observed in the measured data and it is important to recognize the models are driven with modelled wind fields, which inherently add another level of uncertainty.

The mean percent error ranged from 8% to -30% for all comparisons, the maximum error associated with a specific event ranged from 61% to -84% for Lake Ontario and 47% to -178% for Lake Erie. Most of these larger errors are associated with surge comparisons that are less than 20 cm, particularly at the Toronto and Erieau gauges; the exception is Storm 6 at the Burlington gauge (13150) where the model underpredicted the 0.57 m surge event by 61%. Testing showed that the model could not match the surge value of that event regardless of the parameters tested suggesting the wind conditions may not capture this event well.

With respect to waves, not all storm events were captured at the buoys, so information was limited, however, the model consistently overestimated waves on Lake Ontario by 18% to 30% based on the mean percent error. A high-level review of the WRF winds against other wind datasets such as NCAR's Climate Forecast System Reanalysis (CFSR) data showed a difference in the predicted winds that may explain the overestimation in wave height and uncertainty associated with different modelled datasets. This is illustrated in Figure 4.7, which compares the wind speed of both the WRF and CFSR winds at a point on Lake Ontario during Storm Event No. 9 (October 30, 2012). Overall, the trend in wind speeds are similar but the WRF winds are stronger particularly during the peak of the event. This is reflected in the predicted wave heights as the WRF simulation overestimated the event compared to the waves generated using the CFSR winds, which more closely matched the measured data. The purpose of this discussion is to demonstrate that uncertainties exist in the model inputs that can impact the results but overall the model is able to capture the wave and hydrodynamic trends in these storm events.

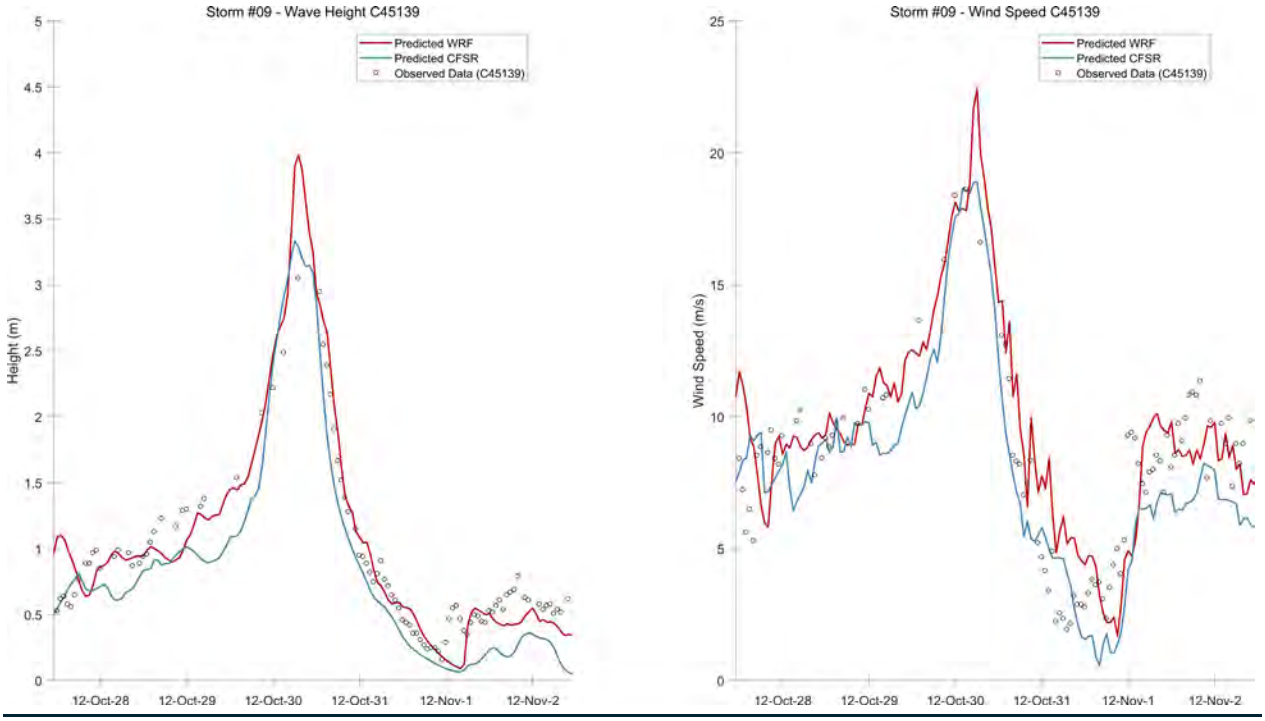

Figure 4.7: Comparison of WRF and CFSR winds and predicted waves for on Lake Ontario for Storm 9.

4.5 Summary of MIKE21 Model Results

The wave and hydrodynamic models were used to complete simulations of the fifteen storm events on Lake Ontario and Lake Erie for the baseline and future conditions. Ice maps were included in all runs with ice. The future scenarios assumed ice free conditions for all events to represent a worst-case condition.

In total, sixty simulations were completed. Each event was run for a period of six days, run times ranged from 20 hours for the wave simulations to 1.5 hours for the hydrodynamic simulations. Figure 4.8 shows a typical 2D map of model results from the wave model simulations. Wave and water level (surface elevation) data were extracted at two points offshore of the case study sites in a water depth of approximately 10 m; these locations are also shown in Figure 4.8. Note, LOP stands for “Lake Ontario Point” and LEP stands for “Lake Erie Point”. Additional points can be extracted as required to support the Stream 2.0 work.

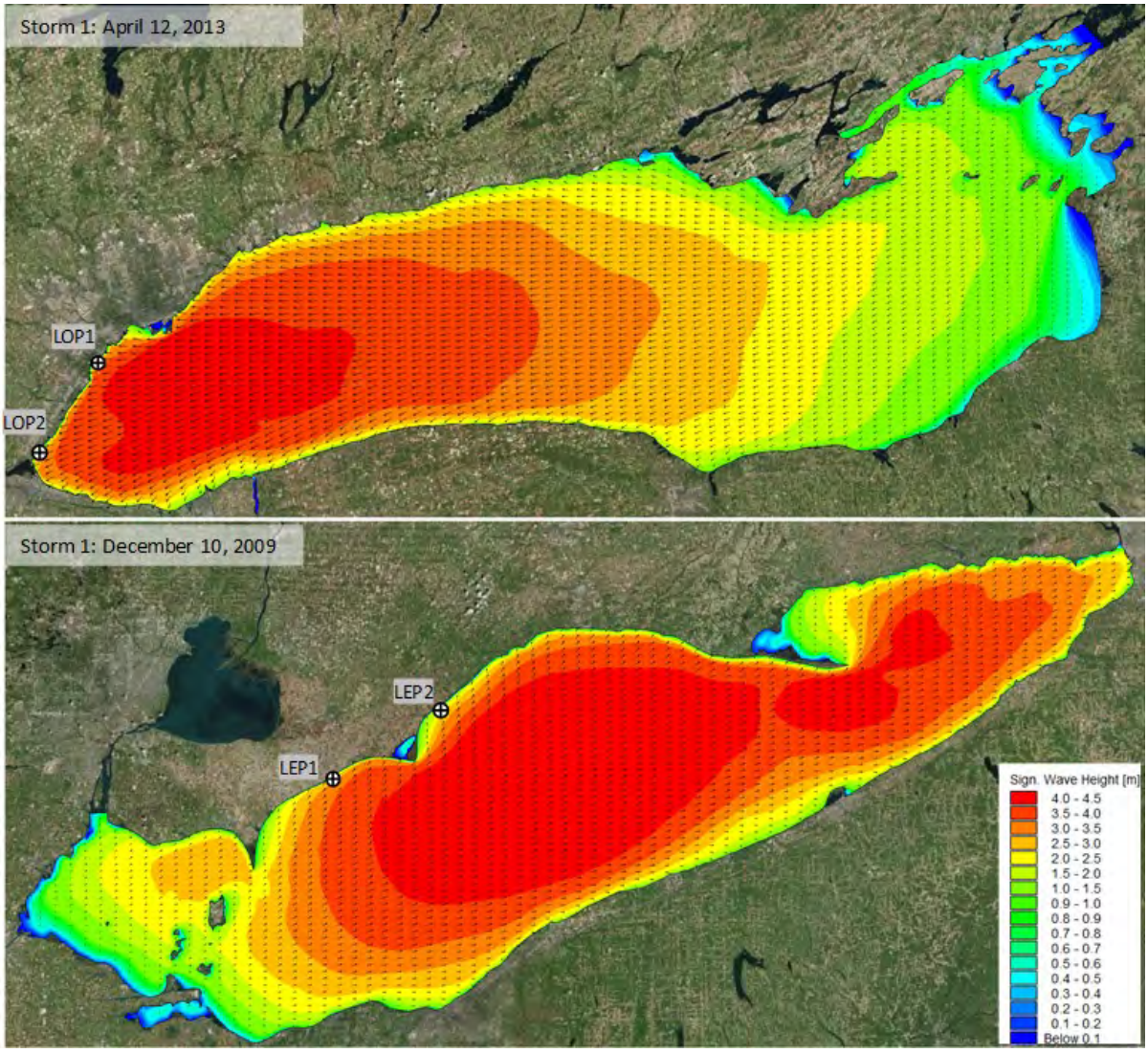

Figure 4.8: 2D map of wave height under baseline conditions and model result extraction locations

The peak wave and surge output from the baseline and projected future scenarios are summarized in Appendix B. Note that wave data were extracted at the LOP and LEP locations and surge levels were compared at the Toronto, Burlington and Erieau gauge locations.

A comparison of the predicted peak wave height at the extraction locations are illustrated in Figure 4.9 and Figure 4.10. Some winter storms generated a wave height of zero due to the existence of ice under baseline conditions. The largest increases and decreases in wave height and surge from the fifteen events are summarized in Table 4.3.

.

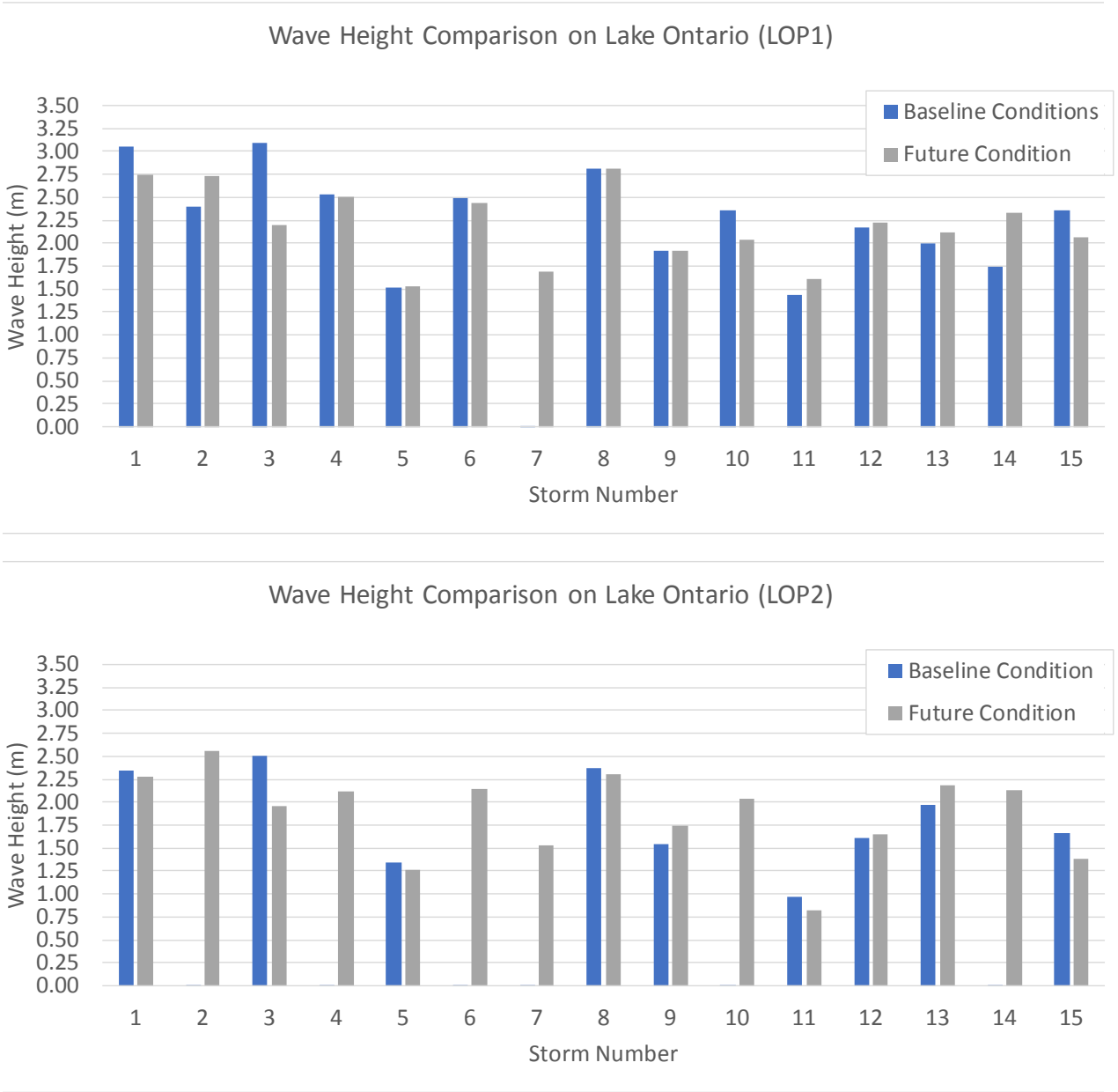

Figure 4.9: Predicted peak wave height on Lake Ontario under baseline and projected future conditions.

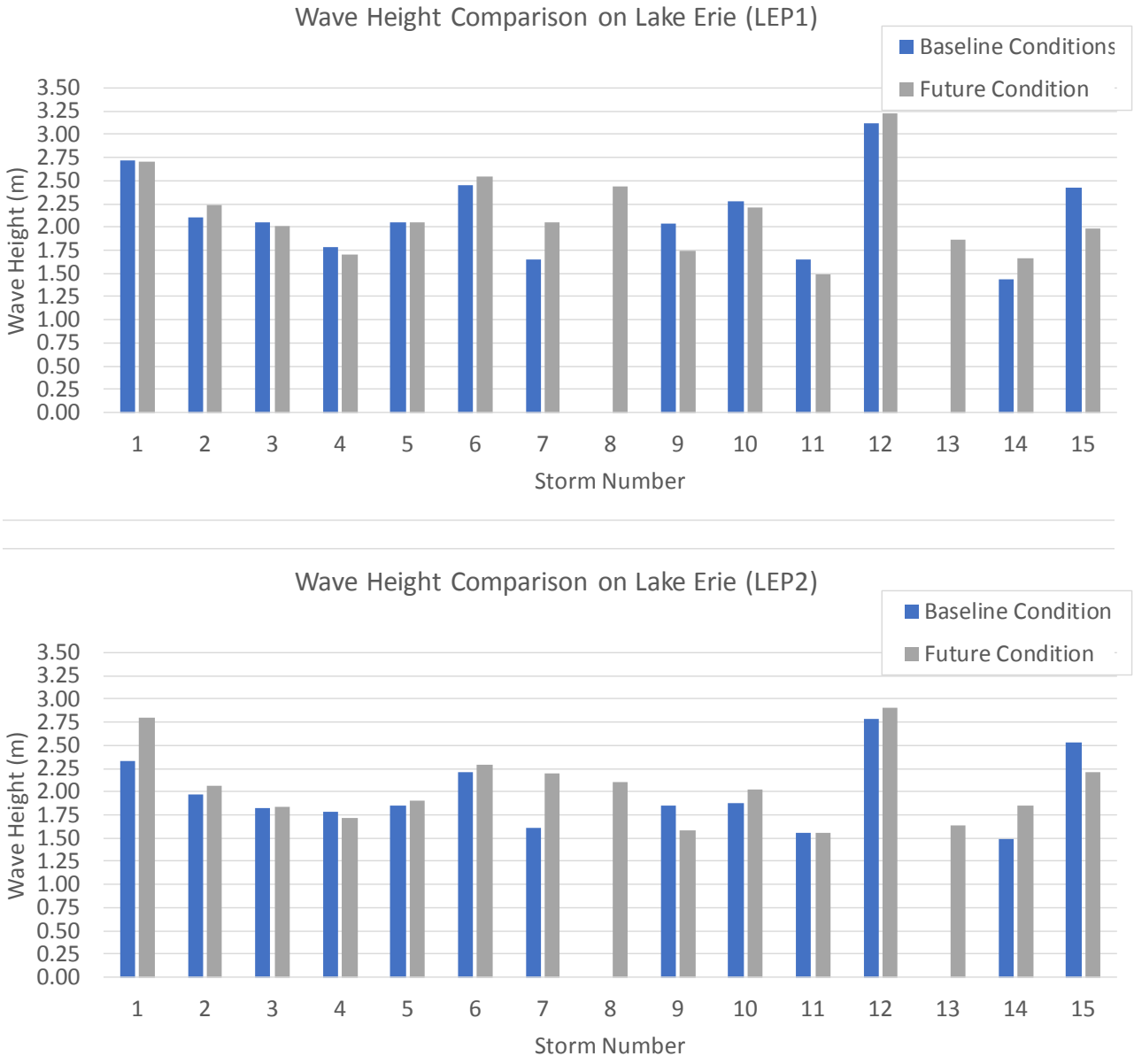

Figure 4.10: Predicted peak wave height on Lake Erie under baseline and projected future conditions.

Table 4.3: Summary of the largest increase and decrease in wave height and surge.

Reference Locations	Largest increase in future conditions compared to baseline	Largest decrease in future conditions compared to baseline
LOP1: Waves	+1.68 m (Storm 7)	- 0.90 m (Storm 3)
LOP2: Waves	+2.55 m (Storm 2)	-0.55 m (Storm 3)
Toronto: Surge	+0.05 m (Storm 14)	-0.02 m (Storm 3)
Burlington: Surge	+0.11 m (Storm 14)	-0.08 m (Storm 3)
LEP1: Waves	+2.43 m (Storm 8)	-0.45 m (Storm 15)
LEP2: Waves	+2.09 m (Storm 8)	-0.32 m (Storm 15)
Erieau: Surge	+0.08 m (Storm 1)	-0.11 m (Storm 15)

The following observations were based on the findings from the model results:

- The results showed no obvious trend with respect to wave and surge levels as the model predicted both larger and smaller wave and water level conditions in the future. This suggests that wind events in the future may not cause a significant change in wave and water level conditions on either lake based on the future emission scenario used for this study.
- There were several events under baseline conditions that resulted in zero wave heights offshore of the case study sites due to the existence of ice. Interestingly, Lake Ontario experienced more impact from ice at the extraction locations compared to Lake Erie, however, the study is limited to only fifteen storm events.
- Under future (ice free) conditions, the coastlines on both lakes would be impacted by all storm events simulated for this study. The results suggest that the disappearance of ice on the Great lakes may pose a bigger threat than wind with respect to wave climatology as the shorelines will be exposed to more storms on an annual basis.
- The average peak wave height for the fifteen events on Lake Ontario was 2.12 m (LOP1) and 1.09 m (LOP2) for the baseline condition and 2.20 m (LOP1) and 1.87 m (LOP2) for the future case. On Lake Erie, the average peak wave height was 1.85 m (LEP1) and 1.71 m (LEP2) for the baseline condition and 2.13 m (LEP1) and 2.05 m (LEP2) for the future condition. The increase in average wave height in the future is mainly due to the absence of ice.
- The results also showed that the change in surge levels is approximately ±0.11 m on the two lakes. The largest increase in surge occurred at the Burlington gauge on Lake Ontario, which makes sense given it is located near the west end of the lake and most storms are easterly. The Toronto gauge is east of the Burlington gauge and does not show a significant change in surge. Erieau is located towards the center of Lake Erie, the largest increase and decrease in surge relative to the baseline simulations was +0.08 m and -0.11 m, respectively.
- The large increase in wave heights that are presented in Table 4.3 reflects the potential change in wave conditions at the study site when ice is not present. The absence of ice during the winter months would mean the shorelines are subjected to more storms annually increasing the risk of flooding and erosion. A key limitation of this modelling approach is the number of storms that were considered (only fifteen per lake). A more robust method would be to simulate the entire thirteen-year period in order to capture all storm events and develop a more statistically relevant dataset. This is discussed in the following section.

5. WAVAD Wave Model Simulations 2000 to 2013

Additional wave modelling was completed using the deepwater wave model WAVAD to continuously simulate wave climatology from 2000 to 2013. The benefit of this approach is that all storm events are modelled over the thirteen-year period, which allows for a more detailed assessment of numerous wave events under future wind and ice regimes. The limitation to this modelling approach is that it cannot simulate shallow water wave effects such as refraction, diffraction, shoaling, reflection and breaking. This is the trade off between modelling specific events with a more computationally expensive nearshore spectral wave transformation model such as MIKE21 SW and simulating continuous wave conditions for long durations using a deepwater spectral wave model such as WAVAD. This model runs very quickly and has been widely and successfully used in various wave hindcasting studies, cyclone storm simulations on various ocean basins and extratropical cyclone events on the Great Lakes.

5.1 WAVAD Model Setup

WAVAD is a 2nd generation directional spectral wave model developed by Dr. Don Resio of the U.S. Army Corps of Engineers (USACE). Inputs to the model include a regular spaced grid defining the shoreline and lake bathymetry as well as spatially and temporally varying wind fields. Similar to the MIKE21 modelling task, the corrected WRF winds from 2000 to 2013 were interpolated to the WAVAD grid and used to drive the wave model. Lake bathymetry and shoreline data were obtained from NGDC. The resolution of the computational grid is 0.02 degrees (2200 m) for both lakes and an hourly timestep was used in the model.

It is important to consider the effects of ice cover when developing an accurate wave climatology for both lakes. Digital daily ice concentration maps from GLERL were used as an input to the model. These data were processed based on an ice concentration threshold of 30% and10%; that is, waves in grid cells with values of ice coverage greater than the threshold were removed from the wave simulation. This was accomplished by preventing both wave generation and wave propagation in model grid cells above the threshold. The WAVAD model was run for the thirteen-year baseline period using both thresholds; for context, the 10% concentration threshold represents more ice coverage on the lakes. The USACE uses 30% on the Great Lakes for the WIS hindcasts, re-running the wave model at 10% provides an upper envelope for ice coverage. These baseline model simulations, which include ice, were then compared against the future (wind) scenario, which assumes no ice during the winter months.

The model outputs standard parameters such as significant wave height, peak wave period and peak wave direction at pre-defined locations around the perimeter of both lakes. Figure 5.1 and Figure 5.2 show the WAVAD grid for Lake Ontario and Lake Erie along with the wave buoys used for model calibration. Similar to the MIKE21 model, this was not intended to be a comprehensive calibration but rather a high-level comparison to ensure the model is capturing the storms and adequately predicting wave heights on both lakes.

The primary objective of this task was to examine the change in wave energy under a future condition where ice free conditions exist on both lakes. While timeseries of hourly wave data from 2000 to 2013 is available offshore of each case study site to support the Stream 2.0 work, the focus of this task was to develop spatial maps showing the change in wave energy around the lake under ice free future conditions.

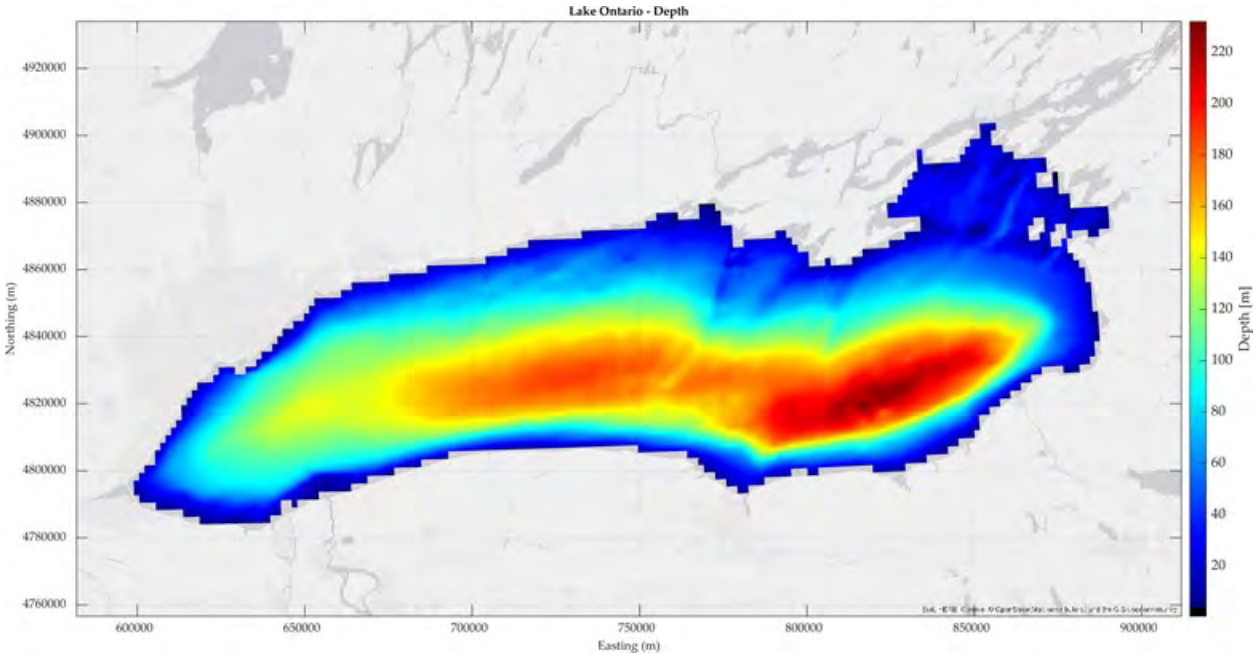

Figure 5.1: WAVAD model grid for Lake Ontario.

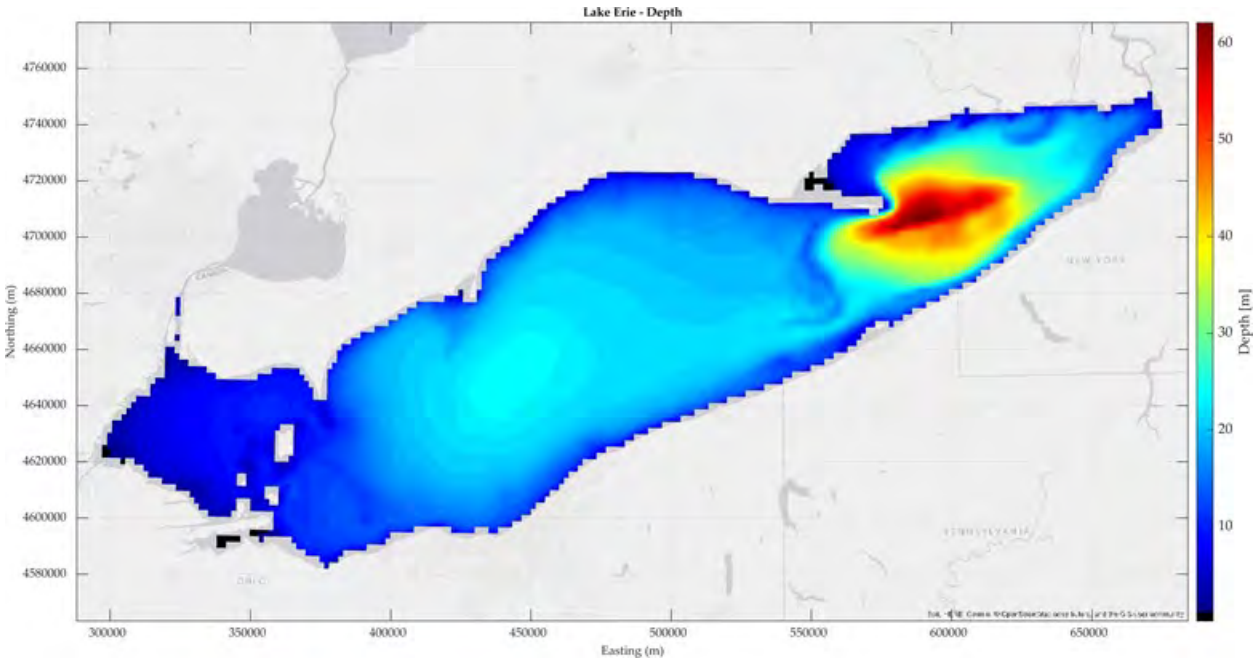

Figure 5.2: WAVAD model grid for Lake Erie.

5.2 WAVAD Model Calibration

The WAVAD model was calibrated to measured wave conditions at two buoy locations on each lake as summarized in Table 2.1. Hourly wave predictions were compared with available hourly measured data over the thirteen-year period, the results are summarized statistically in Appendix C in the form of scatter and Q-Q plots. Figure 5.3 and Figure 5.4 show timeseries comparisons of wave height at the buoy locations on each lake between September 1 and December 31, 2011; this time period was selected as both lakes were subjected to storms that showed up on the storm listings, so it was a particularly energetic period. Key statistics such as the mean, RMSE, and correlation coefficient for wave height is summarized in Table 5.1.

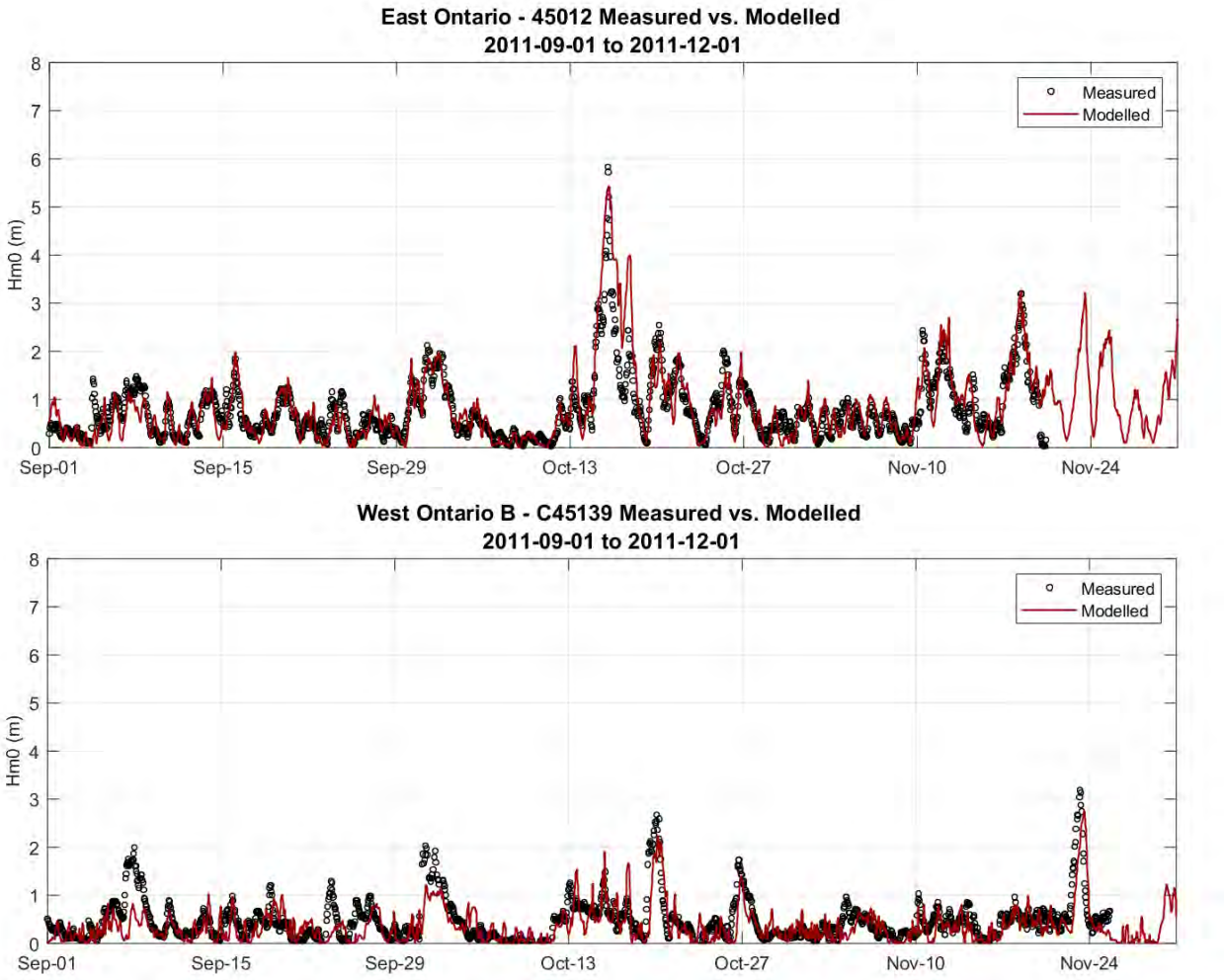

Figure 5.3: Timeseries comparison of wave height on Lake Ontario from Sept 1 to Dec 31, 2011.

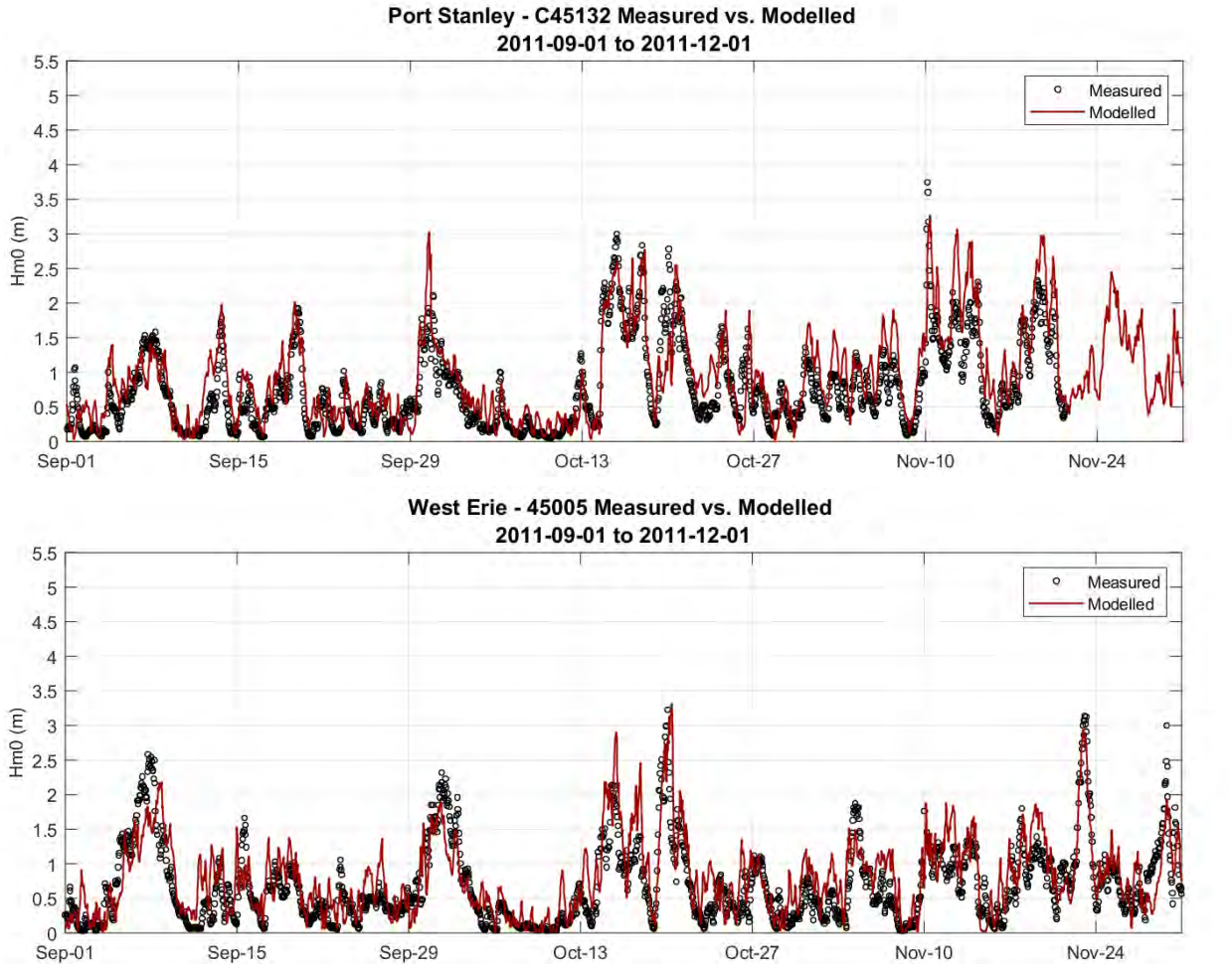

Figure 5.4: Timeseries comparison of wave height on Lake Erie from Sept 1 to Dec 31, 2011.

Table 5.1: Summary of key statistics for wave height.

	Bias (m)	Correlation (r)	RMSE (m)
Lake Ontario			
45012	0.08	0.81	0.39
C45139 A	-0.04	0.58	0.40
C45139 B	-0.03	0.41	0.34
Lake Erie			
45005	0.04	0.60	0.37
C45132	0.16	0.74	0.40

The results showed that the WAVAD model does capture the storm events and trends in wave height observed in the measured data with the model over predicting some events and underpredicting other events. The model compared well with measured data at buoy 45012 but underestimated the larger events at C45139 based on a review of the Q-Q plots for Lake Ontario. The correlation coefficient and RMSE ranged from 0.41 to 0.81 and 0.34 m to 0.40 m, respectively, based on the thirteen-year simulation period. For Lake Erie, the model tended to overestimate waves at C45132 and underestimate the larger wave events at 45002. The correlation coefficient and RMSE ranged from 0.60 to 0.74 and 0.37 m to 0.40 m as shown in Table 5.1.

The thirteen-year wave climate that was developed through the calibration process represents the baseline conditions. The WAVAD model was re-run using the future corrected winds and assuming no ice during the winter months, the results from a comparison of baseline and future conditions is discussed in the next section.

5.3 Summary of WAVAD Model Results

The WAVAD model was used to simulate hourly wave conditions on Lake Ontario and Lake Erie over the thirteen-year period for the baseline and future conditions. The baseline condition was completed as part of the calibration task. The projected future scenario was simulated assuming ice free conditions on both lakes to represent a worst-case condition.

The model output includes timeseries of hourly wave data offshore of the case study sites at the same locations used to examine the MIKE output (i.e. LOP1, LOP2, LEP1, and LEP2). Storm listings were generated at these locations and the results are summarized in Table 5.2.

Table 5.2: Summary of WAVAD storm listing results offshore of the project sites.

Hm0 (m)	**Number of Storms greater than Hm0 Threshold on Lake Ontario**			
	LOP1 Baseline	LOP1 Future	LOP2 Baseline	LOP2 Future
➢ 2.5 m	52	51	34	29
➢ 3.0 m	26	26	13	13
➢ 3.5 m	9	14	4	2
➢ 4.0 m	2	4	0	0
Max (m)	4.39	4.37	3.87	4
Hm0 (m)	**Number of Storms greater than Hm0 Threshold on Lake Erie**			
	LEP1 Baseline	LEP1 Future	LEP2 Baseline	LEP2 Future
➢ 2.5 m	120	157	129	175
➢ 3.0 m	34	50	49	74
➢ 3.5 m	3	5	11	15
➢ 4.0 m	0	0	1	2
Max (m)	3.79	3.88	4.28	4.35

A review of the WAVAD baseline results showed that there were approximately 52 and 34 storm events with waves greater than 2.5 m at LOP1 and LOP2, respectively. This number dropped to 51 and 29 under the future wind and ice scenario. The largest wave heights predicted at these locations was 4.39 m at LOP1 and 3.87 at LOP2 under baseline conditions. For the future case, the maximum wave height decreased slightly at LOP1 to 4.37 and increased by 3% to 4.0 m at LOP1.

Lake Erie experienced more storm events greater than 2.5 m compared with Lake Ontario based on the case study site locations. This trend was also observed in the WIS datasets used to develop the original storm listing for this study. The frequency of storms greater than 2.5 m on Lake Erie under baseline conditions was 120 at LEP1 and 129 at LEP2. These values increased by 30% at LEP1 (157 events) and 35% at LEP2 (175 events) under future conditions. The increased frequency in storms is due to the absence of ice in the future rather than increased wind speeds, this is based on the findings from the wind energy maps discussed below. The maximum wave height at LEP1 increased from 3.79 m for the baseline condition to 3.88 m in the future case. At LEP2, the maximum wave height was predicted to be 4.28 m and 4.35 m for the baseline and future conditions.

Note that the maximum wave heights generated by the WAVAD model were smaller than those predicted by WIS for both lakes and the top storm events do not necessarily match. A detailed comparison and investigation into the differences between model results was not completed as this study was not intended to be a comprehensive review of the WIS data. The objective of this task was to examine the relative change in wave climatology under future wind and ice regime over a thirteen-year period using the WAVAD model.

5.4 Wave Energy Maps

Wave energy maps were generated for each lake by applying the formula below to the hourly wave results at each grid within the computational domain.

$E = \frac{1}{16}\rho g Hm0^2$; where: ρ = density of water (m^3/s)

g = gravity (m/s^2)

Hm0 – wave height (m)

The cumulative wave energy E (presented in Joules/m^2) was calculated for three periods: 1) all seasons over the thirteen-year period, 2) ice season from December 1 to March 31, and 3) ice free season from April 1 to November 30. The energy predicted in the future was divided by the energy calculated under baseline conditions and then multiplied by 100 in order to generate 2D maps showing the percent increase in wave energy. These spatial maps, which are presented in Appendix D, are intended to highlight the relative change in wave energy around the lake under future conditions. Values greater than 100% represent an increase in wave energy. Spatial maps presenting the percent increase in wave energy for the winter (ice) period from December to March is shown in Figure 5.5 and Figure 5.6.

In general, the wave maps in Appendix D showed that during the ice-free season (April to November) there was very little change in wave energy on both lakes suggesting that winds in the future scenario did not have a significant impact on wave climatology.

During the winter months when ice is typically present there was an increase in wave energy in regions of both lakes where ice coverage occurs. This tends to be in the east end of Lake Ontario and over large regions of Lake Erie as shown in Figure 5.5 and Figure 5.6. The 10% ice concentration threshold increased the relative wave energy even more compared with the 30% threshold as more ice coverage is captured under the baseline runs which in turn reduces wave heights in those regions. Ice was not present for the future condition's simulation resulting in more wave energy in those regions where ice was previously present.

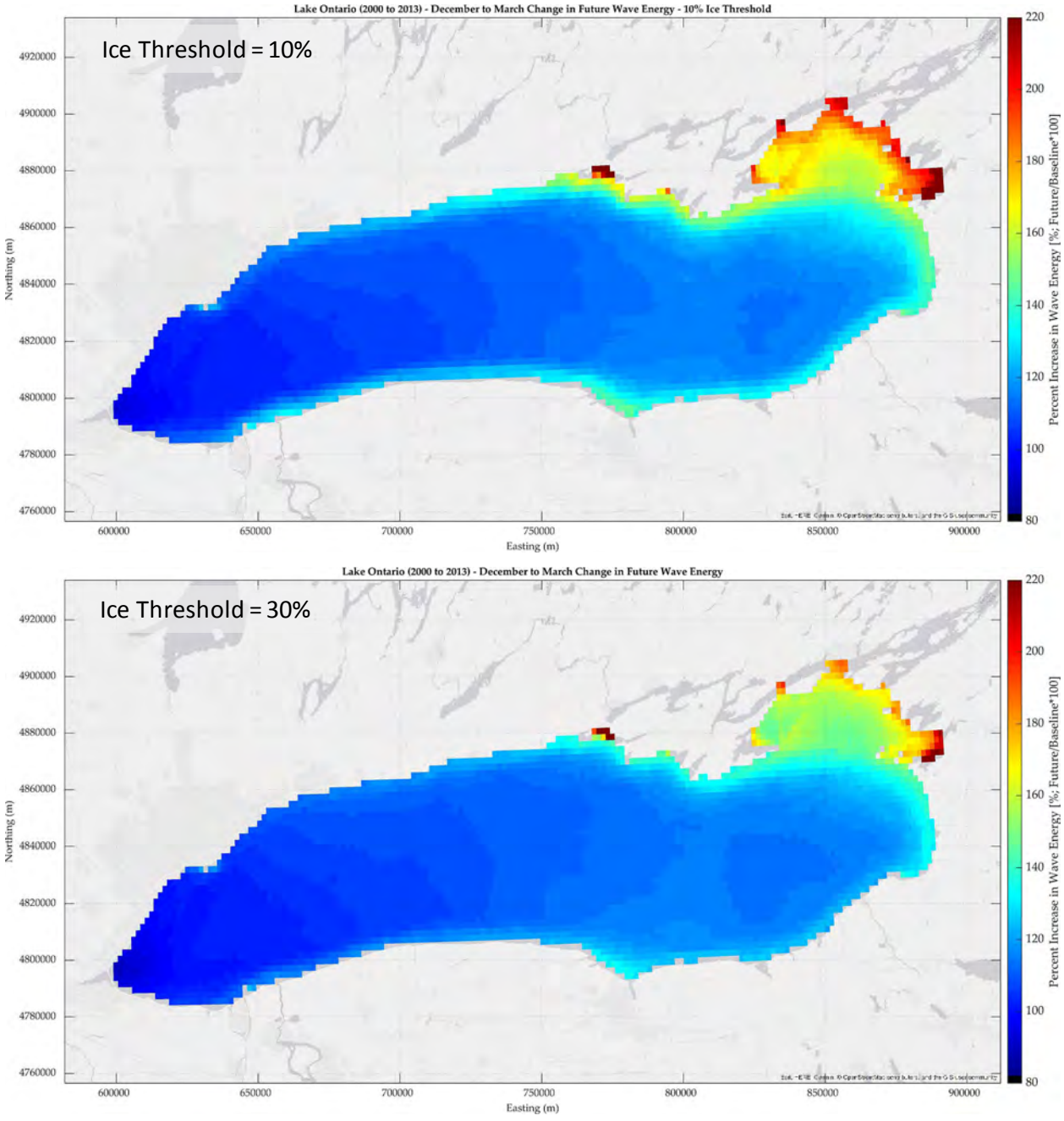

Figure 5.5: Percent increase in wave energy on Lake Ontario during the winter (ice) period for two ice concentration thresholds (2000-2013).

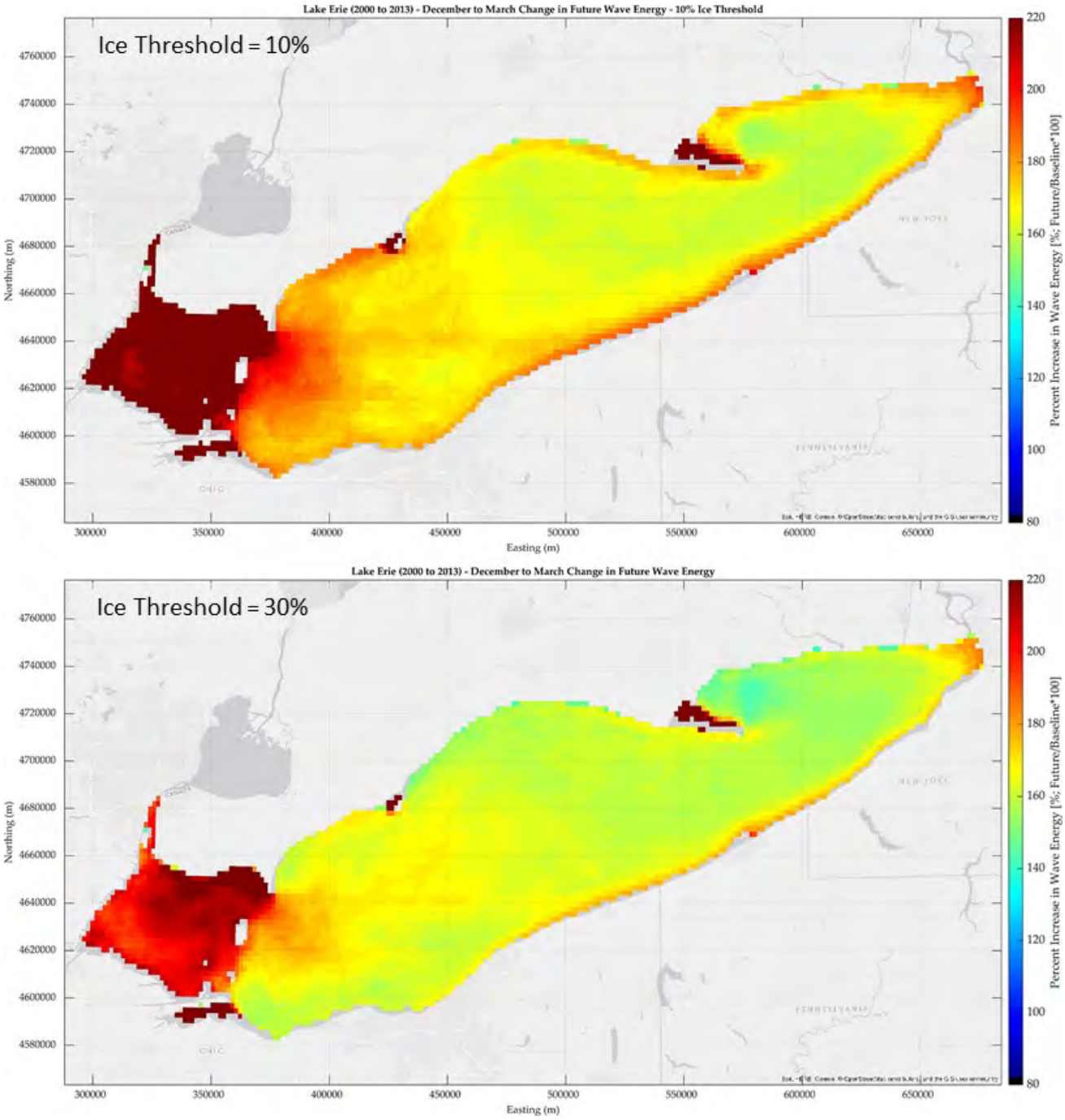

Figure 5.6: Percent increase in wave energy on Lake Erie during the winter (ice) period for two ice concentration thresholds (2000-2013).

The wave energy maps for Lake Ontario showed very little change in wave climatology in the west end of the lake; this is because the future wind scenario considered in this study does not significantly increase wave heights, and ice coverage in this area is minimal during the winter months. An increase in wave energy was observed in the east end of the lake where ice coverage is more frequent under baseline conditions. During the winter months, future wave energy increased by as much as 170% in this region with higher values near shore.

The maps developed for Lake Erie showed an increase in wave energy lake-wide, including the Chatham-Kent shoreline where wave energy increased by approximately 150% to 200% depending on location and ice concentration threshold. Larger values were observed in Rondeau Bay, although these percentages are questionable as the model is not suited for small bays, particularly given the resolution of the WAVAD grid and the size of the bay and shallow bathymetry.

A key observation on both lakes was that any increase in wave energy occurred during the winter months and is due to the absence of ice in the future condition; the differences in wave energy were small during the ice-free periods. This means the shoreline is exposed to more storm events during the winter months, increasing the potential for erosion and flooding. It should also be noted however that the lowest lake levels typically occur during the winter months, which can offset the impact of waves, runup and inundation along the shoreline.

6. Conclusions

Wave and hydrodynamic models were developed for Lake Ontario and Lake Erie as part of an effort to examine the impact of future wind scenarios and ice regimes on wave climatology. NCAR developed two thirteen-year wind dataset using 2000 to 2013 as a baseline condition and then re-running this period and adding the CMIP5 ensemble mean of the high emission scenario to account for climate change.

Initially, the MIKE modelling system was used to simulate wave and hydrodynamic conditions on both lakes for fifteen storm events under baseline and projected future climate conditions. The USACE WIS wave hindcast dataset, which provides continuous hourly wave climatology on the Great Lakes from 1979 to 2014, was used to select the fifteen storm events. Measured water levels at select gauges were also analysed to provide information on surge levels at the case study sites as part of the Stream 2.0 work. The case study sites for Lake Ontario include the Credit Valley Conservation Authority shoreline and Burlington shoreline, both of which are located along the west end of the lake. The case study site for Lake Erie is the Chatham-Kent shoreline which is centrally located along the north shore.

An assessment of the wind datasets showed that the future scenario considered in this study was not significantly different from the baseline condition suggesting the strength of storms (i.e. wind speed) may not increase significantly in the future. However, increased warming trends could result in the loss of ice on the Great Lakes in the future exposing the shoreline to more extreme events during the winter months and increasing the risk (and rate) of erosion and flooding. Based on this, the future scenarios were run assuming ice free conditions to generate an upper limit (worst case) condition.

The MIKE models were calibrated to select wave and water level data using the fifteen storm events. Digital ice concentration maps were defined when ice was present on the lakes for a storm event. Overall, the model captured the trends in wave height and water levels at select wave buoy and water level gauges on both lakes as the mean percent error was within ±30%. It should be noted that this was not intended to be a comprehensive calibration exercise. The objective was to confirm the model was generating reasonable results for the purpose of the study, which was to examine the relative change in waves and water levels under projected future climate conditions.

The MIKE models were run for the baseline and future storm conditions on both lakes. Model results from the production runs were extracted at two locations on each lake near the case study sites. This information is to be used to support the Stream 2.0 work although additional points can be extracted as required to meet the Stream 2.0 study objectives.

A review of the model results showed a relatively small change in wave height and surge levels for the future wind condition considered in this study. In some cases, the wave heights were lower in the future compared with baseline conditions. Large increases in wave heights were observed for those storm events that occurred during the winter months when ice was present on the lakes and around the study sites. For these runs, wave heights were zero under baseline conditions as ice was present at the extraction locations. Wave heights of 1.68 m to 2.55 m were predicted under future conditions with no ice. The results suggest that future storm events are not expected to generate significantly larger wave and surge levels as projected future winds were not much different than the baseline case. However, the loss of ice on the lakes will subject the shoreline to increased wave energy increasing the risk of structural damage, flooding and erosion.

A limitation of this numerical modelling exercise was that the number of storms simulated were limited to fifteen per lake. While the results provided insight on the impact of future wind and ice assumptions on wave climatology, it is difficult to comment on long term trends. To address this, Baird developed wave models of both lakes using the less computationally demanding deep-water spectral model WAVAD to simulate the entire

thirteen-year period under baseline and future conditions. The baseline condition was run twice assuming two different ice concentration thresholds of 30% and 10%. The ice sheet is larger for the 10% ice concentration threshold reducing the area impacted by waves. These results were compared against the future condition, which assumed no ice coverage.

Wave energy maps were generated to examine the change in wave climatology for different seasonal periods such as the winter months (ice period) and non-winter months (ice free period). These spatial maps show the percent increase in wave energy, which was calculated as the total energy from the future run divided by the total energy from the baseline run multiplied by 100.

The findings showed very little change in wave energy on both lakes during the non-winter months (generally less than 30%) confirming that the future wind scenario considered in this study does not significantly increase wave conditions on either lake during this seasonal period.

During the winter months, the percent increase in wave energy in the west end of Lake Ontario was small and (in some areas) less than baseline conditions. Wave energy increased in the east end of the lake by 170% with higher values near shore; this makes sense as ice growth is historically present in this region during the winter months. The percent increase in wave energy was also higher for the 10% ice concentration threshold compared to the 30% threshold as this assumption resulted in more ice coverage under baseline conditions. The case study sites for Lake Ontario are at the west end of the lake and therefore do not see much difference in wave climatology in the future.

There was a notable increase in wave energy on Lake Erie and along the case study shoreline of Chatham-Kent during the winter months. Historically, Lake Erie experiences more ice coverage than Lake Ontario, this resulted in an increase in wave energy of 150% to 200% along the Chatham-Kent shoreline if lake ice disappears in the future.

Note that the model output from these numerical simulations are available offshore of the case study sites in the form of hourly timeseries data of wave height, period and direction; this information will be used to support the Stream 2.0 work.

7. References

Rasmussen, R., and C. Liu. (2017). *High Resolution WRF Simulations of the Current and Future Climate of North America.* Research Data Archive at the National Center for Atmospheric Research, Computational and Information Systems Laboratory. https://doi.org/10.5065/D6V40SXP.

Risk Assessment, Mapping and Planning Partners. (2012). Final Report Lake Erie Storm Surge Study: FEMA Region V.

RWDI (2020). Adapting to the Future Storm and Ice Regime in the Great Lakes: Future Storm Frequencies.

Saha, S., Moorthi, S., Pan, H.-L., Wu, X., & Coauthors. (2010). The NCEP Climate Forecast System Reanalysis. *Bulletin of the American Meteorological Society*, *91*(8), 1015–1058. https://doi.org/10.1175/2010bams3001.1

Skamarock, W. C., Klemp, J. B., Dudhia, J., Gill, D. O., Barker, D. M., Wang, W., & Powers, J. G. (2005). *A description of the Advanced Research WRF Version 2* (NCAR Tech. Note NCAR/TN-468+STR). Retrieved from http://opensky.ucar.edu/islandora/object/technotes:479

W.F. Baird & Associates Ltd. (2012). FEMA Lake Ontario Wave and Surge Modeling.

Appendix A

MIKE21 Model Calibration

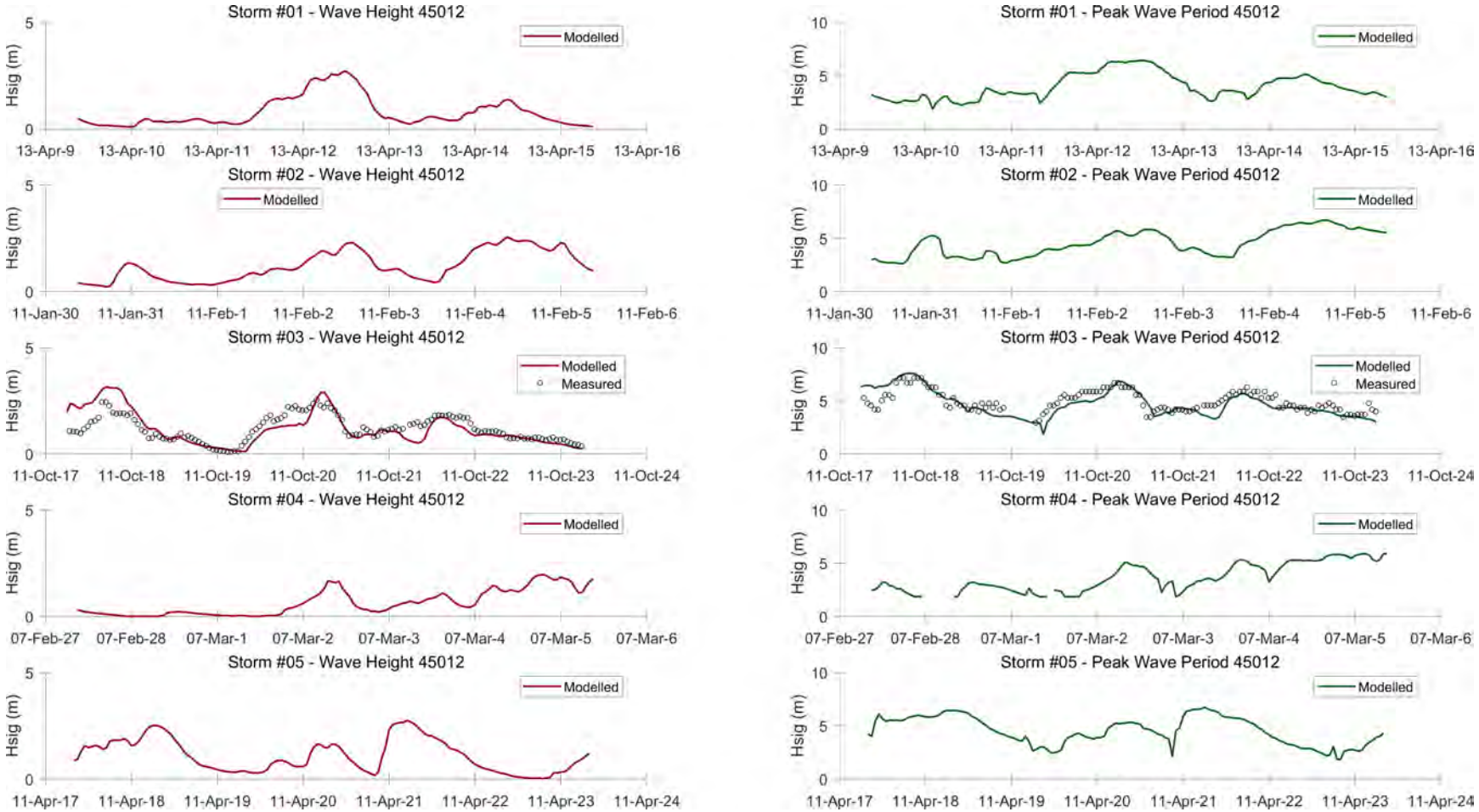

Figure A.1 MIKE21 spectral wave comparison on Lake Ontario at buoy 45012 for Storms 1 to 5.

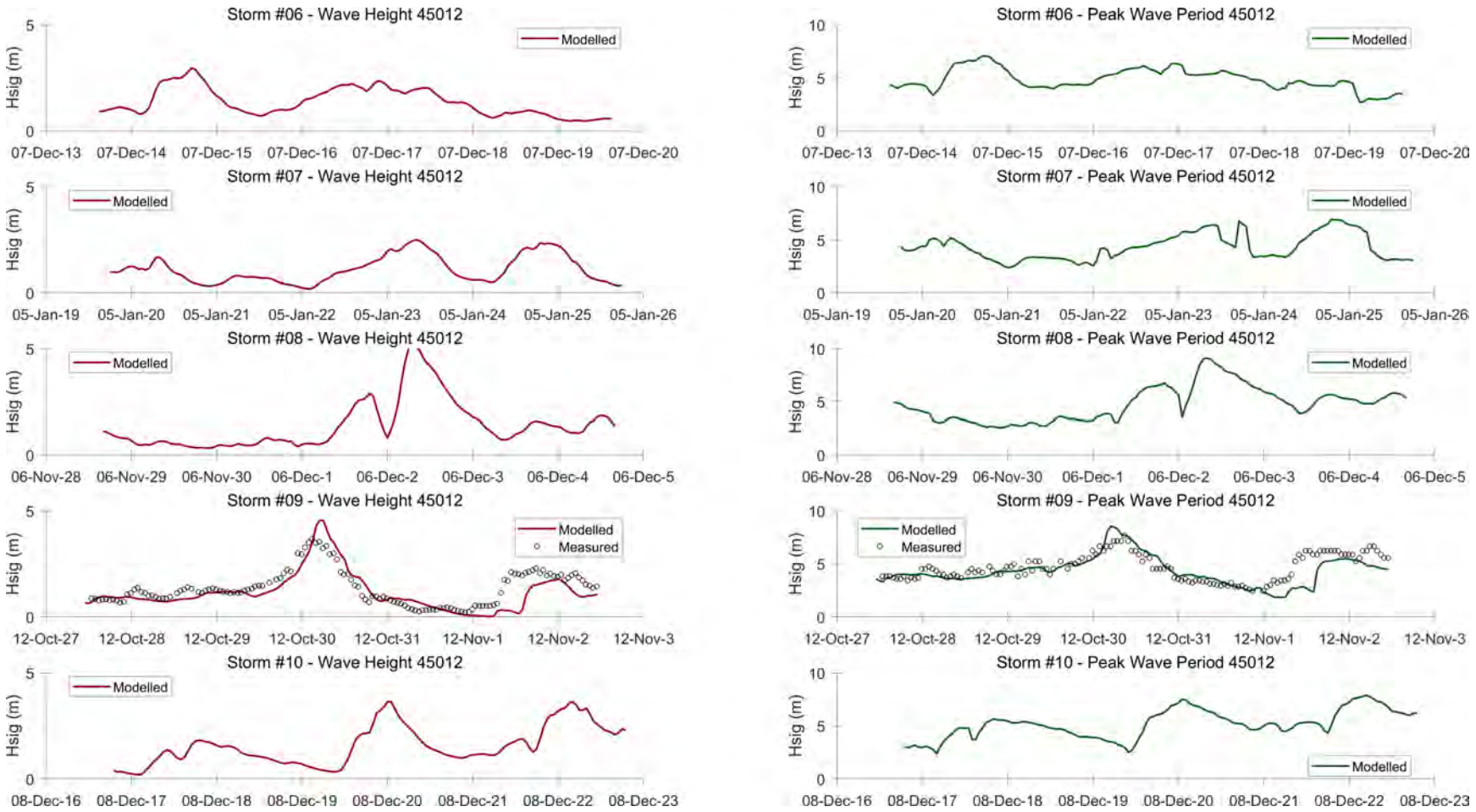

Figure A.2 MIKE21 Spectral wave comparison on Lake Ontario at buoy 45012 for Storms 6 to 10.

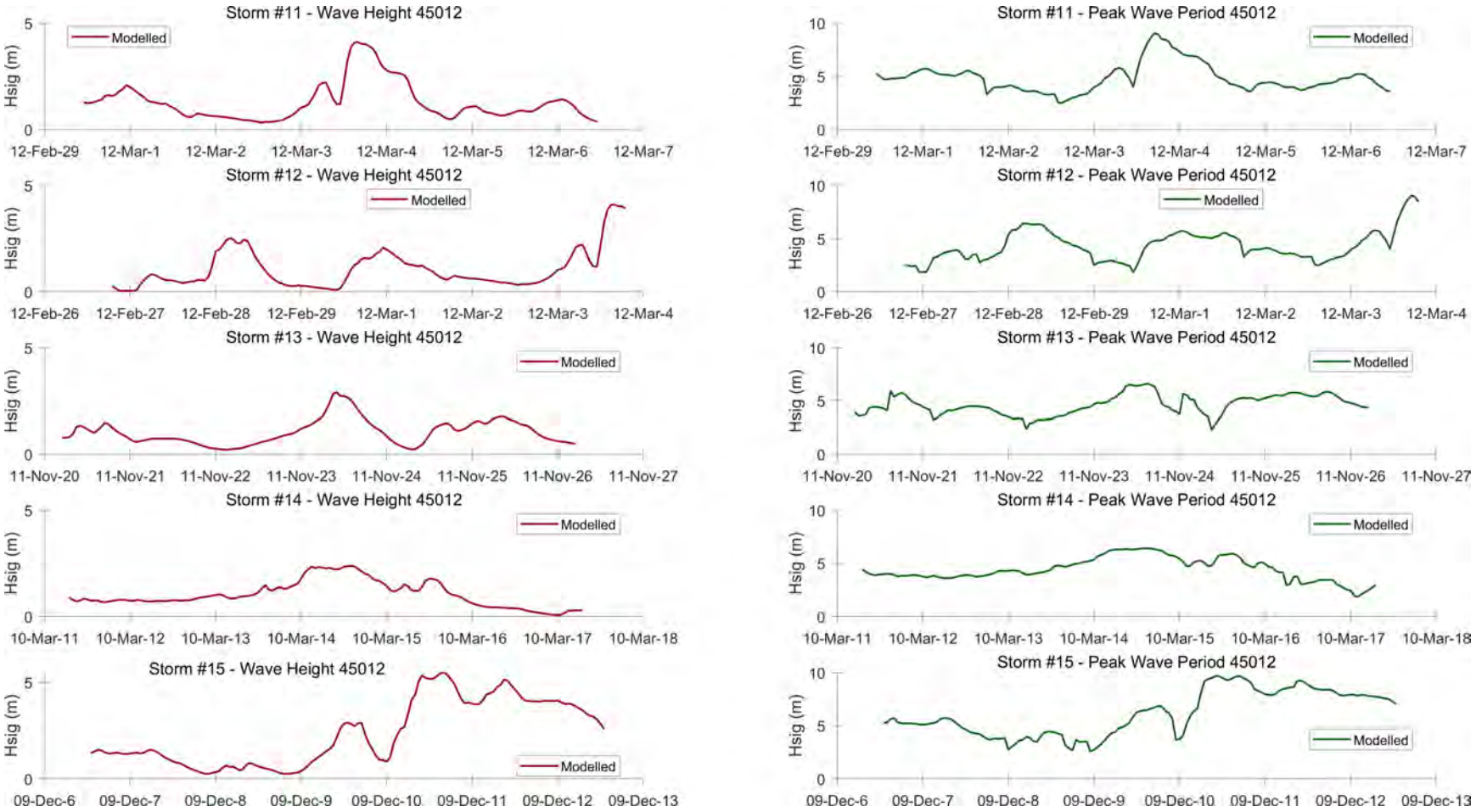

Figure A.3 MIKE21 Spectral wave comparison on Lake Ontario at buoy 45012 for Storms 11 to 15.

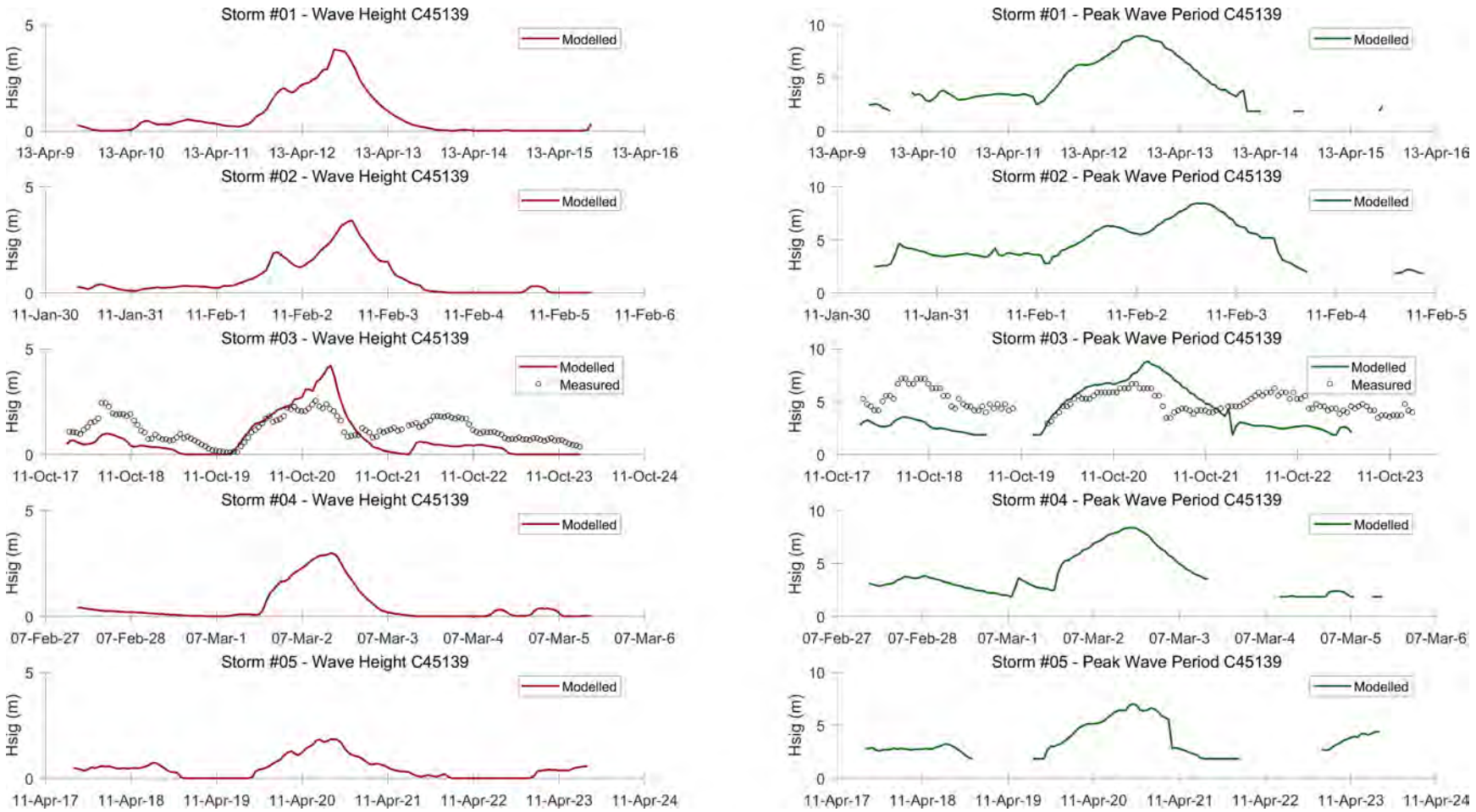

Figure A.4 MIKE21 Spectral wave comparison on Lake Ontario at buoy C45139 for Storms 1 to 5.

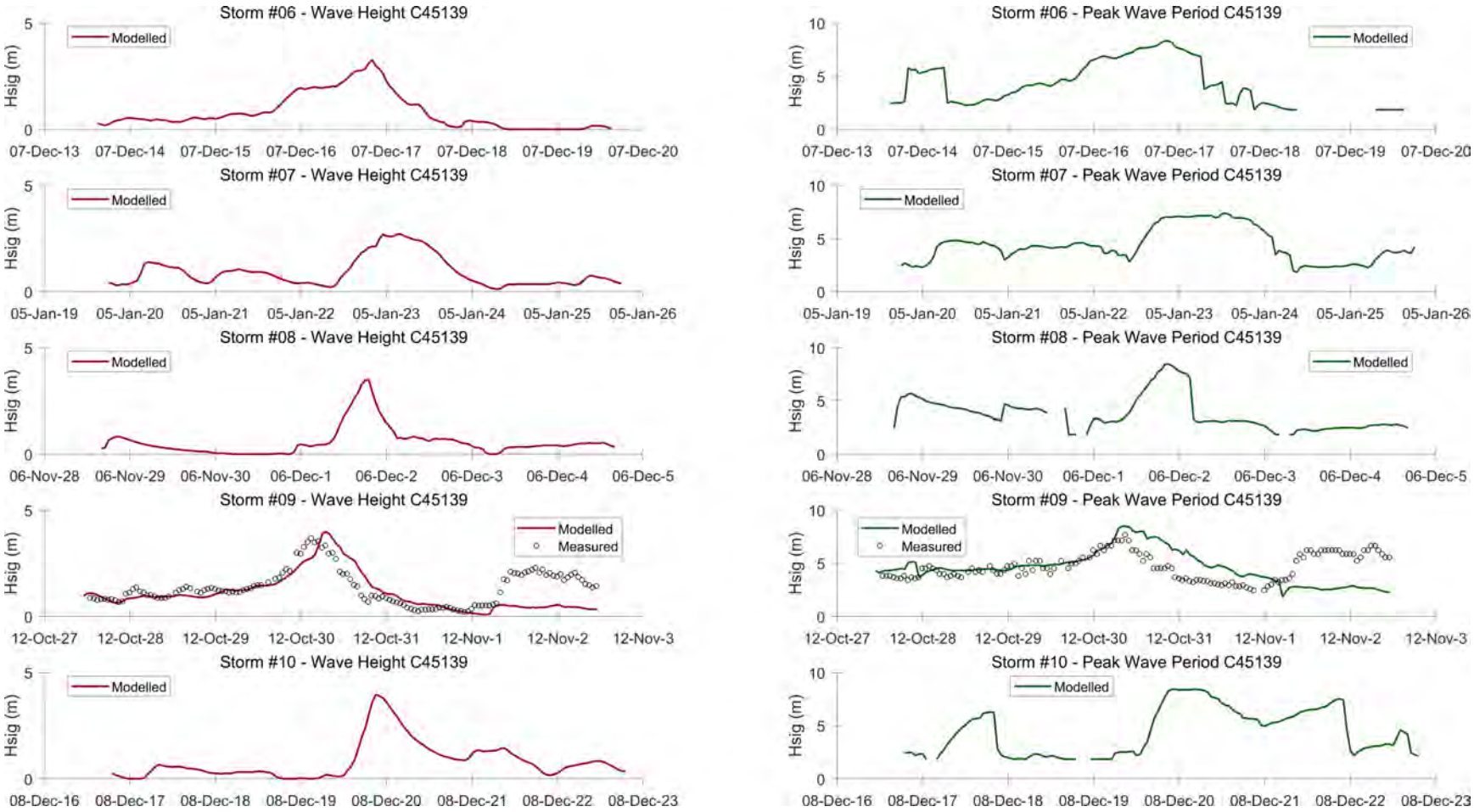

Figure A.5 MIKE21 Spectral wave comparison on Lake Ontario at buoy C45139 for Storms 6 to 10.

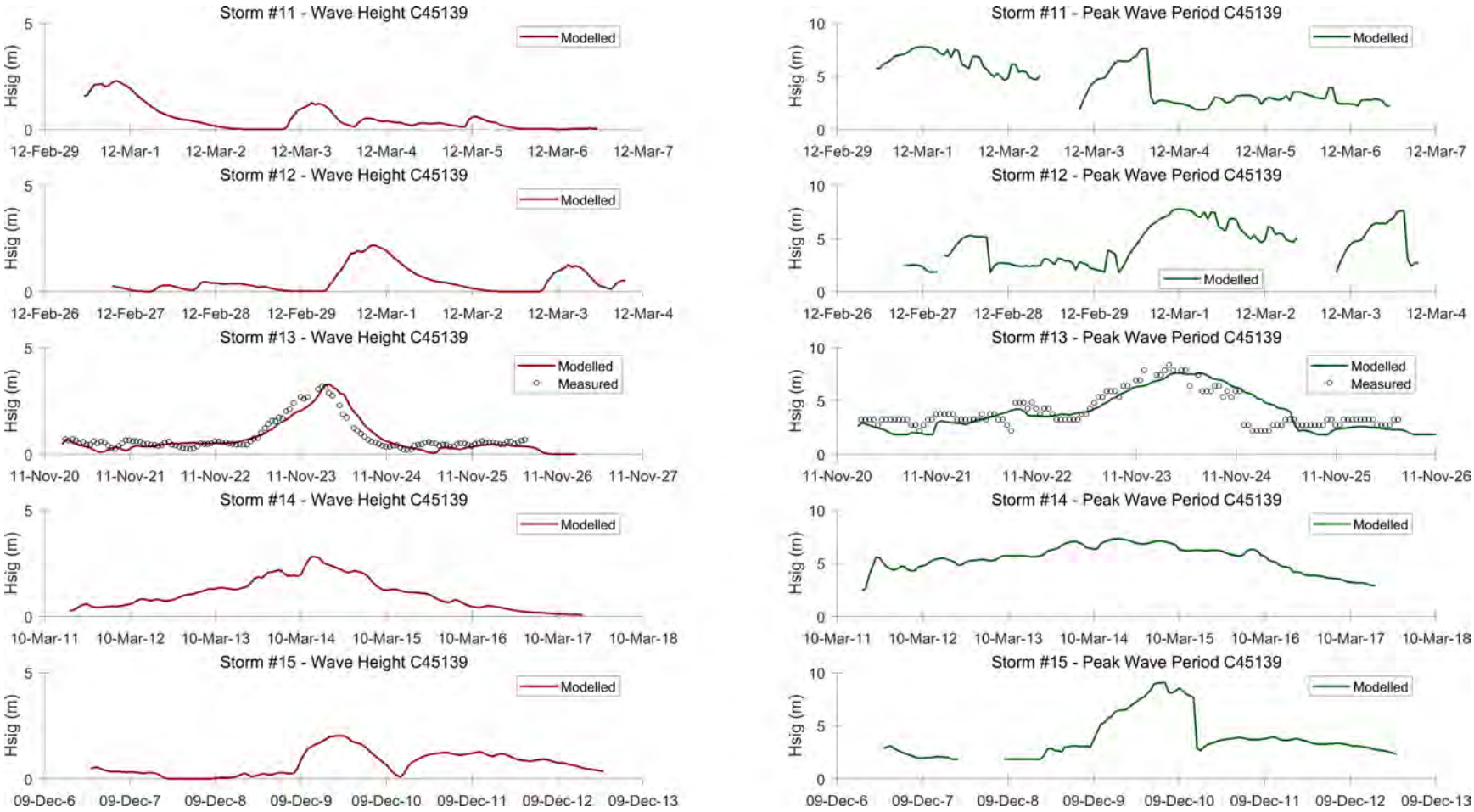

Figure A.6 MIKE21 Spectral wave comparison on Lake Ontario at buoy C45139 for Storms 11 to 15.

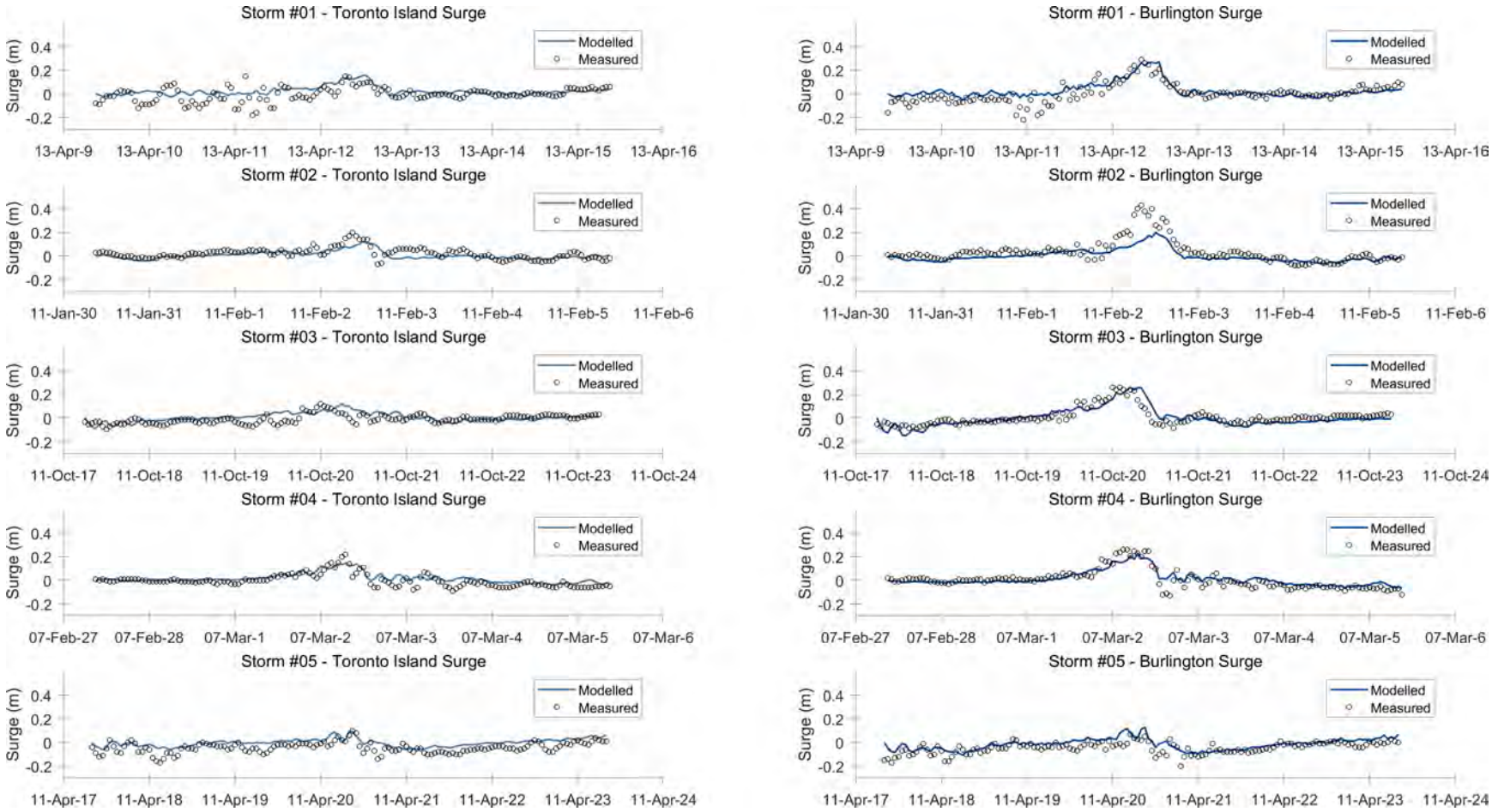

Figure A.7 MIKE21 surge comparisons on Lake Ontario at the Toronto (13320) and Burlington (13150) gauges for Storms 1 to 5.

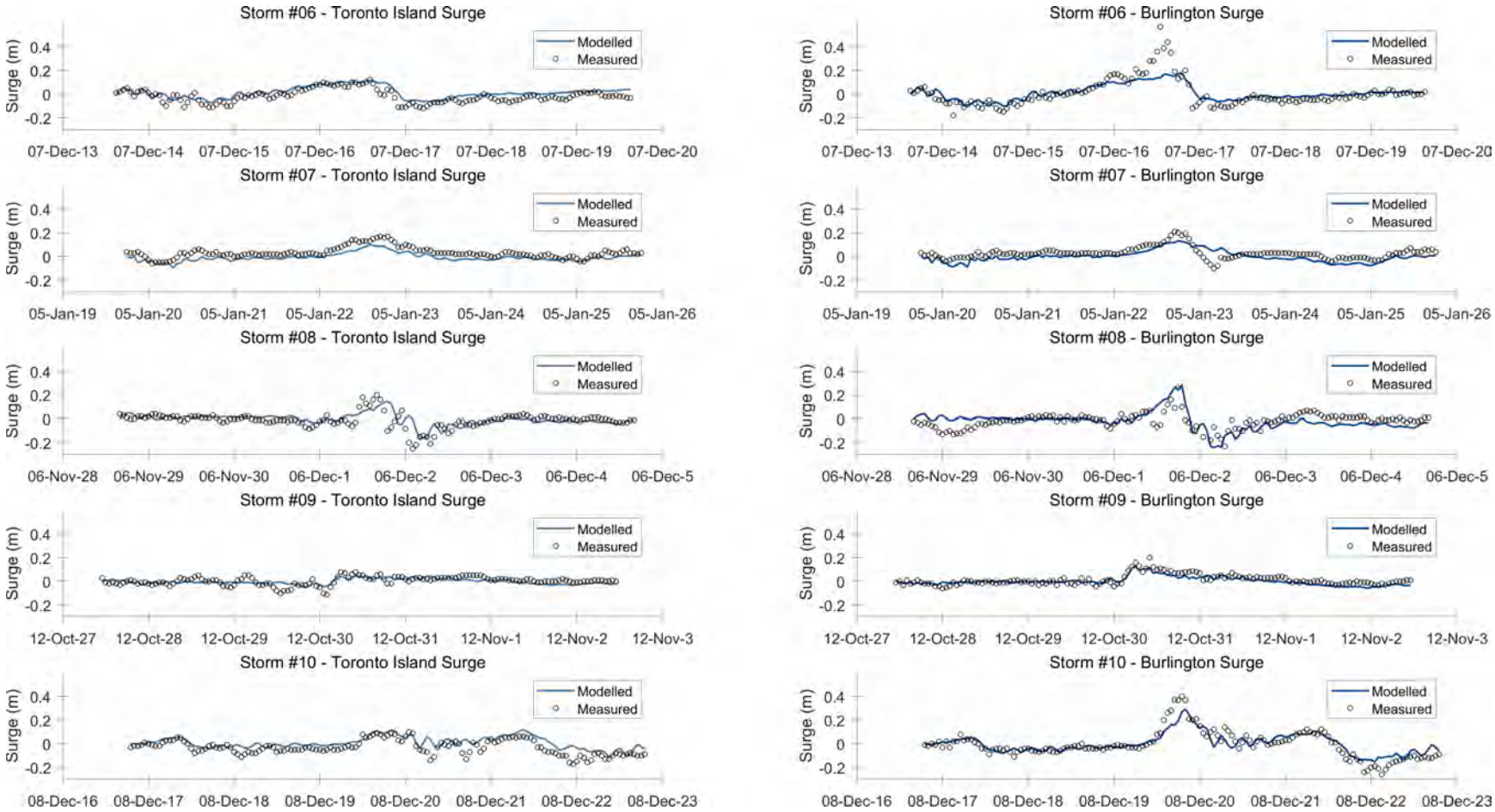

Figure A.8 MIKE21 surge comparisons on Lake Ontario at the Toronto (13320) and Burlington (13150) gauges for Storms 6 to 10.

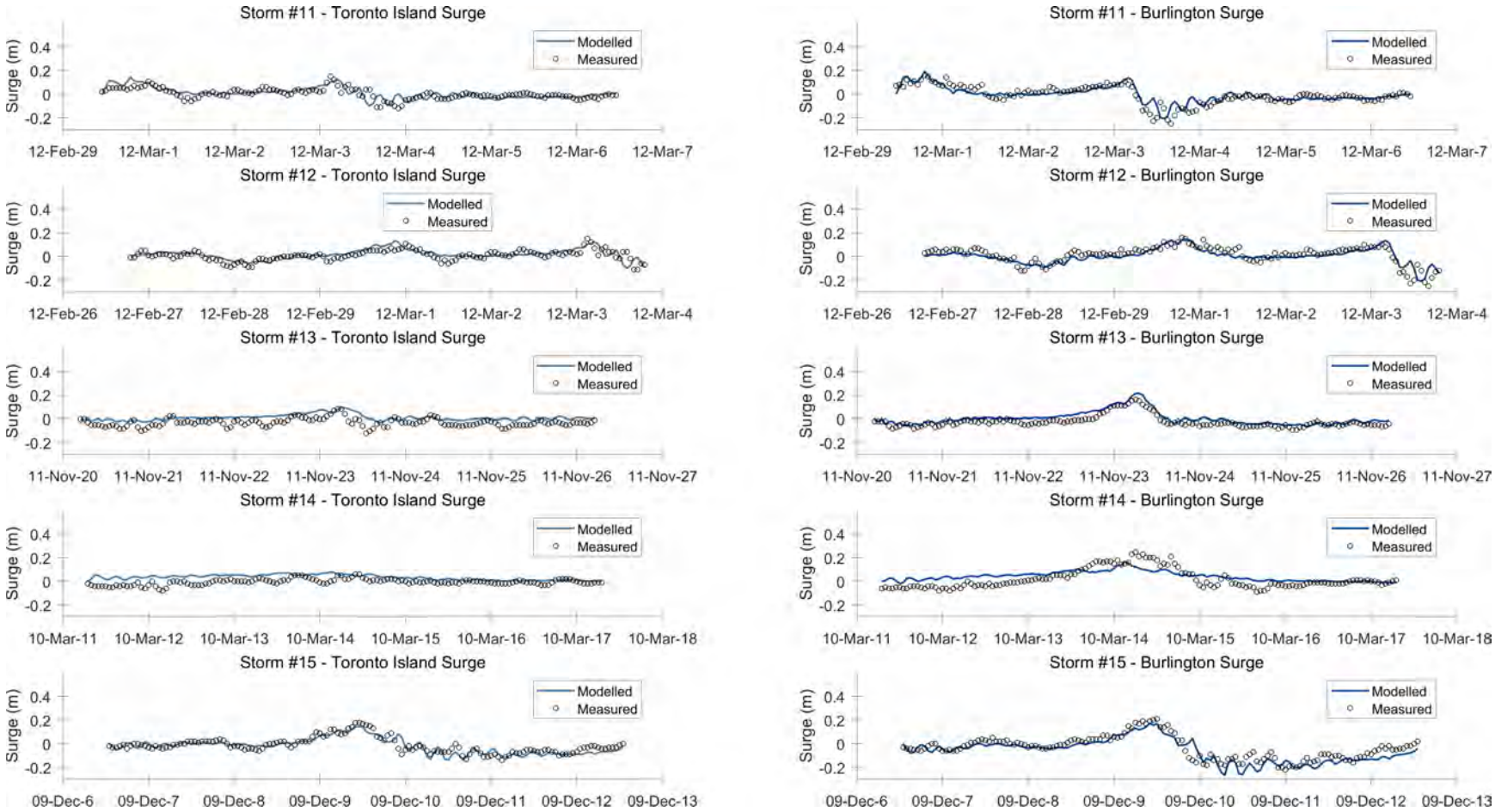

Figure A.9 MIKE21 surge comparisons on Lake Ontario at the Toronto (13320) and Burlington (13150) gauges for Storms 11 to 15.

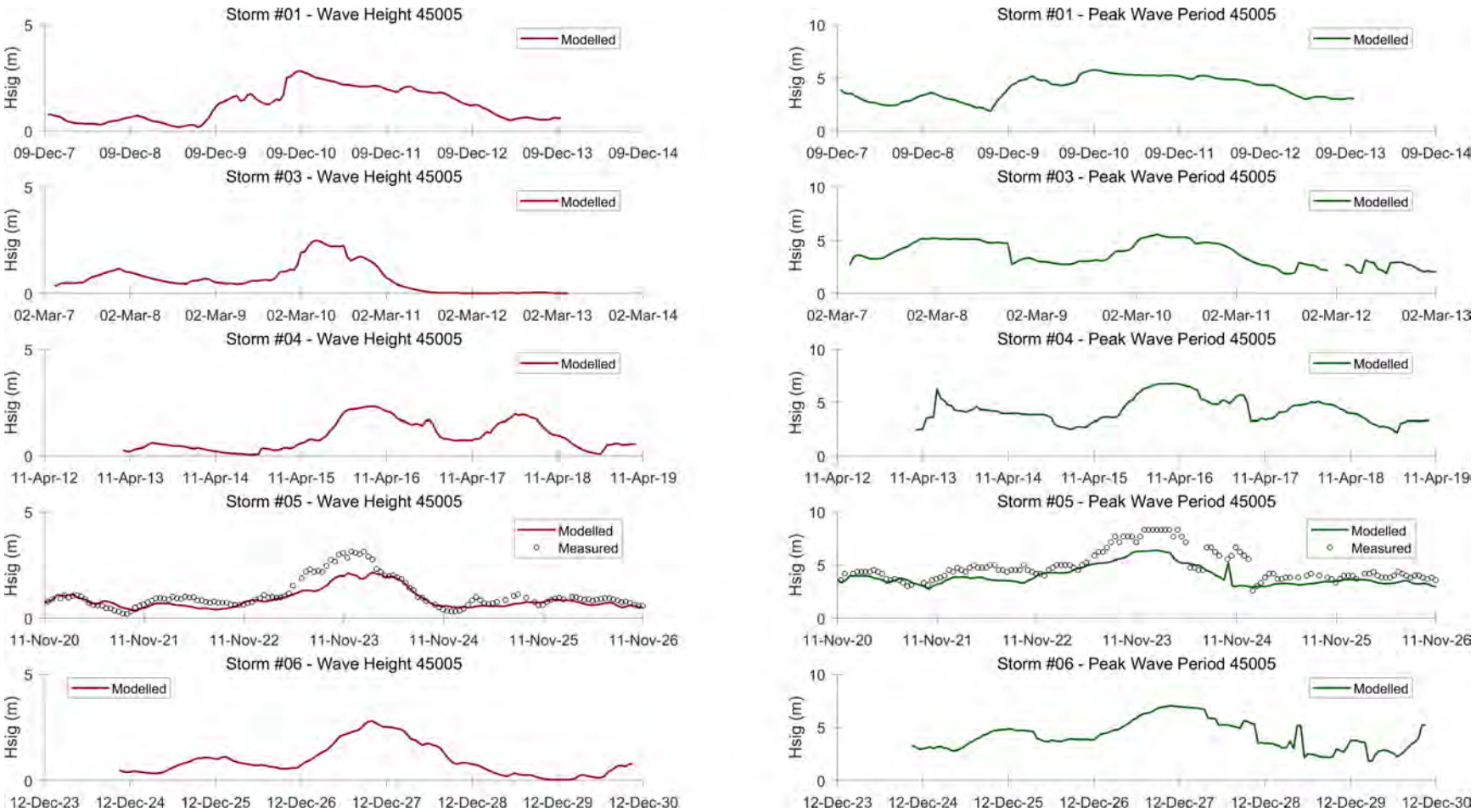

Figure A.10 MIKE21 spectral wave comparison on Lake Erie at buoy 45005 for Storms 1 to 5.

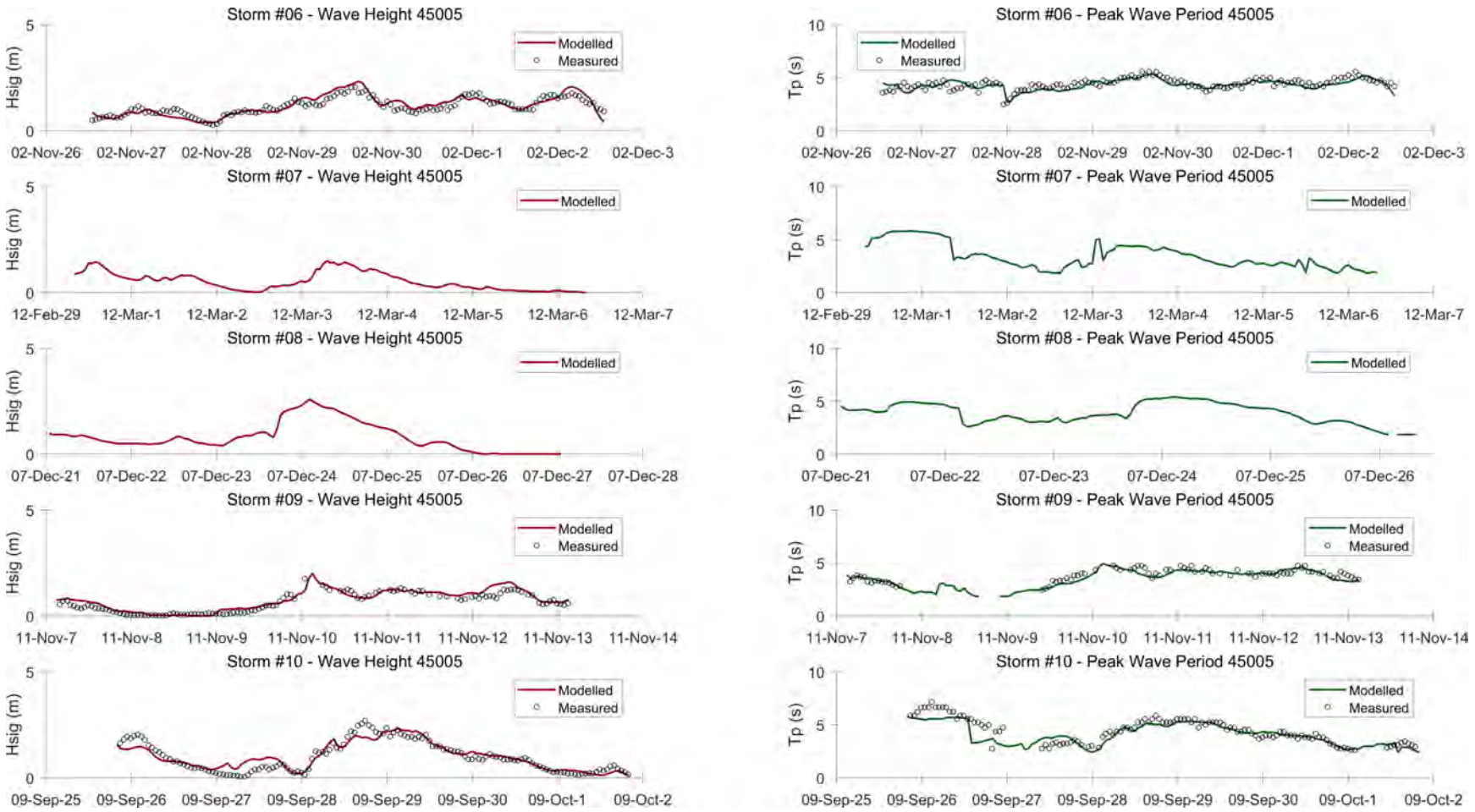

Figure A.11 MIKE21 spectral wave comparison on Lake Erie at buoy 45005 for Storms 6 to 10.

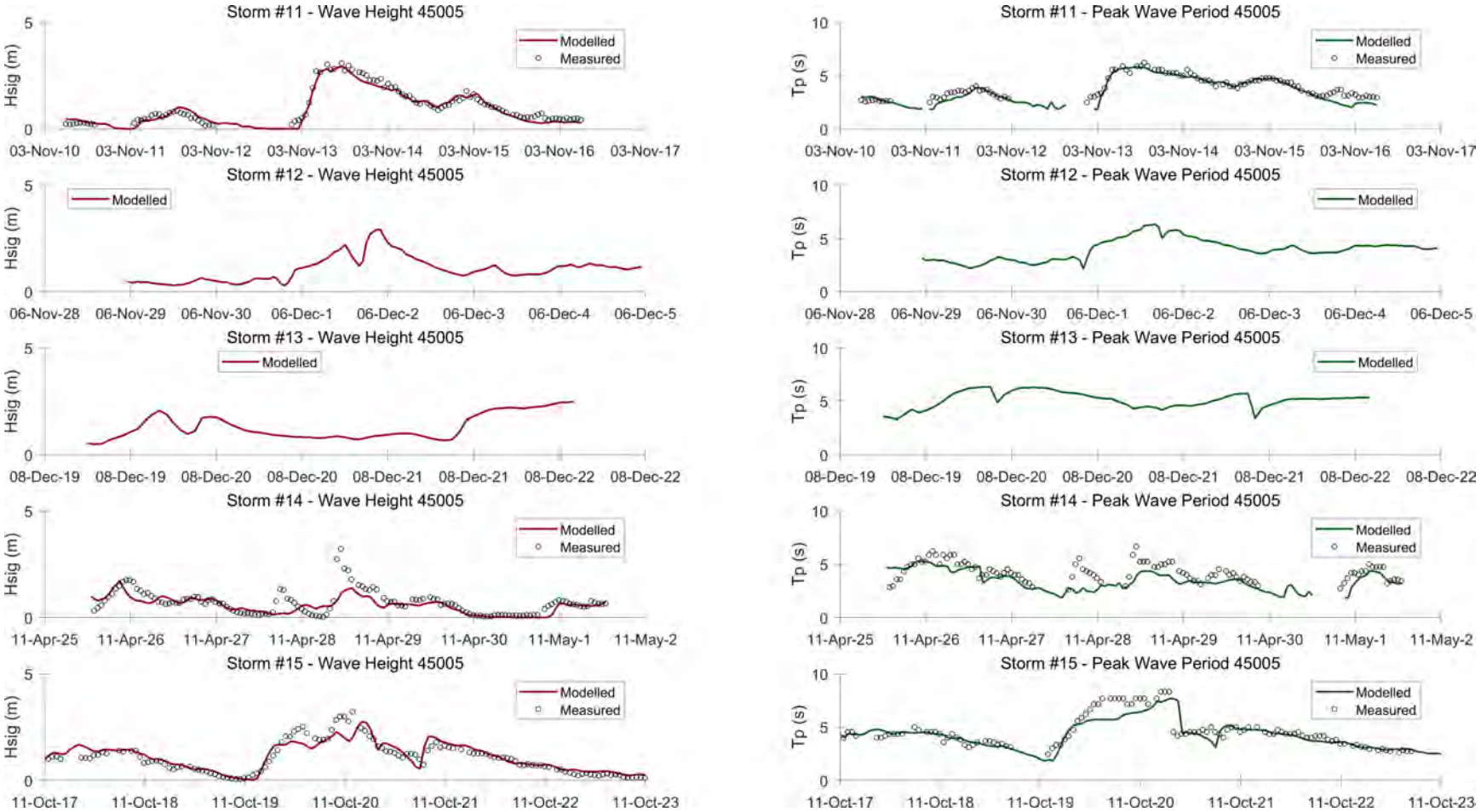

Figure A.12 MIKE21 spectral wave comparison on Lake Erie at buoy 45005 for Storms 11 to 15.

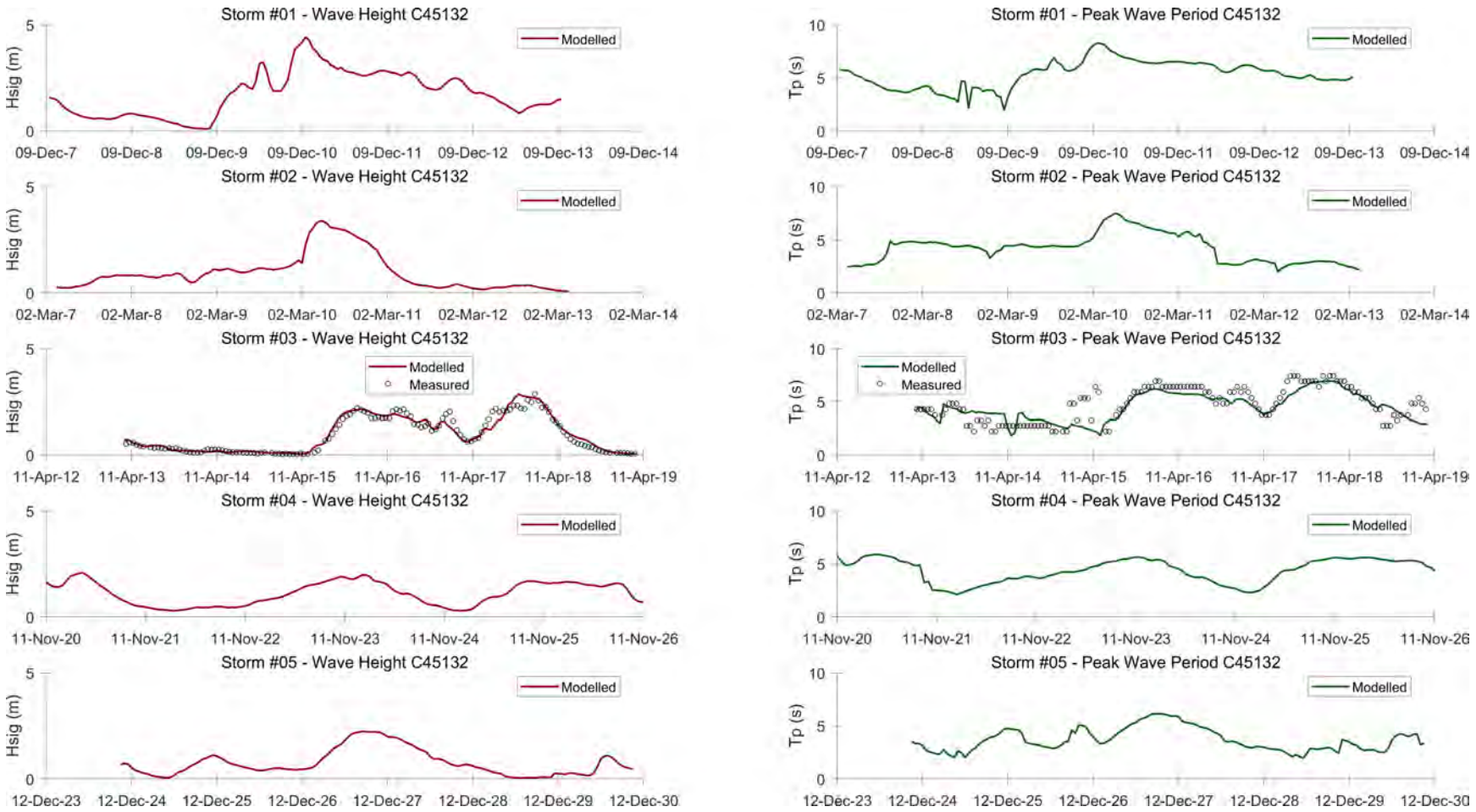

Figure A.13 MIKE21 spectral wave comparison on Lake Erie at buoy C45132 for Storms 1 to 5.

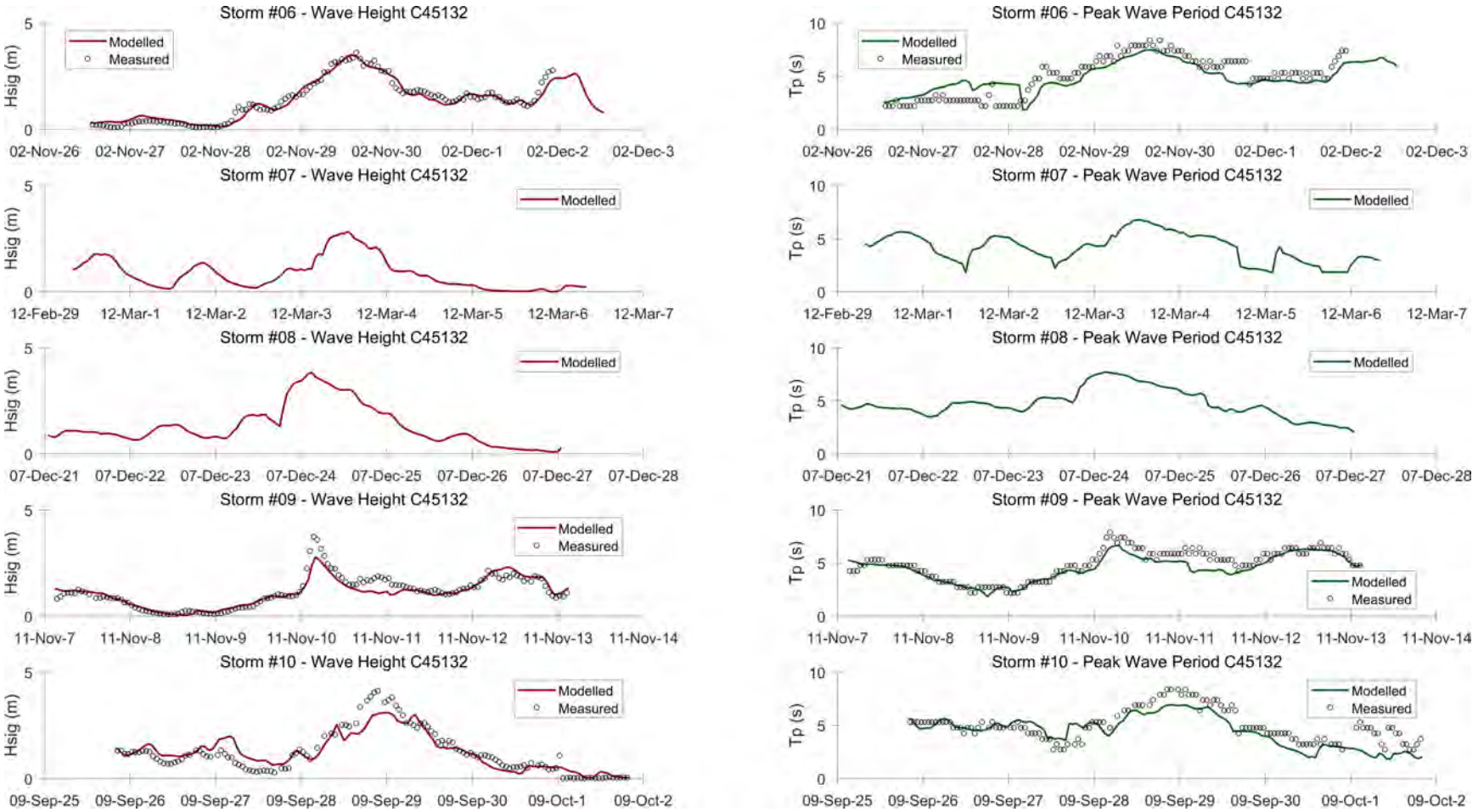

Figure A.14 MIKE21 spectral wave comparison on Lake Erie at buoy C45132 for Storms 6 to 10.

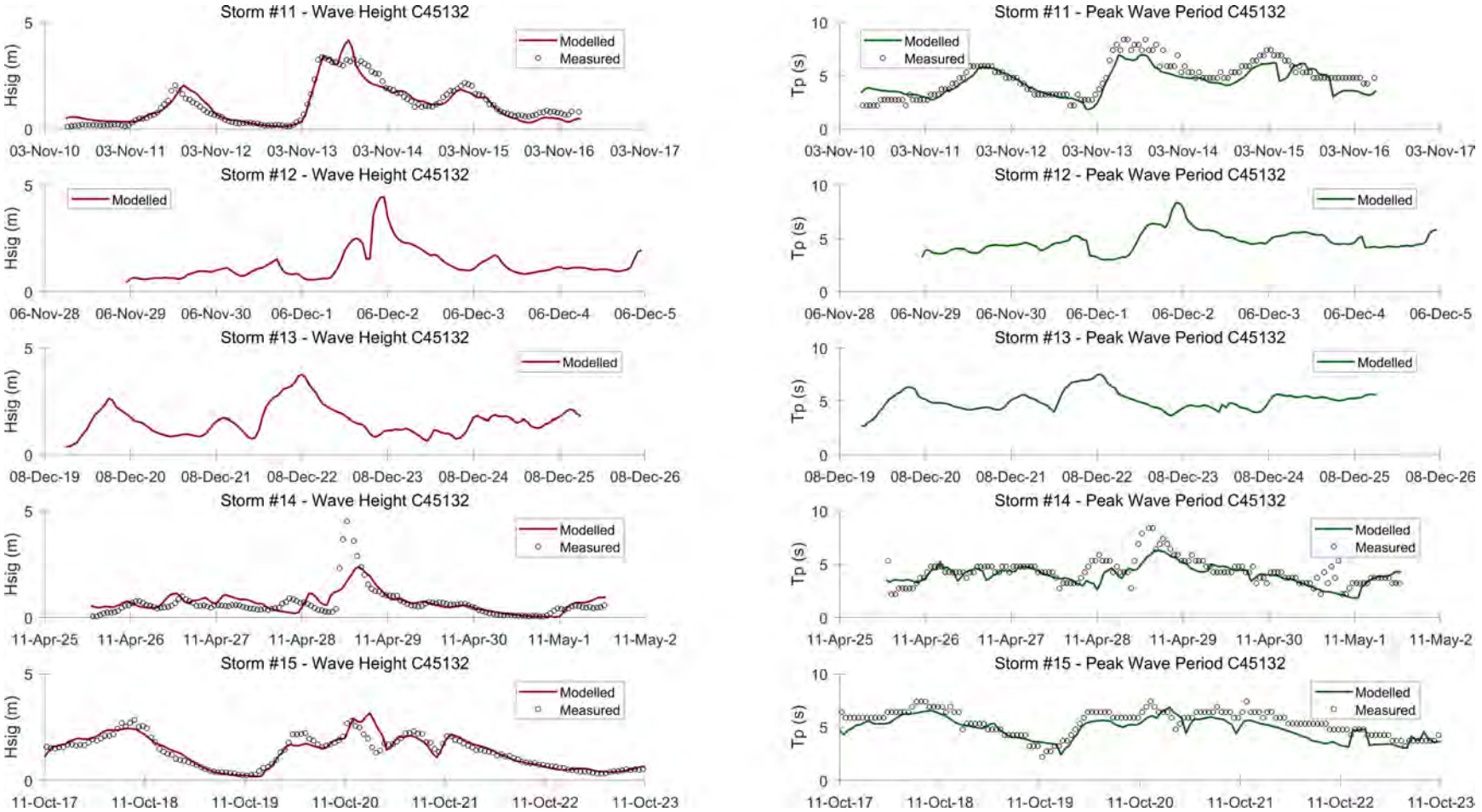

Figure A.15 MIKE21 spectral wave comparison on Lake Erie at buoy C45132 for Storms 11 to 15.

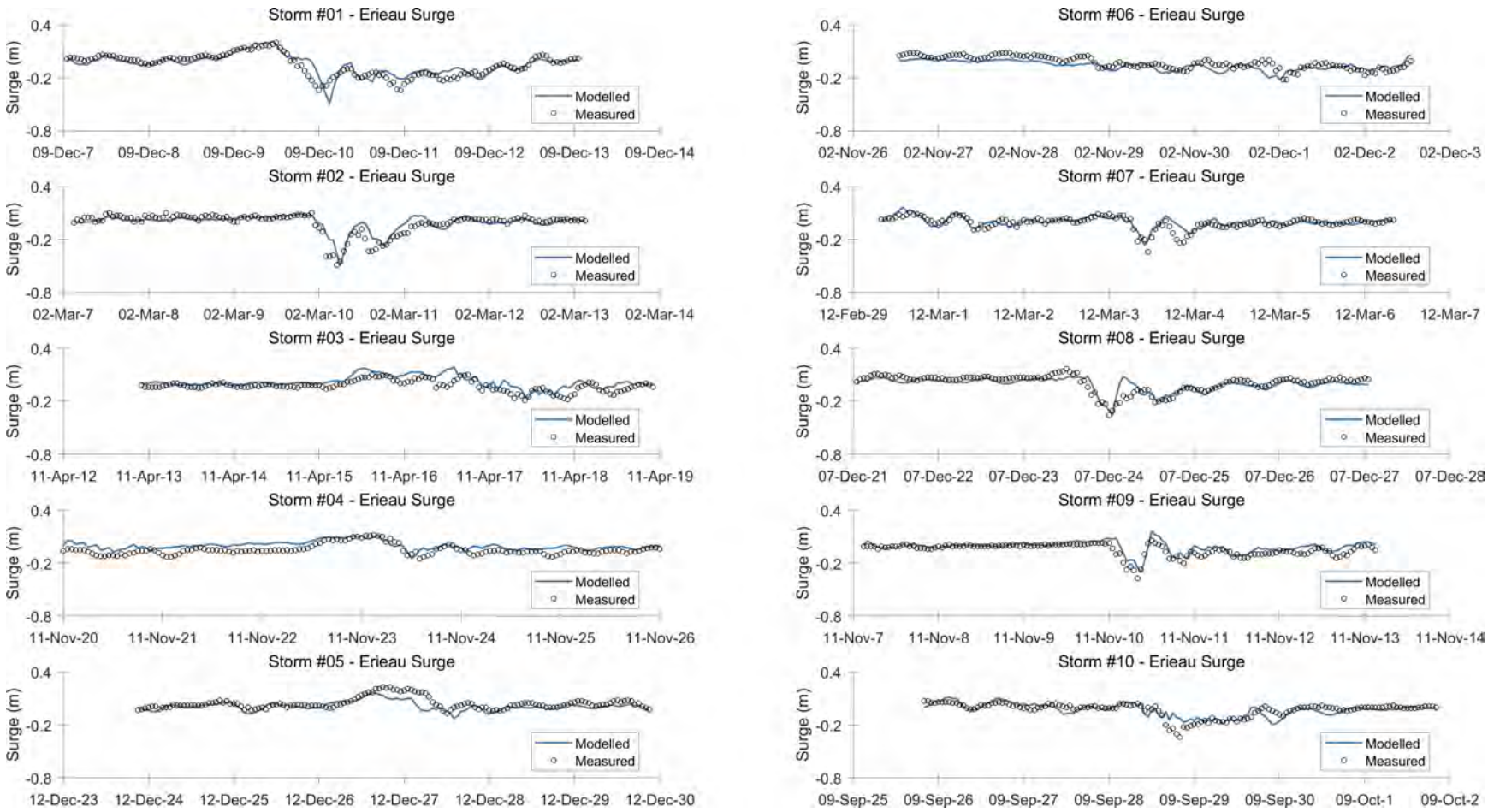

Figure A.16 MIKE21 surge comparisons on Lake Erie at the Erieau gauge (12250) for Storms 1 to 10.

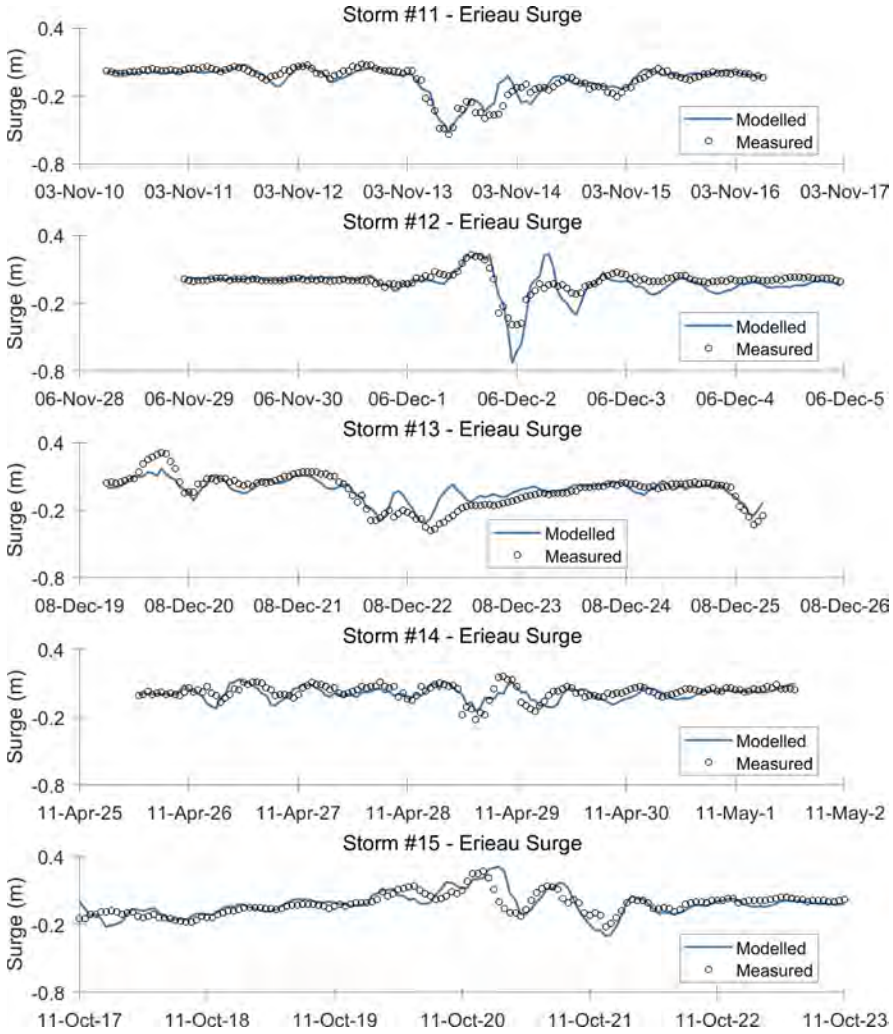

Figure A.17 MIKE21 surge comparisons on Lake Erie at the Erieau gauge (12250) for Storms 11 to 15.

Appendix B

MIKE21 Model Results – Baseline and Future Conditions

Table B.1 Summary of Peak Wave and Surge Conditions on Lake Ontario.

Storm	Hm0 (m) LOP1		Hm0 (m) LOP2		Surge (m) Toronto		Surge (m) Burlington	
No.	Baseline	Future	Baseline	Future	Baseline	Future	Baseline	Future
1	3.04	2.74	2.34	2.27	0.16	0.17	0.27	0.27
2	2.39	2.72	0.00	2.56	0.13	0.15	0.20	0.30
3	3.09	2.19	2.51	1.96	0.12	0.10	0.26	0.18
4	2.54	2.51	0.00	2.12	0.15	0.17	0.23	0.26
5	1.52	1.53	1.34	1.27	0.09	0.09	0.13	0.11
6	2.48	2.44	0.00	2.15	0.12	0.14	0.18	0.22
7	0.00	1.69	0.00	1.53	0.10	0.11	0.13	0.14
8	2.81	2.82	2.37	2.30	0.15	0.18	0.28	0.29
9	1.92	1.92	1.54	1.74	0.05	0.06	0.13	0.14
10	2.36	2.04	0.00	2.03	0.11	0.12	0.22	0.25
11	1.43	1.62	0.97	0.82	0.14	0.14	0.19	0.12
12	2.17	2.22	1.61	1.66	0.13	0.15	0.14	0.16
13	1.99	2.12	1.97	2.18	0.09	0.13	0.22	0.26
14	1.74	2.33	0.00	2.13	0.07	0.13	0.16	0.27
15	2.35	2.06	1.67	1.39	0.15	0.15	0.17	0.15

Table B.2 Summary of Peak Wave and Surge Conditions on Lake Erie.

Storm	Hm0 (m) LEP1		Hm0 (m) LEP2		Surge (m) Erieau	
No.	Baseline	Future	Baseline	Future	Baseline	Future
1	2.72	2.70	2.34	2.80	0.21	0.29
2	2.11	2.24	1.97	2.07	0.09	0.10
3	2.05	2.01	1.83	1.84	0.19	0.18
4	1.78	1.70	1.78	1.72	0.12	0.12
5	2.04	2.05	1.85	1.91	0.17	0.18
6	2.46	2.54	2.21	2.29	0.06	0.08
7	1.65	2.05	1.61	2.20	0.16	0.15
8	0.00	2.44	0.00	2.10	0.08	0.12
9	2.04	1.75	1.85	1.58	0.17	0.13
10	2.27	2.21	1.88	2.03	0.11	0.15
11	1.65	1.49	1.56	1.56	0.08	0.08
12	3.12	3.23	2.78	2.91	0.24	0.22
13	0.00	1.86	0.00	1.63	0.17	0.20
14	1.44	1.66	1.49	1.85	0.13	0.18
15	2.43	1.98	2.53	2.22	0.31	0.20

Appendix C

WAVAD Calibration QQ Plots

Lake Ontario - Quantile-Quantile (WAVAD versus Buoy)

Station:	EAST_ONTARIO_NDBC_45012	Points:	21,480
Latitude:	43.6200	Start:	2002-04-12
Longitude:	-77.4000	End:	2013-06-26

Statistic	Hm0	Tp
Bias	0.077	-0.174
RMSE	0.386	0.787
SI	0.380	0.170
SIB	0.372	0.166
r	0.807	0.720

Series	Average	Maximum
Buoy Hm0 (m)	1.02	7.57
WAVAD Hm0 (m)	1.09	5.75
Buoy Tp (sec)	4.62	10.81
WAVAD Tp (s)	4.45	9.67

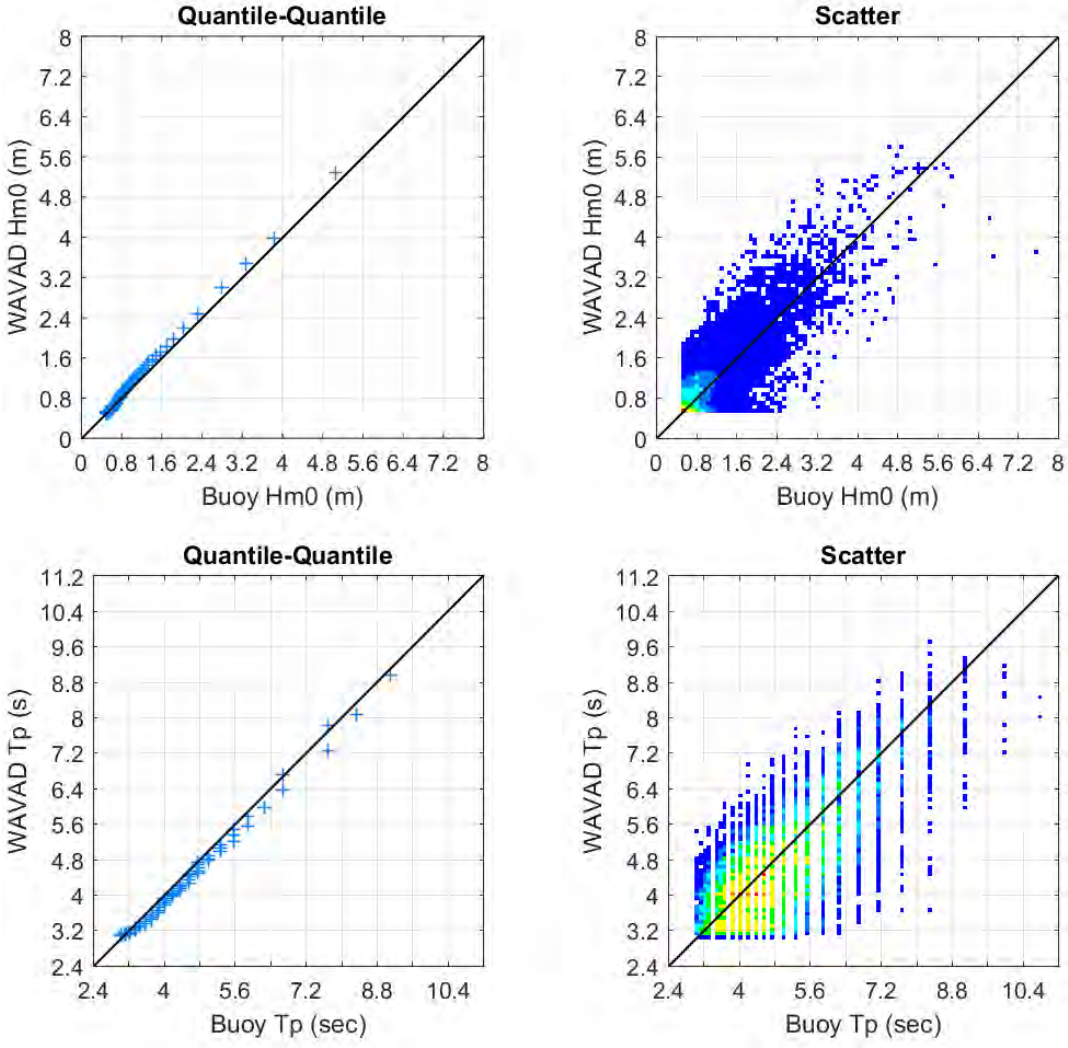

Figure C.1 QQ plot comparison on Lake Ontario at buoy 45012.

Lake Ontario - Quantile-Quantile (WAVAD versus Buoy)

Station:	WEST_ONTARIO_A_MEDS_45139_C	Points:	3,619
Latitude:	43.4000	Start:	2001-07-26
Longitude:	-79.4400	End:	2004-09-07

Statistic	Hm0	Tp
Bias	-0.040	-0.774
RMSE	0.402	1.101
SI	0.431	0.215
SIB	0.429	0.153
r	0.575	0.724

Series	Average	Maximum
Buoy Hm0 (m)	0.93	3.97
WAVAD Hm0 (m)	0.89	3.77
Buoy Tp (s)	5.13	8.98
WAVAD Tp (s)	4.36	8.66

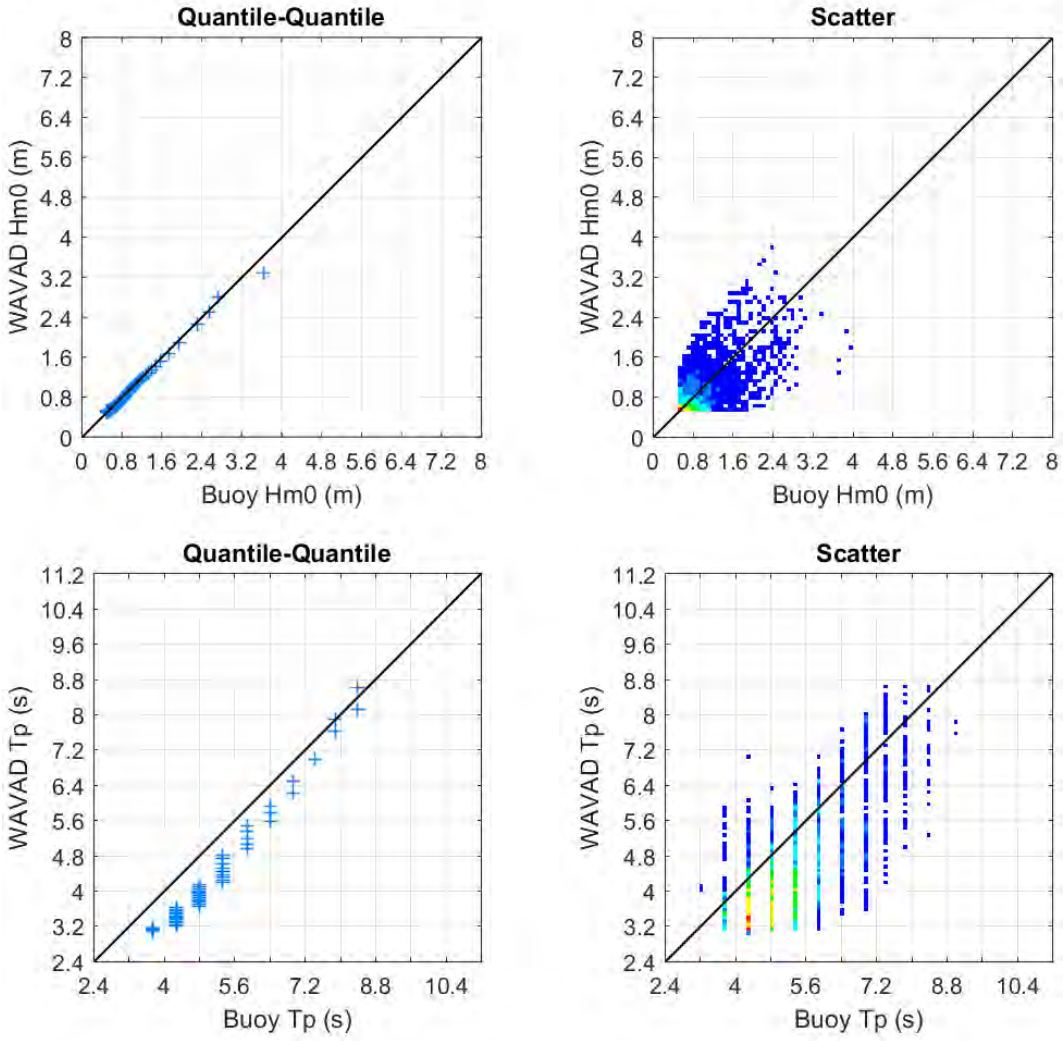

Figure C.2 QQ plot comparison on Lake Ontario at buoy C45139 (2001 to 2004).

Lake Ontario - Quantile-Quantile (WAVAD versus Buoy)

Station:	WEST_ONTARIO_B_MEDS_45139_A	Points:	5,888
Latitude:	43.2600	Start:	2006-04-13
Longitude:	-79.5400	End:	2013-05-12

Statistic	Hm0	Tp
Bias	-0.029	-0.149
RMSE	0.335	0.860
SI	0.429	0.188
SIB	0.428	0.185
r	0.418	0.669

Series	Average	Maximum
Buoy Hm0 (m)	0.78	3.23
WAVAD Hm0 (m)	0.75	2.71
Buoy Tp (s)	4.58	11.13
WAVAD Tp (s)	4.43	8.87

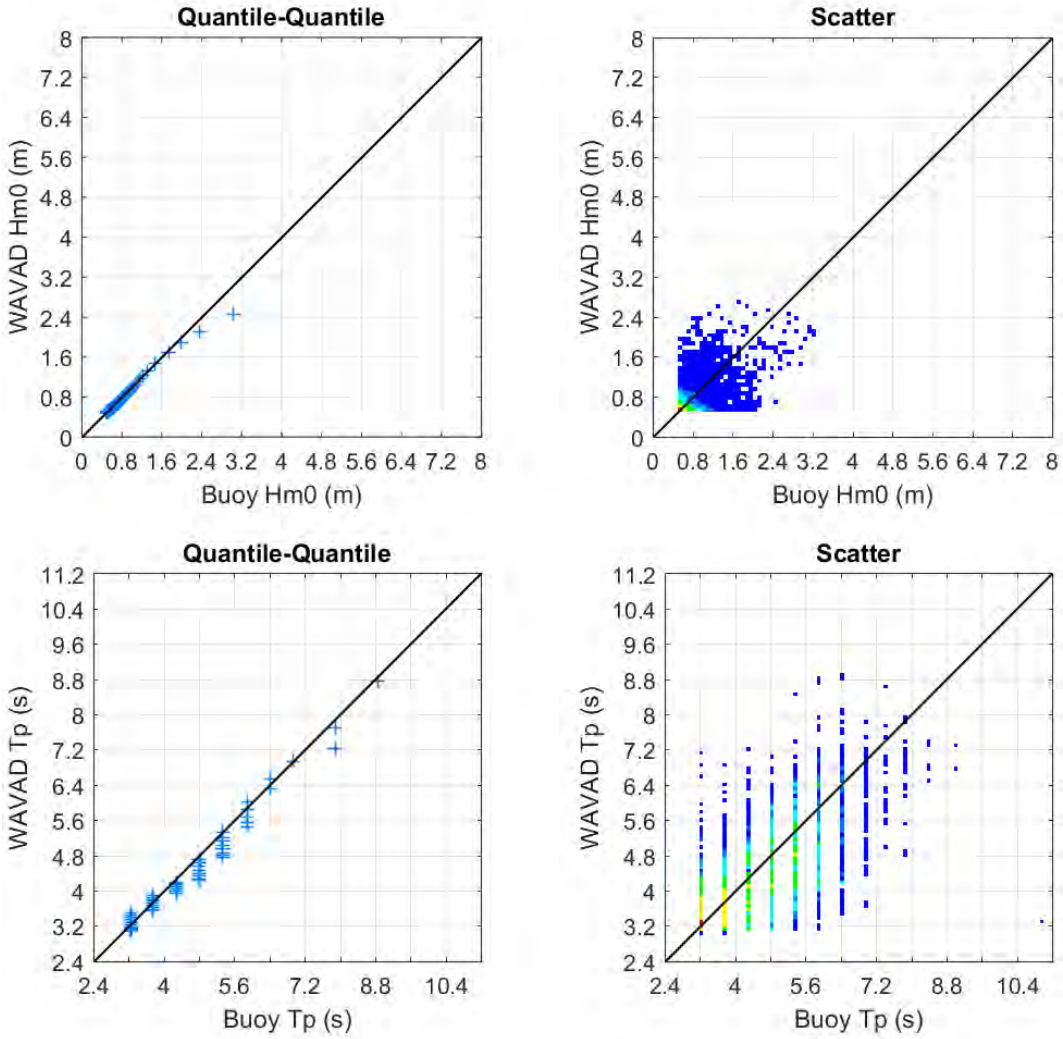

Figure C.3 QQ plot comparison on Lake Ontario at buoy C45139 (2006 to 2013).

Lake Erie - Quantile-Quantile (WAVAD versus Buoy)

Station:	PORT_STANLEY_C45132	Points:	19,923
Latitude:	42.4800	Start:	2000-10-01
Longitude:	-81.2200	End:	2013-06-26

Statistic	Hm0	Tp
Bias	0.159	-0.223
RMSE	0.402	0.853
SI	0.423	0.180
SIB	0.389	0.174
r	0.744	0.656

Series	Average	Maximum
Buoy Hm0 (m)	0.95	4.52
WAVAD Hm0 (m)	1.11	4.15
Buoy Tp (s)	4.74	8.39
WAVAD Tp (s)	4.51	8.92

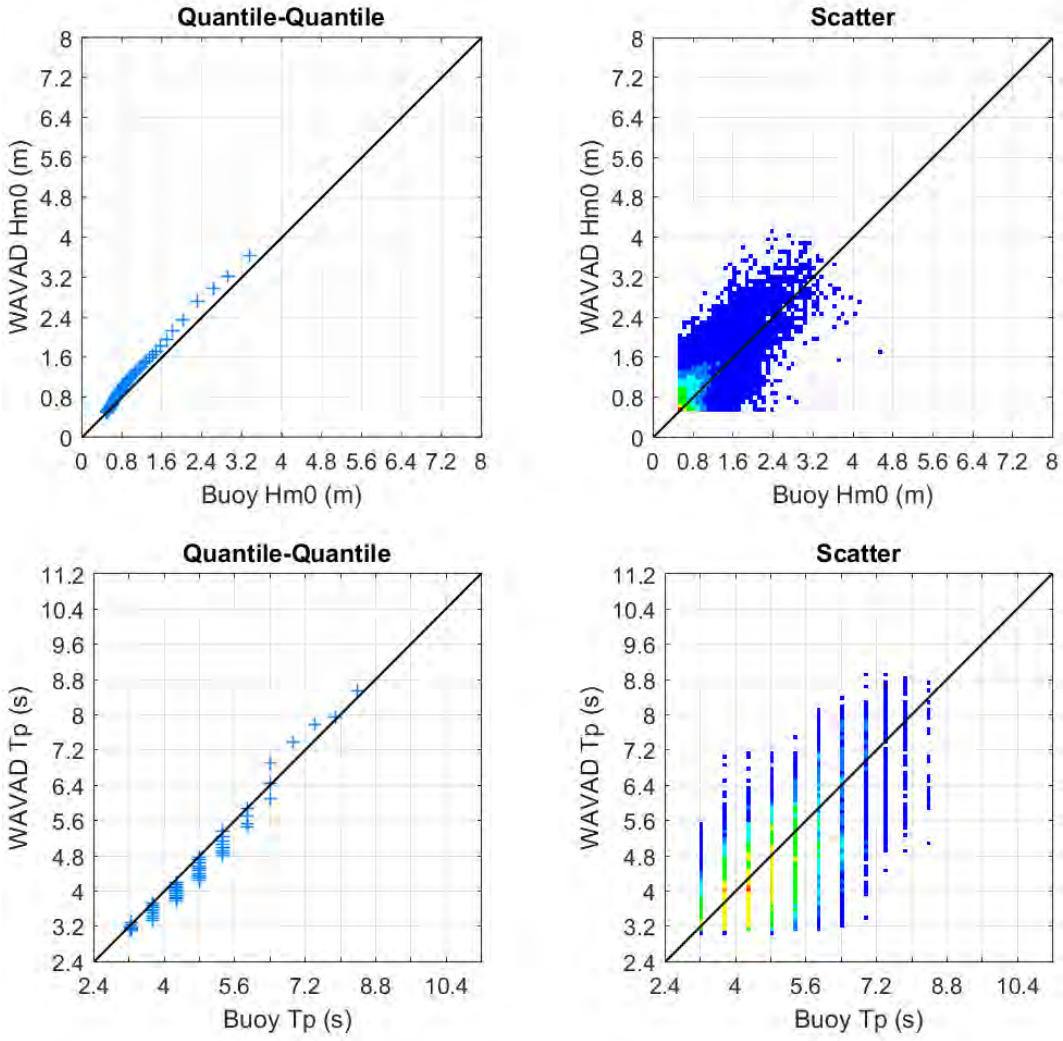

Figure C.4 QQ plot comparison on Lake Erie at buoy C45132.

Lake Erie - Quantile-Quantile (WAVAD versus Buoy)

Station:	WEST_ERIE_45005	Points:	24,168
Latitude:	41.6800	Start:	2000-10-01
Longitude:	-82.4000	End:	2013-06-30

Statistic	Hm0	Tp
Bias	0.035	0.000
RMSE	0.372	0.783
SI	0.402	0.178
SIB	0.401	0.178
r	0.599	0.593

Series	Average	Maximum
Buoy Hm0 (m)	0.92	4.26
WAVAD Hm0 (m)	0.96	3.31
Buoy Tp (sec)	4.41	12.50
WAVAD Tp (s)	4.41	8.31

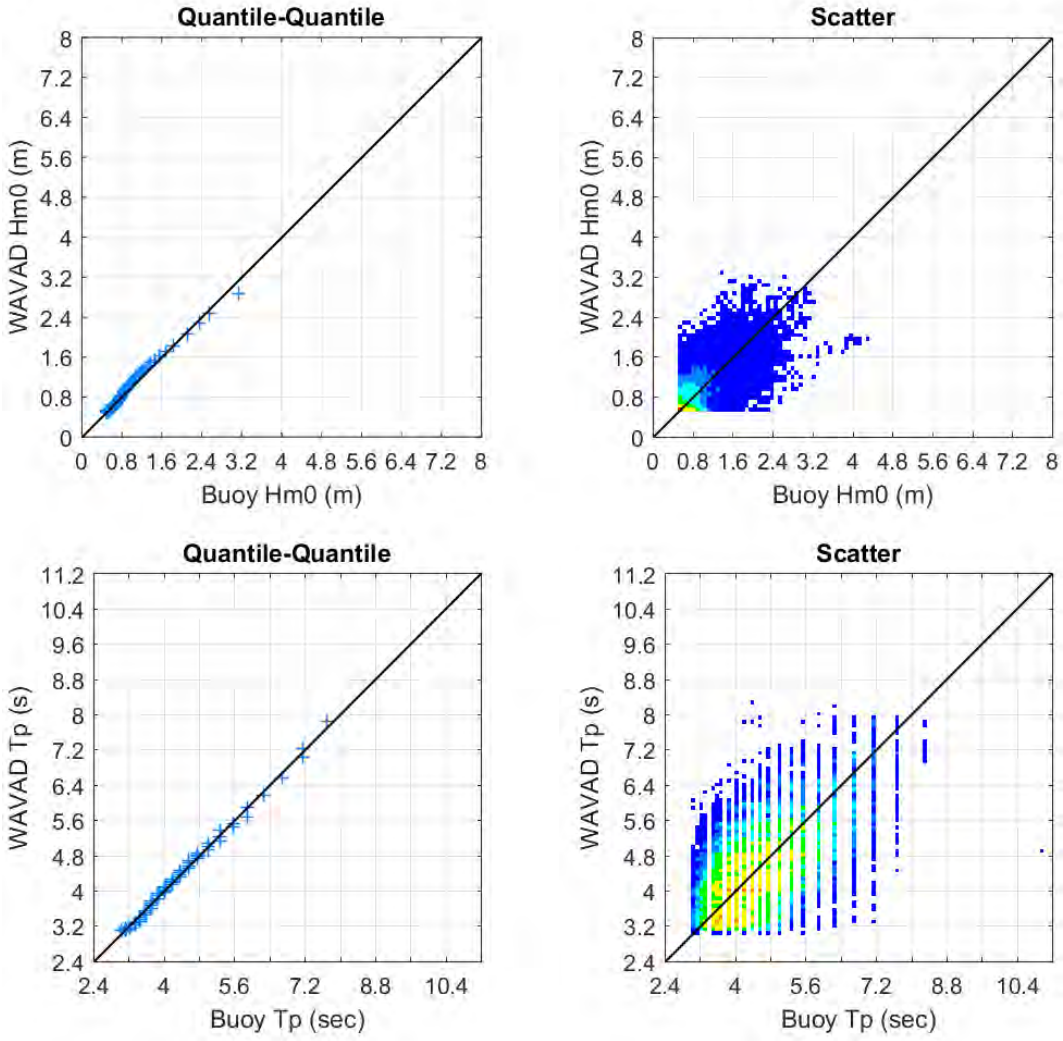

Figure C.5 QQ plot comparison on Lake Erie at buoy 45005.

Appendix D

WAVAD Wave Energy Maps

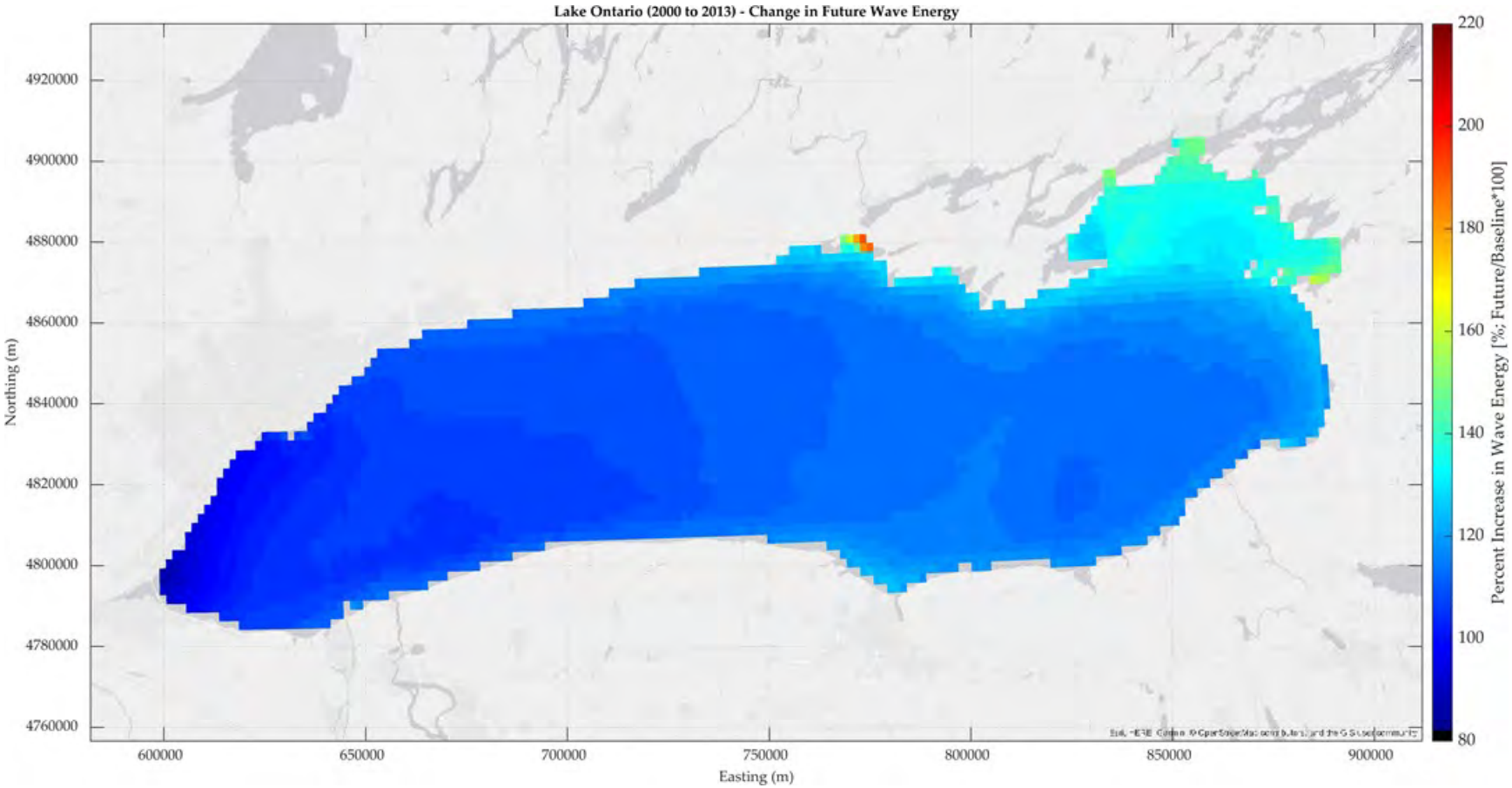

Figure D.1 Percent increase in wave energy in the future on Lake Ontario for the period 2000-2013 (30% ice threshold).

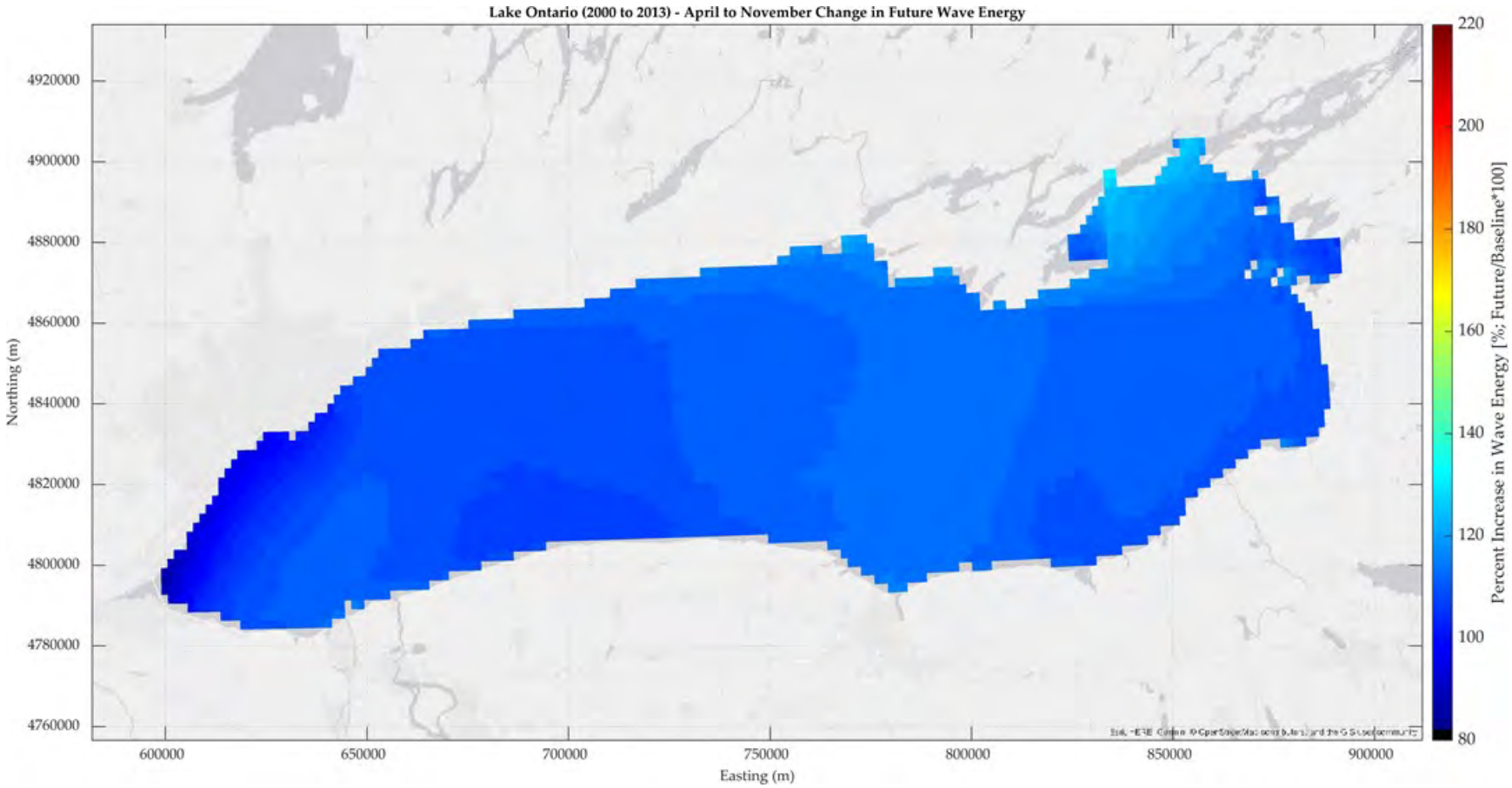

Figure D.2 Percent increase in wave energy in the future on Lake Ontario for the ice-free (April to November) periods between 2000-2013 (30% ice threshold).

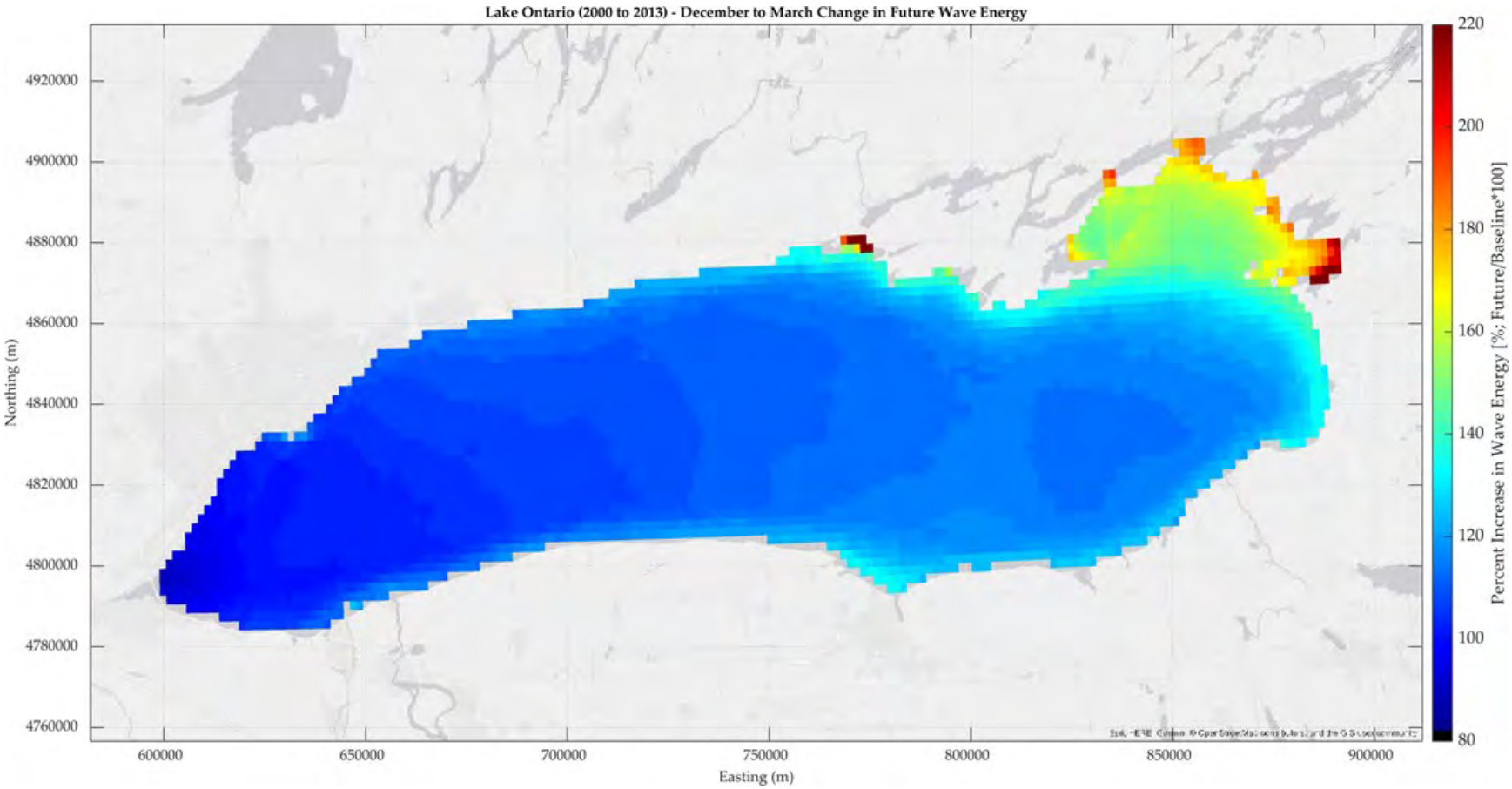

Figure D.3 Percent increase in wave energy in the future on Lake Ontario for the ice (December to March) periods between 2000-2013 (30% ice threshold).

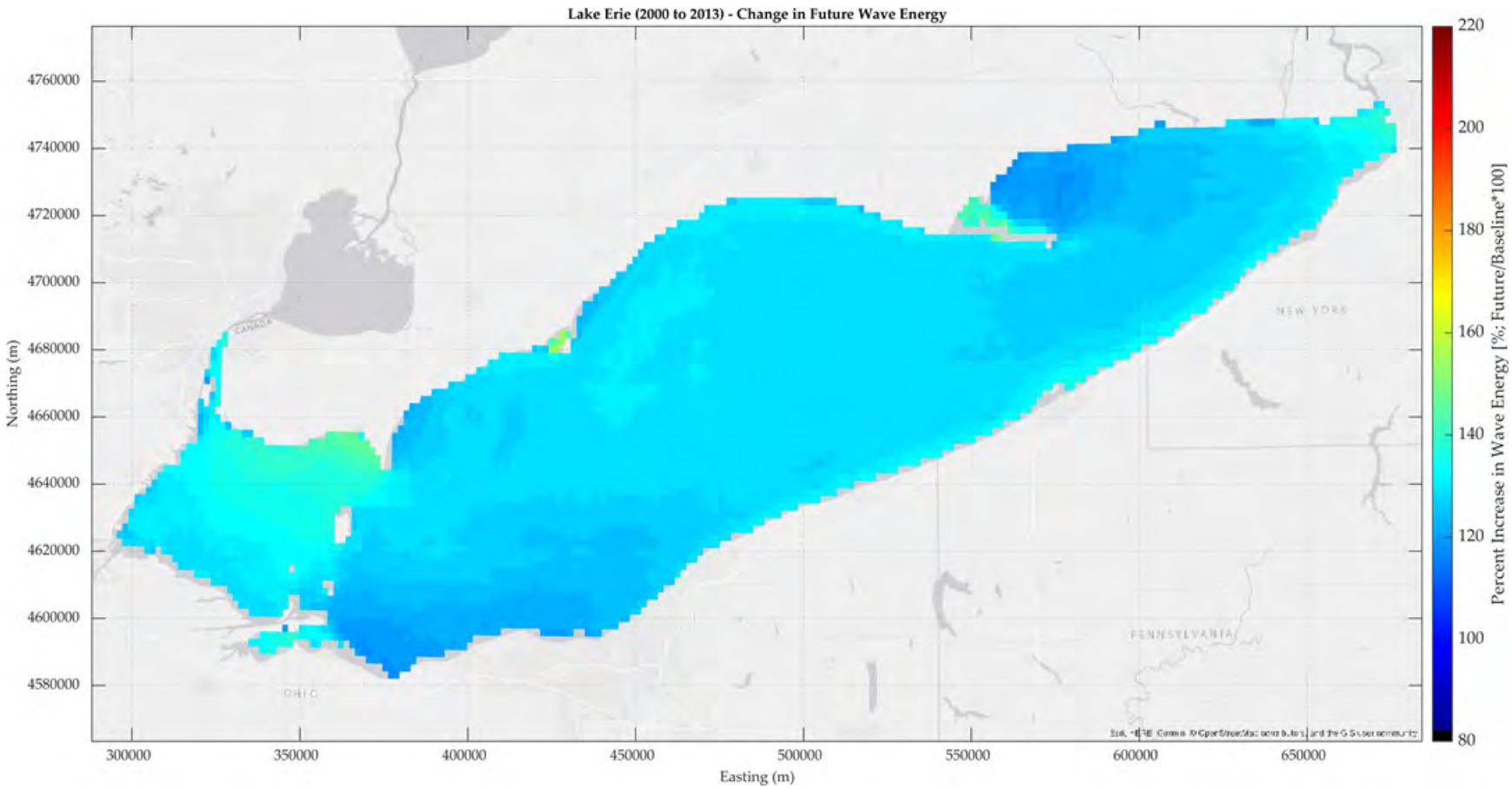

Figure D.4 Percent increase in wave energy in the future on Lake Erie for the period 2000-2013 (30% ice threshold).

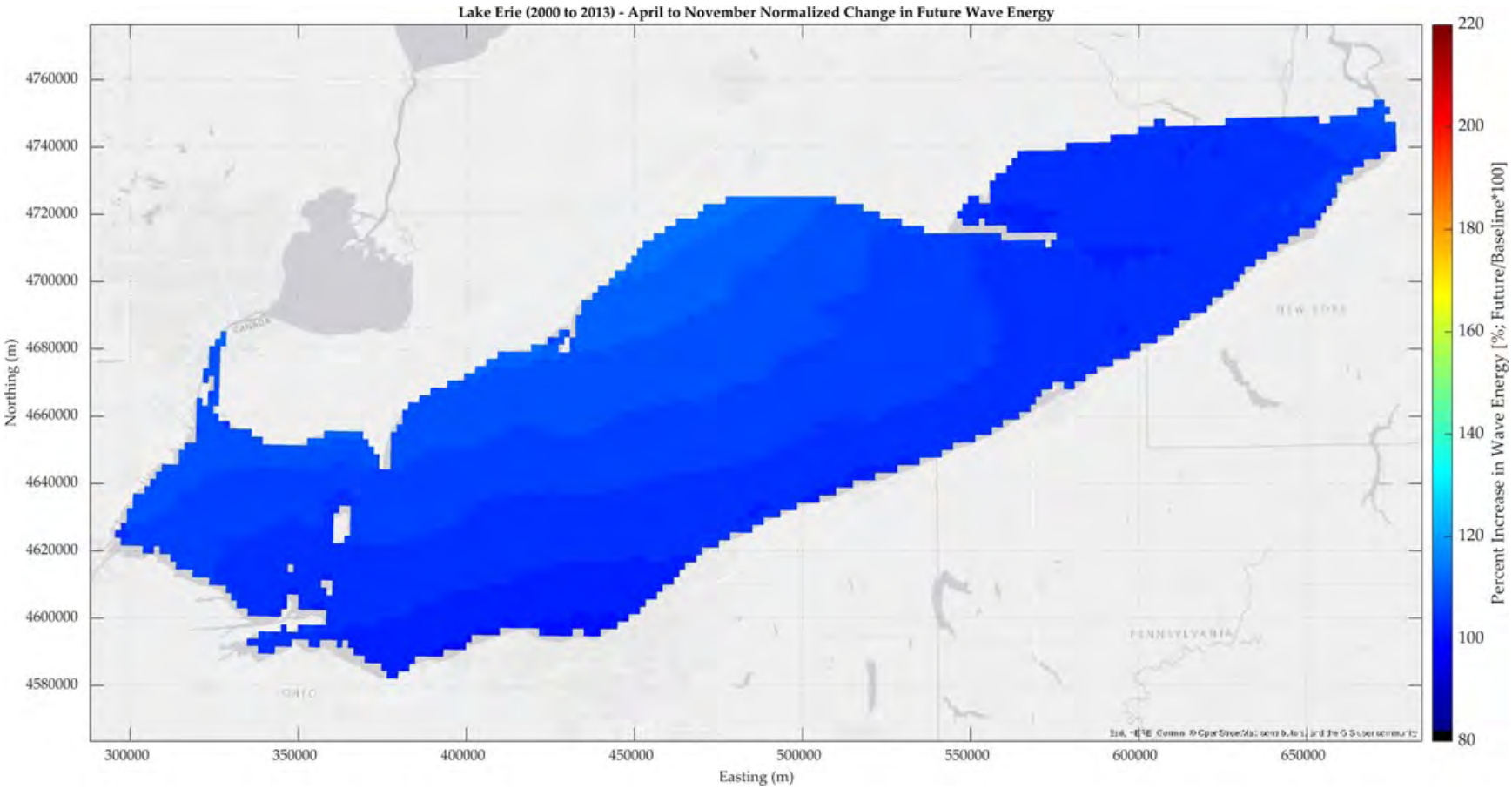

Figure D.5 Percent increase in wave energy in the future on Lake Erie for the ice-free (April to November) periods between 2000-2013 (30% ice threshold).

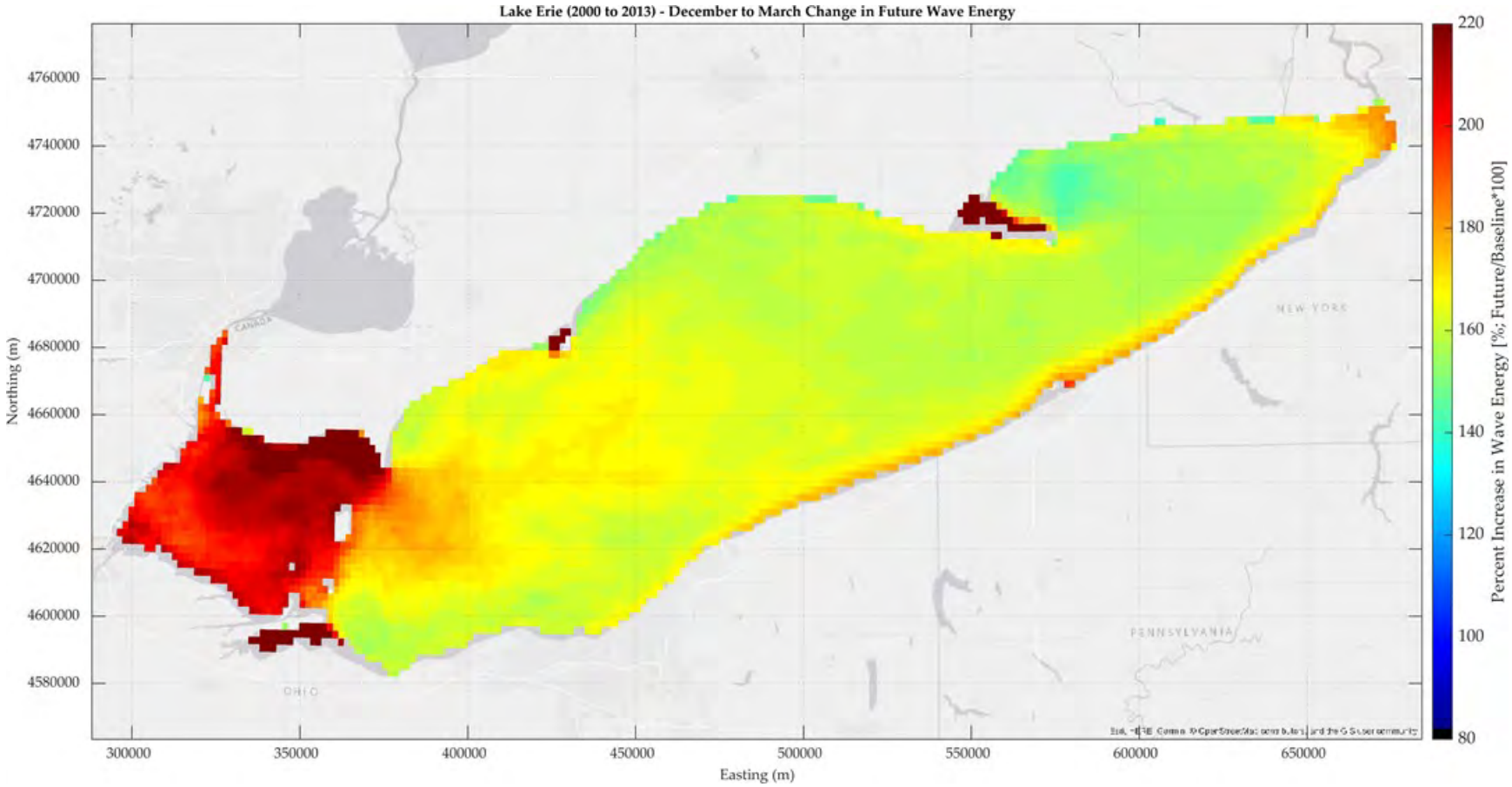

Figure D.6 Percent increase in wave energy in the future on Lake Erie for the ice (December to March) periods between 2000-2013 (30% ice threshold).

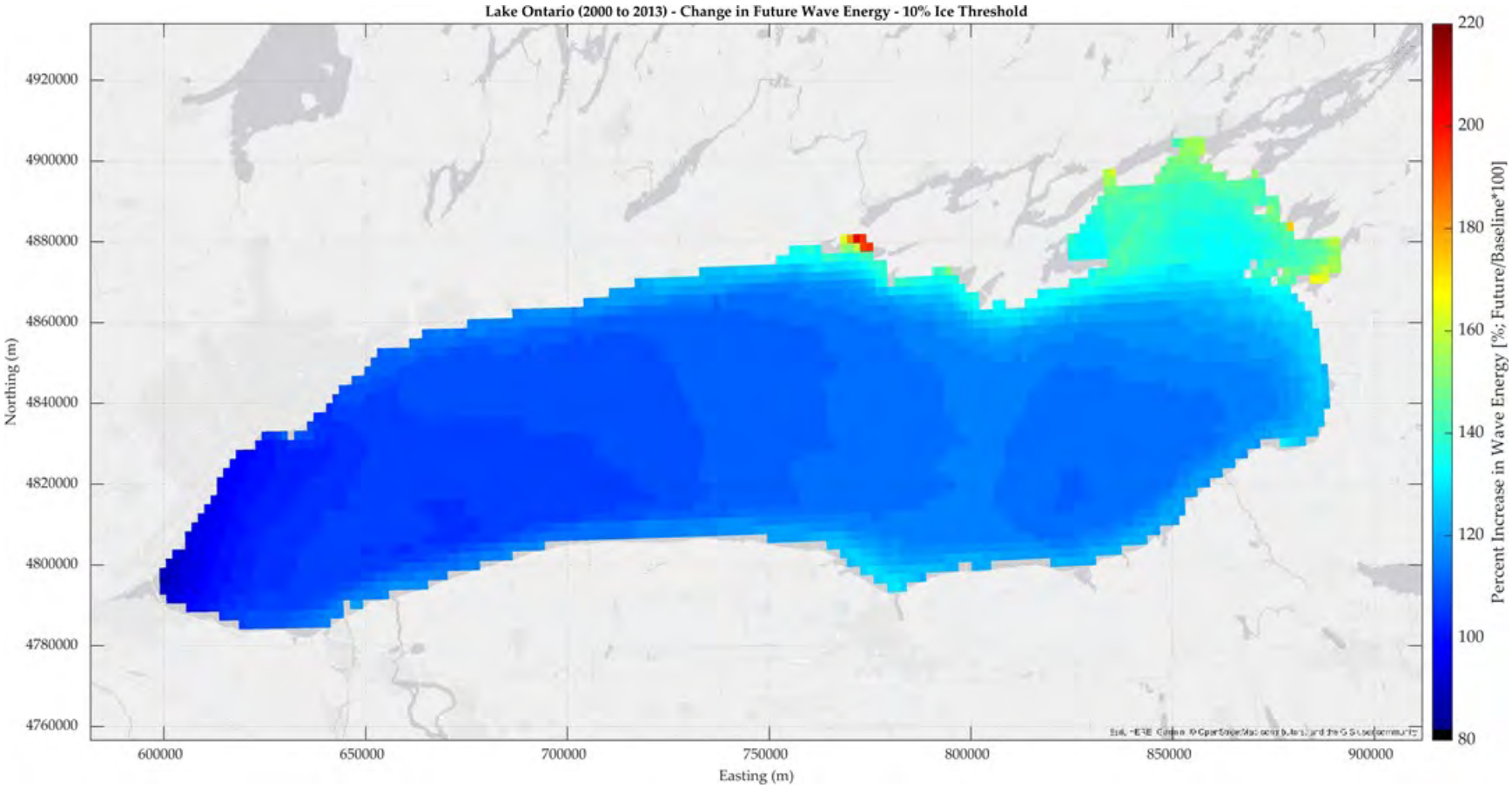

Figure D.7 Percent increase in wave energy in the future on Lake Ontario for the period 2000-2013 (10% ice threshold).

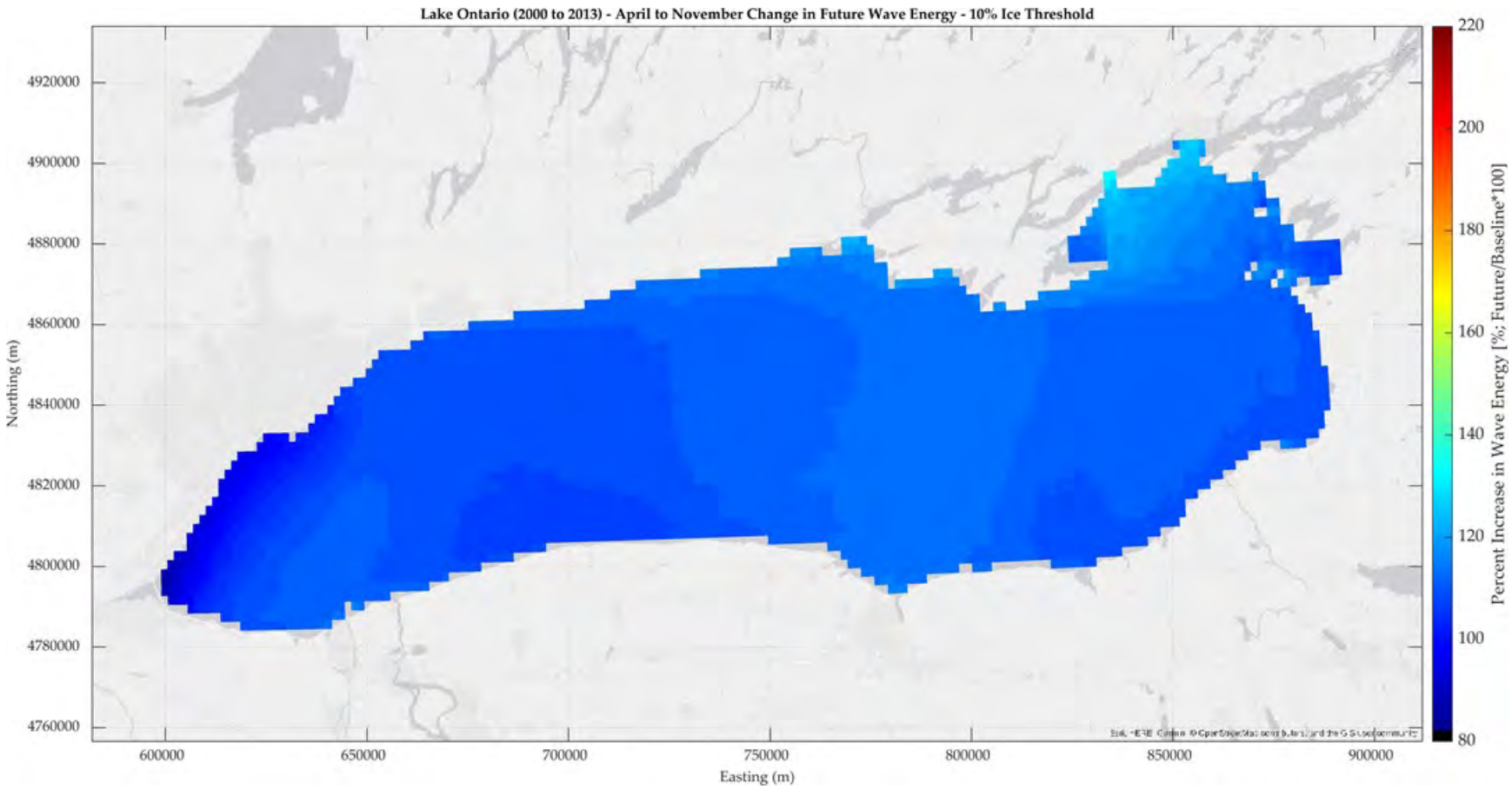

Figure D.8 Percent increase in wave energy in the future on Lake Ontario for the ice-free (April to November) periods between 2000-2013 (10% ice threshold).

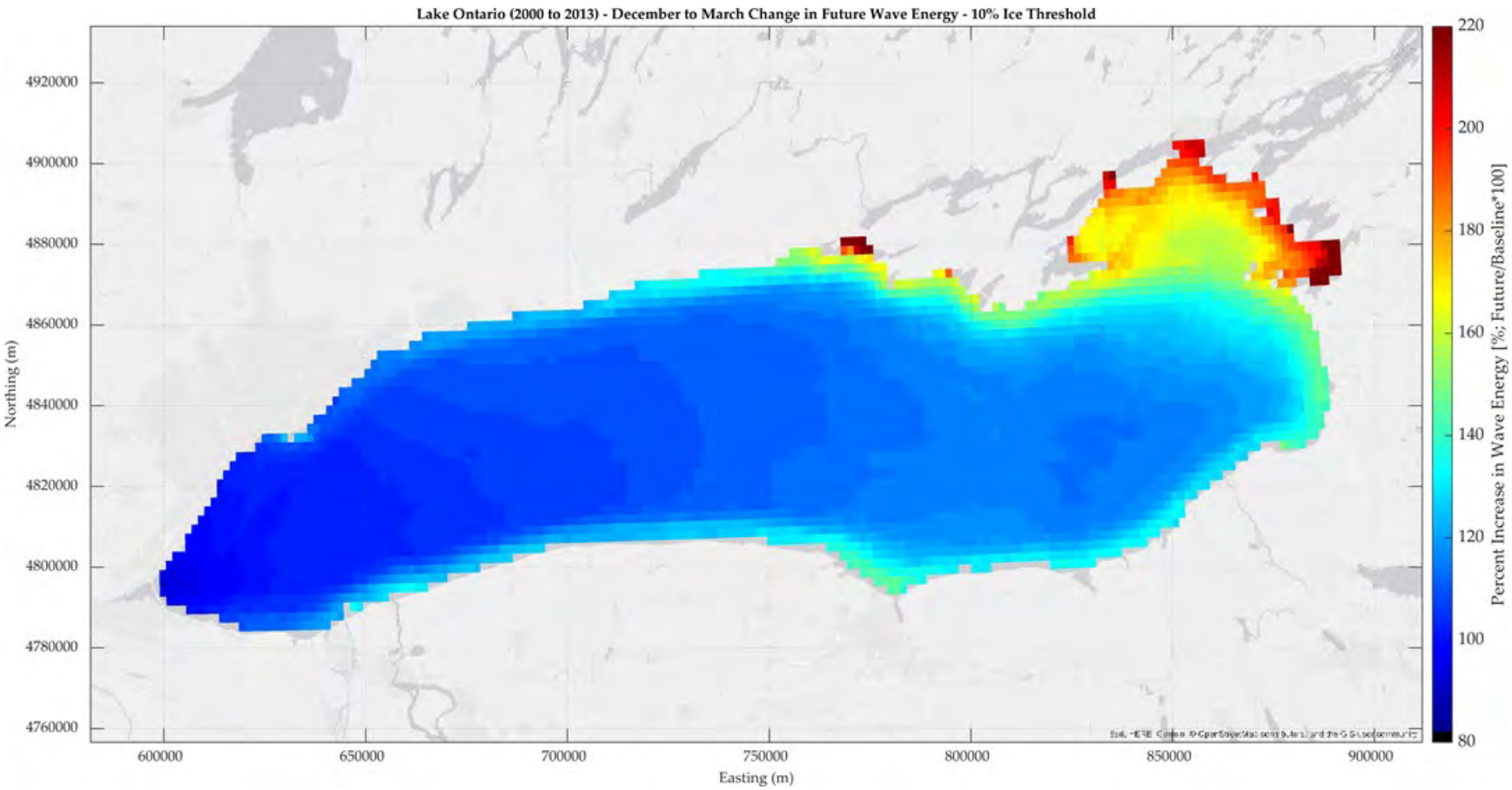

Figure D.9 Percent increase in wave energy in the future on Lake Ontario for the ice (December to March) periods between 2000-2013 (10% ice threshold).

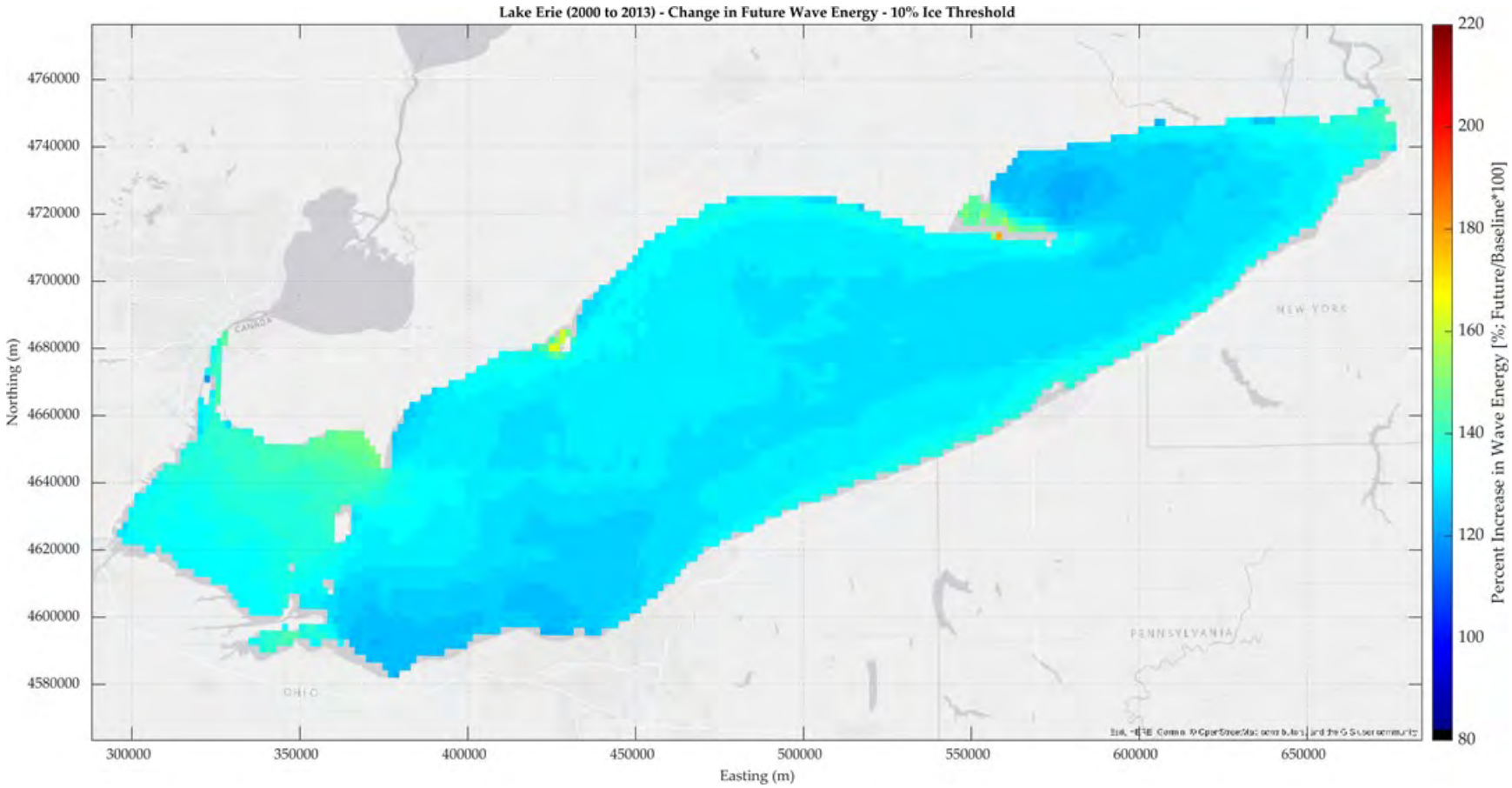

Figure D.10 Percent increase in wave energy in the future on Lake Erie for the period 2000-2013 (10% ice threshold).

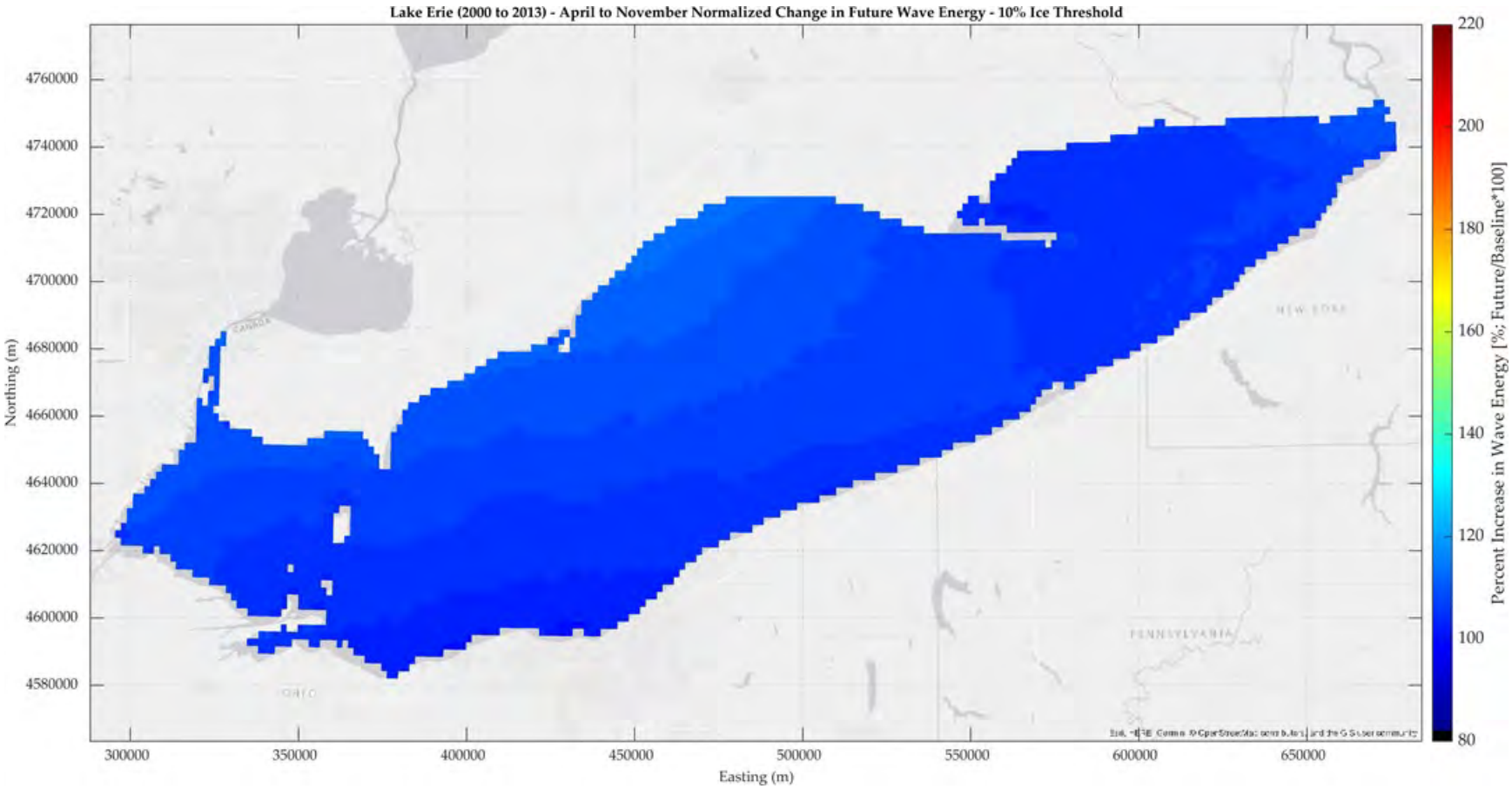

Figure D.11 Percent increase in wave energy in the future on Lake Erie for the ice-free (April to November) periods between 2000-2013 (10% ice threshold).

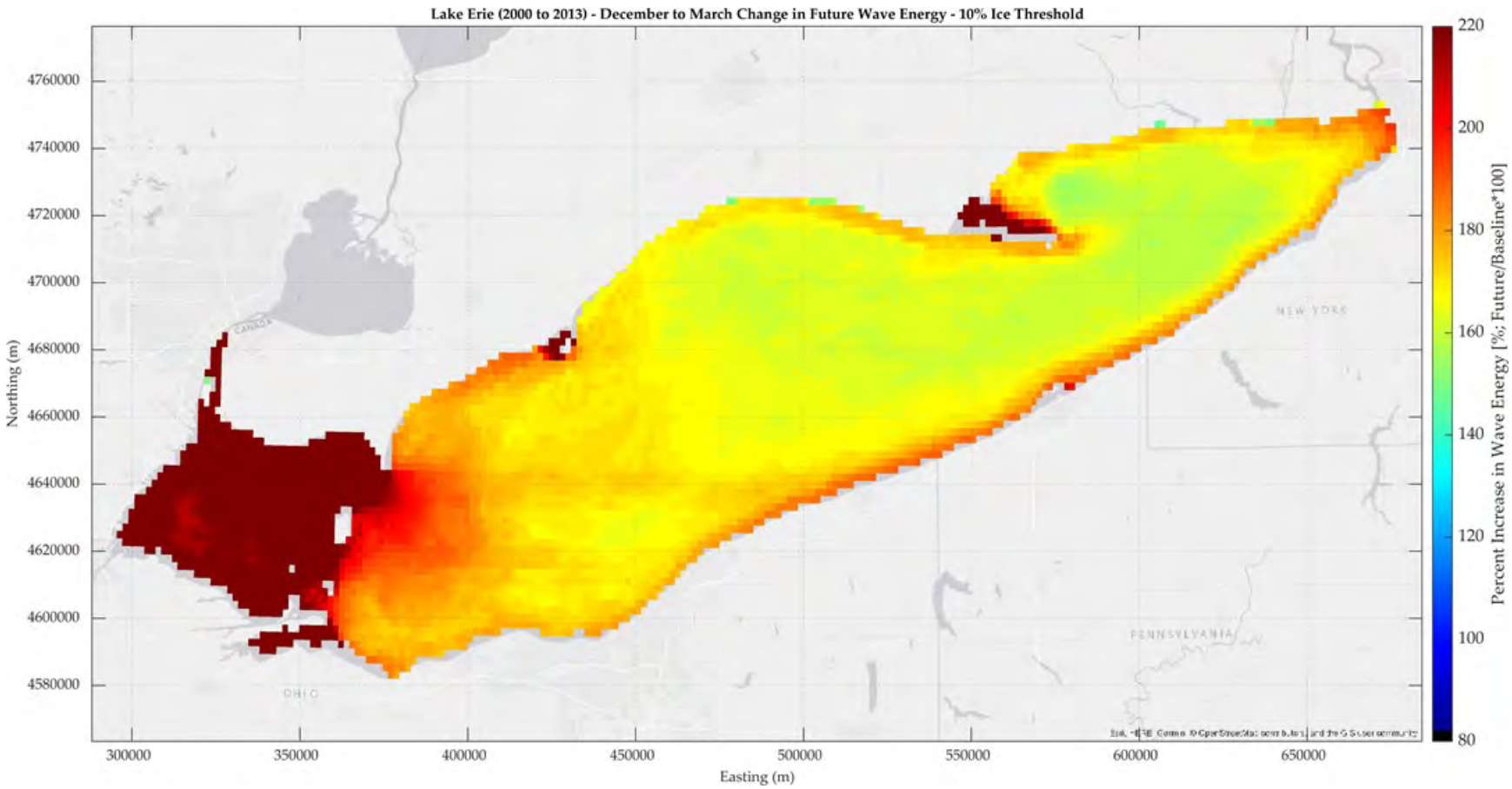

Figure D.11 Percent increase in wave energy in the future on Lake Erie for the ice (December to March) periods between 2000-2013 (10% ice threshold).